



## Disaggregation of SMOS soil moisture in southeastern Australia

Olivier Merlin, Christoph Rüdiger, Al Bitar Ahmad, Philippe Richaume,  
Jeffrey P. Walker, Yann H. Kerr

### ► To cite this version:

Olivier Merlin, Christoph Rüdiger, Al Bitar Ahmad, Philippe Richaume, Jeffrey P. Walker, et al.. Disaggregation of SMOS soil moisture in southeastern Australia. *IEEE Transactions on Geoscience and Remote Sensing*, 2012, 50 (5), pp.1556-1571. 10.1109/TGRS.2011.2175000 . ird-00658335

HAL Id: ird-00658335

<https://ird.hal.science/ird-00658335>

Submitted on 10 Jan 2012

**HAL** is a multi-disciplinary open access archive for the deposit and dissemination of scientific research documents, whether they are published or not. The documents may come from teaching and research institutions in France or abroad, or from public or private research centers.

L'archive ouverte pluridisciplinaire **HAL**, est destinée au dépôt et à la diffusion de documents scientifiques de niveau recherche, publiés ou non, émanant des établissements d'enseignement et de recherche français ou étrangers, des laboratoires publics ou privés.

# Disaggregation of SMOS Soil Moisture in Southeastern Australia

Olivier Merlin, Christoph Rüdiger, Ahmad Al Bitar, Philippe Richaume, Jeffrey P. Walker, and Yann H. Kerr

**Abstract**—Disaggregation based on Physical And Theoretical scale Change (DisPATCh) is an algorithm dedicated to the disaggregation of soil moisture observations using high-resolution soil temperature data. DisPATCh converts soil temperature fields into soil moisture fields given a semi-empirical soil evaporative efficiency model and a first-order Taylor series expansion around the field-mean soil moisture. In this study, the disaggregation approach is applied to soil moisture and ocean salinity (SMOS) data over the 500 km by 100 km AACES (Australian Airborne Calibration/validation Experiments for SMOS) area. The 40-km resolution SMOS surface soil moisture pixels are disaggregated at 1-km resolution using the soil skin temperature derived from moderate resolution imaging spectroradiometer (MODIS) data, and subsequently compared with the AACES intensive ground measurements aggregated at 1-km resolution. The objective is to test DisPATCh under various surface and atmospheric conditions. It is found that the accuracy of disaggregation products varies greatly according to season: while the correlation coefficient between disaggregated and *in situ* soil moisture is about 0.7 during the summer AACES, it is approximately zero during the winter AACES, consistent with a weaker coupling between evaporation and surface soil moisture in temperate than in semi-arid climate. Moreover, during the summer AACES, the correlation coefficient between disaggregated and *in situ* soil moisture is increased from 0.70 to 0.85, by separating the 1-km pixels where MODIS temperature is mainly controlled by soil evaporation, from those where MODIS temperature is controlled by both soil evaporation and vegetation transpiration. It is also found that the 5-km resolution atmospheric correction of the official MODIS temperature data has a significant impact on DisPATCh output. An alternative atmospheric correction at 40-km resolution increases the correlation coefficient between disaggregated and *in situ* soil moisture from 0.72 to 0.82 during the summer AACES. Results indicate that

DisPATCh has a strong potential in low-vegetated semi-arid areas where it can be used as a tool to evaluate SMOS data (by reducing the mismatch in spatial extent between SMOS observations and localized *in situ* measurements), and as a further step, to derive a 1-km resolution soil moisture product adapted for large-scale hydrological studies.

**Index Terms**—AACES, calibration/validation, disaggregation, Disaggregation based on Physical And Theoretical scale Change (DisPATCh), field campaign, moderate resolution imaging spectroradiometer (MODIS), soil moisture and ocean salinity (SMOS).

## I. INTRODUCTION

PASSIVE MICROWAVE remote sensing has the capability to provide key elements of the terrestrial hydrological cycle such as surface soil moisture [1], [2] and overland precipitation [3], [4]. Nevertheless, due to the large discrepancy between the observation scale (several tens of km) and the scale of physical interactions with the land surface (one wavelength or several cm), the radiative transfer models applied to passive microwave remote sensing data are only semiphysically based. Consequently, the retrieval process of land surface parameters from microwave brightness temperatures requires ancillary data for calibration and validation purposes [5]. It also requires a strategy to use such ancillary data since ground-based sampling is often made over a small area/point, which constrains with the large integrated extent of spaceborne passive microwave observations.

The soil moisture and ocean salinity (SMOS), [6] satellite was launched on November 2, 2009. Over land, the SMOS mission aims at providing  $\sim 5$  cm surface soil moisture data at a spatial resolution better than 50 km and a repeat cycle of less than 3 days. The payload is a 2-D interferometer equipped with 69 individual L-band antennas regularly spaced along Y-shaped arms. This new concept allows observing all pixels in the 1000 km wide field of view at a range of incidence angles. It also allows reconstructing brightness temperatures on a fixed sampling grid [7].

Since the SMOS launch, various field experiments (the HOBE site in Denmark [8], the Mali site in Western Africa [9], the SMOSMANIA site in Southwestern France [10] just to name a few) have been undertaken to validate SMOS reconstructed brightness temperatures and soil moisture retrievals. The AACES (Australian Airborne Calibration/validation Experiment for SMOS, [11]) is one of the most comprehensive campaigns worldwide dedicated to SMOS calibration/validation. A series of two experiments were undertaken in 2010, AACES-1 in January–February (Austral summer) and

Manuscript received March 31, 2011; revised September 1, 2011; accepted October 30, 2011. The AACES participants are gratefully acknowledged for their participation in collecting this extensive data set. The Australian Airborne Calibration/validation Experiments for SMOS have been made possible through infrastructure (LE0453434) and research (DP0879212) funding from the Australian Research Council, and the collaboration of a large number of scientists from throughout Australia, United States and Europe. Initial setup and maintenance of the study catchments was funded by two research Grants (DP0343778, DP0557543) from the Australian Research Council and by the CRC for Catchment Hydrology. This work was funded by the CNES TOSCA (Terre solide, Océan, Surfaces Continentales et Atmosphère) program and the Centre National de la Recherche Scientifique.

O. Merlin is with the Centre d'Etudes Spatiales de la Biosphère (CESBIO), 31401 Toulouse, France (e-mail: olivier.merlin@cesbio.cnes.fr).

C. Rüdiger (e-mail: chris.rudiger@monash.edu).

A. Al Bitar (e-mail: ahmad.albitar@cesbio.cnes.fr).

P. Richaume (e-mail: philippe.richaume@cesbio.cnes.fr).

J. P. Walker (e-mail: jeff.walker@monash.edu).

Y. H. Kerr (e-mail: yann.kerr@cesbio.cnes.fr).

Color versions of one or more of the figures in this paper are available online at <http://ieeexplore.ieee.org>.

Digital Object Identifier 10.1109/TGRS.2011.2175000

83 AACES-2 in September (Austral winter). The data collected  
 84 in AACES include 1-km resolution airborne L-band brightness  
 85 temperature mapped over a 500 km by 100 km area, 20 days  
 86 of very intensive ground measurements and 20 5 km by 2 km  
 87 ground sampling areas.

88 Even though the AACES ground measurements are very  
 89 extensive, it is not feasible to cover the whole extent of a  
 90 SMOS pixel by ground sampling alone. This is the reason why  
 91 most validation strategies of spaceborne passive microwave  
 92 data using *in situ* measurements have been based on the as-  
 93 sumption that local observations are representative of a much  
 94 larger spatial extent (i.e., the size of a microwave pixel). In the  
 95 heterogeneous case where this assumption does not hold, up-  
 96 scaling approaches [12], [13] have been developed to relate the  
 97 available ground observations to satellite scale soil moisture.  
 98 Such approaches are very useful over sites which have been  
 99 monitored for a long time and where extensive measurements  
 100 have been made over a range of spatial scales. However, aggrega-  
 101 tion rules are difficult to build over sites which have been set  
 102 up recently, or where no extensive field campaigns have been  
 103 undertaken.

104 This study develops a methodology to facilitate the cali-  
 105 bration and validation of SMOS data using localized ground  
 106 measurements, such as those collected during AACES. The  
 107 methodology combines upscaling (aggregation) and downscal-  
 108 ing (disaggregation) approaches to make remote sensing and  
 109 *in situ* observations match at an intermediate spatial resolution  
 110 of 1 km. The key step in the procedure is a disaggregation  
 111 algorithm of passive microwave soil moisture using kilometric  
 112 optical data [14]–[16]. Disaggregating SMOS soil moisture can  
 113 solve the disparity of spatial scales between satellite and *in situ*  
 114 observations. However, the validation of spaceborne data by  
 115 means of a disaggregation approach requires the uncertainties  
 116 and potential error sources in downscaled data to be assessed.  
 117 Generally speaking, disaggregation is a compromise between  
 118 downscaling resolution and accuracy. The higher downscaling  
 119 resolution, the more disaggregated values are spatially repre-  
 120 sentative of ground observations, but typically have a lower  
 121 accuracy and vice versa [17]. In this context, a disaggrega-  
 122 tion algorithm named Disaggregation based on Physical And  
 123 Theoretical scale Change (DisPATCH) is applied to 40-km  
 124 resolution SMOS soil moisture over the AACES area using 1-  
 125 km resolution Moderate resolution Imaging Spectroradiometer  
 126 (MODIS) data. The objective is to test DisPATCH under various  
 127 surface and atmospheric conditions. Specifically, the impact  
 128 of climatic (evaporative demand), meteorologic (presence of  
 129 clouds), and vegetation (cover and water status) conditions on  
 130 1-km resolution disaggregated soil moisture is evaluated both  
 131 qualitatively by visual assessment of disaggregation images and  
 132 quantitatively by comparing DisPATCH output with AACES  
 133 intensive ground measurements.

134 The AACES, SMOS, and MODIS data used in this study  
 135 are first described. Next, the disaggregation methodology is  
 136 presented followed by a step-by-step description of the Dis-  
 137 PATCH algorithm. Results of the comparison between disag-  
 138 ggregated SMOS soil moisture and *in situ* measurements are  
 139 then reported. To test DisPATCH under various surface and  
 140 atmospheric conditions, the algorithm is run during AACES-1

and AACES-2 in different modes, by including (or not) a 141  
 correction for vegetation and atmospheric effects. Finally, some 142  
 perspectives in the use of DisPATCH for validating SMOS data 143  
 using ground-based sampling are given. 144

## II. DATA COLLECTION AND PREPROCESSING 145

The AACES experiments were planned to provide ground 146  
 and airborne soil moisture data over an area of approximately 147  
 500 km by 100 km during the two main seasons in the 148  
 Murrumbidgee river catchment, in southeastern Australia. The 149  
 first AACES campaign (AACES-1) was undertaken in summer 150  
 2010 from January 18 to February 21, and the second campaign 151  
 (AACES-2) was undertaken in the following Austral winter 152  
 from September 11 to September 24 [11]. Fig. 1 presents the 153  
 study area including the 20 5 km by 2 km ground sampling 154  
 focus areas. The background image is the MODIS 250-m res- 155  
 olution 16-day normalized difference vegetation index (NDVI) 156  
 product of February 2, 2010. The climate of the Murrumbidgee 157  
 catchment area ranges from semi-arid in the west to alpine in 158  
 the east, with a strong rainfall and potential evapotranspiration 159  
 gradient in the west-east direction. Land use is extensive graz- 160  
 ing in the west, cropping in the center, and mostly grazing/forest 161  
 in the east (refer to [11] for a detailed account of AACES). 162

### A. HDAS 163

During both AACES-1 and AACES-2, a spatially enabled 164  
 platform (Hydraprobe Data Acquisition System, HDAS) was 165  
 used to collect extensive measurements of near-surface soil 166  
 moisture. HDAS is a handheld system combining a soil dielec- 167  
 tric sensor (Hydraprobe) and a pocket PC with GPS receiver, 168  
 allowing for direct storage of location and measurement within 169  
 the GIS software. HDAS measurements were calibrated using 170  
 the approach presented in [18] with a root mean square error 171  
 of point estimate of about  $0.03 \text{ m}^3/\text{m}^3$ . The sampling coverage 172  
 was two 5 km by 2 km farms per day during AACES-1 and one 173  
 5 km by 2 km farm per day during AACES-2. Within each farm, 174  
 a total of six adjacent 5 km long transects separated by 330 m 175  
 were walked to cover each area of  $10 \text{ km}^2$ , and three separate 176  
 HDAS measurements were made along transects every 50 m. 177

In this study, HDAS soil moisture data are aggregated at 178  
 1-km resolution by averaging all measurements made within 179  
 each pixel of the MODIS resolution grid. Out of concern for 180  
 spatial representativeness of *in situ* observations, only the 1-km 181  
 pixels whose ground sampling covers more than two third of 182  
 its surface area are kept for comparison with disaggregation 183  
 results. The 1-km average of HDAS measurements is denoted 184  
 $\langle \text{SM}_{\text{HDAS}} \rangle$  and the standard deviation of *in situ* measurements 185  
 (denoted  $\sigma_{\text{HDAS}}$ ) computed to estimate the subpixel variability 186  
 at 1-km resolution. 187

### B. SMOS 188

The version-4 SMOS level-2 soil moisture product is used. 189  
 This product (released on March 24, 2011) was produced from 190  
 the reprocessed level 1C data, and the version-4 level-2 soil 191  
 moisture algorithm. SMOS has a 6 am (ascending) and 6 pm 192

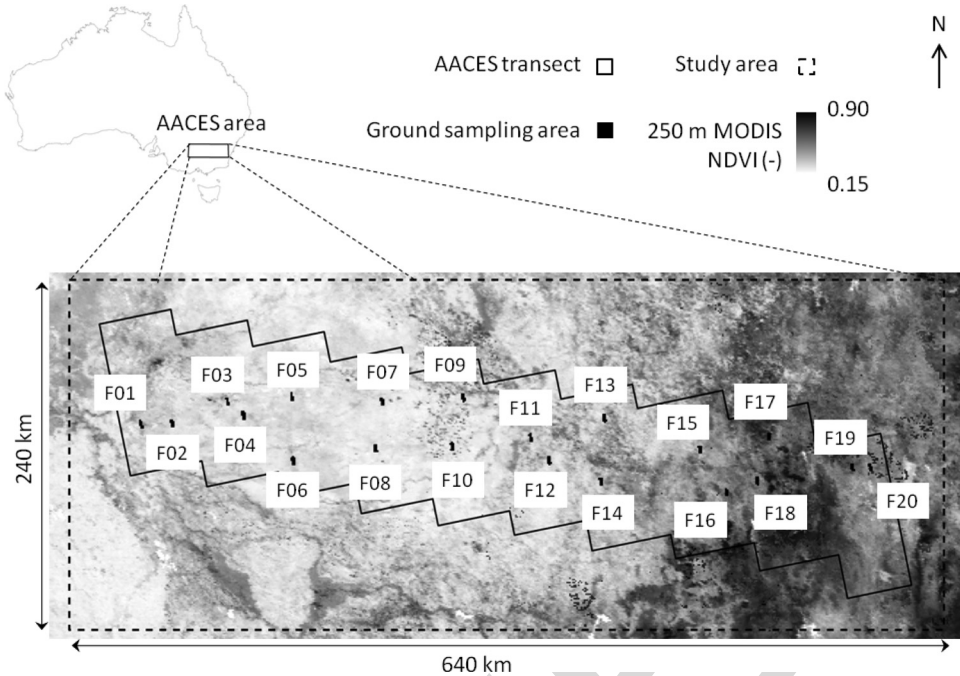


Fig. 1. Overview of the study area. During AACES, ten 100 km by 50 km patches were overflowed by an airborne L-band radiometer. Within each patch, two 5 km by 2 km subareas were sampled to collect spatial soil moisture measurements. In this study, DisPATCH is run over a 640 by 240 km area including the whole AACES area, and disaggregation results are evaluated over the ground sampling areas.

193 (descending) equator crossing time. The sampling grid of the  
 194 SMOS level-2 soil moisture product is called DGG or discrete  
 195 global grid [19], [20] and has a node separation of about  
 196 15 km. The DGG provides a discretization that is higher than  
 197 the SMOS natural pixel size, which is 40 km on average,  
 198 ranging from 30 km at boresight to 90 km at high incidence  
 199 angles. In this study, the disaggregation procedure takes advan-  
 200 tage of the oversampling of SMOS data to potentially reduce  
 201 (and provide an estimate of) random errors in disaggregated  
 202 SMOS data. Instead of using a single snapshot SMOS im-  
 203 age, DisPATCH uses four (overlapping) independent snapshots,  
 204 which are generated by: 1) sliding a 40-km resolution grid; and  
 205 2) extracting the DGG nodes approximately centered on each  
 206 40 km pixel. The extraction of SMOS DGG nodes is presented  
 207 in [21]. The DGG node(s) that fall(s) near the center of the  
 208 40-km resolution pixels with a  $\pm 10$ -km tolerance are se-  
 209 lected. If more than one DGG is selected, the associated soil  
 210 moisture values are averaged to produce a single value for each  
 211 40-km resolution pixel. The 40-km resolution grid that fits the  
 212 study area corresponds to what is termed here Resampling 1.  
 213 Similarly, Resampling 2, 3, and 4 are performed by sliding the  
 214 40-km resolution grid to coordinates  $(+20 \text{ km}, 0)$ ,  $(0, -20 \text{ km})$ ,  
 215 and  $(+20 \text{ km}, -20 \text{ km})$ , respectively. The four 40-km resolu-  
 216 tion SMOS data sets are then used independently as input to  
 217 DisPATCH.

### 218 C. MODIS

219 The MODIS data used in this paper are composed of:

- 220 • Version-5 MODIS/Terra land surface temperature and  
 221 emissivity daily level-3 global 1-km grid product  
 222 (MOD11A1) and version-5 MODIS/Aqua land surface

temperature and emissivity daily level-3 global 1-km grid 223  
 product (MYD11A1). The land surface temperature data 224  
 set is the main component of DisPATCH. It is used to 225  
 estimate 1-km resolution soil evaporative efficiency at 226  
 10 am (Terra data) and 1 pm (Aqua data) [22]. 227

- Version-5 MODIS/Terra vegetation indices 16-day level-3 228  
 global 1-km grid product (MOD13A2). The NDVI data set 229  
 is used in DisPATCH to estimate the fractional vegetation 230  
 cover at 1-km resolution [23]. 231
- Version-5 MODIS/Terra+Aqua albedo 16-day level-3 232  
 global 1-km grid product (MCD43B3). The surface albedo 233  
 data set is used in DisPATCH to estimate the vegetation 234  
 temperature at maximum water stress from the space land 235  
 surface temperature albedo [24]. The MCD43B3 product 236  
 provides 1-km data describing both directional hemispher- 237  
 ical reflectance (black-sky albedo) at local solar noon 238  
 and bihemispherical reflectance (white-sky albedo). In this 239  
 study, surface albedo refers to the MODIS shortwave white 240  
 sky albedo. 241
- MODIS/Terra level-1B calibrated radiances swath 1-km 242  
 grid product (MOD021KM) and MODIS/Aqua level- 243  
 1B calibrated radiances swath 1-km grid product 244  
 (MYD021KM). The radiance data set is used to derive 245  
 a land surface temperature data set that differs from the 246  
 official MOD11A1 and MYD11A1 products with respect 247  
 to atmospheric correction. 248

Products MOD11A1, MYD11A1, MOD13A2, and 249  
 MCD43B3 were downloaded through the NASA Warehouse 250  
 Inventory Search Tool (WIST <http://wist.echo.nasa.gov/>) and 251  
 products MOD021KM and MYD021KM were downloaded 252  
 through the NASA Level 1 and Atmosphere Archive and Dis- 253  
 tribution System (LAADS <http://ladsweb.nascom.nasa.gov>). 254

TABLE I  
SCALE AND OFFSET VALUES USED TO CONVERT TERRA (AND AQUA)  
MODIS RADIANCE DATA TO PHYSICAL RADIANCE  
VALUES OVER THE AACES AREA

Thermal band	Scale ( $\text{W m}^{-2} \text{ sr}^{-1}$ )	Offset (-)
31	$8.4002 \cdot 10^{-4}$ ( $6.5081 \cdot 10^{-4}$ )	1577 (2036)
32	$7.2970 \cdot 10^{-4}$ ( $5.7100 \cdot 10^{-4}$ )	1658 (2119)

255 All products were projected in UTM 55 South with a sampling  
256 interval of 1000 m using the MODIS reprojection tool.

257 The level-1B calibrated radiance data ( $R_{31}$  and  $R_{32}$  for bands  
258 31 and 32, respectively) were converted from digital number  
259 (DN) to radiance in  $\text{W m}^{-2} \text{ sr}^{-1}$  using the radiance scales and  
260 offsets provided with each MODIS granule as listed in Table I

$$R_\lambda = \text{Scale}_\lambda \times (\text{DN}_\lambda - \text{Offset}_\lambda) \quad (1)$$

261 The radiance values were then converted to brightness temper-  
262 ature in K using the inverse of the Planck function [25]

$$Tb_\lambda = \frac{c_2}{\lambda \ln \left( 1 + \frac{c_1}{R_\lambda \lambda^5} \right)} \quad (2)$$

263 with  $c_1 = 1.19107 \times 10^8 \mu\text{m}^5 \text{ W m}^{-2} \text{ sr}^{-1}$  and  $c_2 =$   
264  $1.43883 \times 10^4 \mu\text{m K}$ , for center wavelength of the given band  
265 (11.0186  $\mu\text{m}$  and 12.0325  $\mu\text{m}$  for 31 and 32 band, respectively).

#### 266 D. Overlapping HDAS, SMOS, and MODIS Data and 267 Generating an Input Data Set

268 As indicated in Table II, HDAS soil moisture, SMOS soil  
269 moisture, and cloud-free MODIS land surface temperature data  
270 have overlapped on five days during AACES-1 (on January  
271 28 and 30 and February 15, 18, and 20) and on five days  
272 during AACES-2 (on September 11, 13, 21, 22, and 24). On  
273 each sampling day, two farms were sampled during AACES-1  
274 (except on February 18 when three farms were sampled), and  
275 one farm was sampled during AACES-2, so that disaggregation  
276 results can be evaluated for ten date-farm units during AACES-  
277 1 and five date-farm units during AACES-2.

278 DisPATCh is applied to an input ensemble composed of the  
279 different combinations of available SMOS (ascending orbit at  
280 6 am and/or descending orbit at 6 pm) and MODIS (onboard  
281 Terra platform at 10 am and/or Aqua platform at 1 pm) data. To  
282 increase the quantity of input data sets, the MODIS data col-  
283 lected on the day before and the day after the SMOS overpass  
284 date are also included. For SMOS data on day of year (DoY)  
285 51, the clear sky MODIS data collected on DoY 54 are used.  
286 Note that one implicitly assumes that no rainfall occurs between  
287 MODIS and SMOS overpasses, and that the spatial variability  
288 captured by MODIS is relatively similar to the actual variabil-  
289 ity of surface soil moisture at the time of SMOS overpass.  
290 Moreover, the SMOS data oversampling is used to generate  
291 four (overlapping) 40-km resolution SMOS grids on which  
292 DisPATCh is run independently, thus increasing the number  
293 of downscaled data that could be used in the validation. It is  
294 reminded that the spacing (about 15 km) between neighboring  
295 SMOS DGG nodes is smaller than the SMOS resolution (about

40 km). By combining the four SMOS grids, the two potential 296 SMOS data sets (two orbits in one day) and the six potential 297 MODIS data sets (three days including two overpasses each), 298 the maximum number of input data sets is 48. The generation 299 of input data sets is shown in Fig. 2 and the number of daily 300 input data sets is indicated for each date-farm unit in Table II. 301

### III. DISAGGREGATION ALGORITHM

DisPATCh converts 1-km resolution MODIS-derived soil 303 temperature fields into 1-km resolution surface soil moisture 304 fields given a semi-empirical soil evaporative efficiency model 305 [26] and a first-order Taylor series expansion around the 306 40-km resolution SMOS observation. DisPATCh is an im- 307 proved version of the algorithms in [16] and [27], and mainly 308 differs with regard to the representation of the vegetation water 309 status. In previous versions [16], [27], the soil temperature was 310 derived from MODIS land surface temperature by assuming 311 that vegetation was unstressed so that vegetation temperature 312 was uniformly set to the minimum surface temperature ob- 313 served within the SMOS pixel. In this study, the approach in 314 [28] is implemented to take into account vegetation water status 315 in the estimation of soil temperature. 316

#### A. Disaggregation Methodology

The disaggregation procedure decouples the soil evaporation 318 from the 0–5 cm soil layer and the vegetation transpiration 319 from the root-zone soil layer by separating MODIS surface 320 temperature into its soil and vegetation components as in the 321 triangle or trapezoidal method [28], [29]. MODIS-derived soil 322 temperature is then used to estimate soil evaporative efficiency, 323 which is known to be relatively constant during the day on clear 324 sky conditions. MODIS-derived soil evaporative efficiency is 325 finally used as a proxy for surface (0–5 cm) soil moisture 326 variability within the SMOS pixel. The link between surface 327 soil moisture and soil evaporative efficiency at different scales 328 is ensured by a downscaling relationship and a soil evapo- 329 rative efficiency model, as described below in more detail. 330 The originality of DisPATCh relies on a dynamical land cover 331 classification (based on the hourglass approach in [28]) that 332 takes into account the subpixel variability of the sensitivity of 333 soil evaporative efficiency to surface soil moisture. 334

1) Downscaling Relationship: The downscaling relation- 335 ship can be written as 336

$$\text{SM}_{1 \text{ km}} = \text{SM}_{\text{SMOS}} + \frac{\partial \text{SM}_{\text{mod}}}{\partial \text{SEE}} \times (\text{SEE}_{\text{MODIS}, 1 \text{ km}} - \langle \text{SEE}_{\text{MODIS}, 1 \text{ km}} \rangle_{40 \text{ km}}) \quad (3)$$

with  $\text{SM}_{\text{SMOS}}$  being the SMOS soil moisture (for clarity, 337 the variables defined at SMOS scale are written in bold), 338  $\text{SEE}_{\text{MODIS}}$  the MODIS-derived soil evaporative efficiency (ra- 339 tio of actual to potential evaporation),  $\langle \text{SEE}_{\text{MODIS}} \rangle_{40 \text{ km}}$  its 340 average within a SMOS pixel and  $\partial \text{SM}_{\text{mod}} / \partial \text{SEE}$  the partial 341 derivative evaluated at SMOS scale of soil moisture with re- 342 spect to soil evaporative efficiency. Note that the linearity of (3) 343 implies that a possible bias in SMOS data would produce the 344

TABLE II  
LIST OF OVERLAPPING HDAS, SMOS, AND MODIS (MOD11A1 AND MYD11A1) DATA DURING AACES-1 AND AACES-2. ONLY THE SMOS DATA COLLECTED ON THE SAME DAY AS GROUND SAMPLING HAVE BEEN CONSIDERED. THE MODIS DATA CONSIDERED AS INPUT TO DisPATCH HAVE BEEN COLLECTED WITHIN PLUS OR MINUS ONE DAY EITHER SIDE THE GROUND SAMPLING (AND SMOS OVERPASS) DATE. ON EACH SAMPLING DATE, THE RESULTANT NUMBER OF INPUT DATA SETS TO DisPATCH IS ALSO INDICATED

Experiment	Sampling date	DoY	Farm	SMOS overpass time	Cloud free MODIS data (DoY)	Number of input data sets to DisPATCH
AACES-1	28 January	28	F05	6 am	Terra (27,29) & Aqua (29)	3
	30 January	30	F07	6 am	Terra (29,30) & Aqua (29)	12
	,	,	F08	6 am	Terra (29,30) & Aqua (29)	9-12
	15 February	46	F15	6 am & 6 pm	Terra (46) & Aqua (47)	8-14
	,	,	F16	6 am & 6 pm	Terra (46) & Aqua (47)	8-10
	18 February	49	F17	6 am & 6 pm	Terra (48,50) & Aqua (48,49,50)	30-38
	,	,	F18	6 am & 6 pm	Terra (48,50) & Aqua (48,49,50)	24-30
	,	,	F20	6 am & 6 pm	Terra (48,50) & Aqua (48,49,50)	34-40
	20 February	51	F19	6 am & 6 pm	Terra (54) & Aqua (54)	6-8
	,	,	F20	6 am & 6 pm	Terra (54) & Aqua (54)	16
AACES-2	11 September	254	F09	6 am & 6 pm	Terra (253,254) & Aqua (254)	6-14
	13 September	256	F07	6 am & 6 pm	Terra (256)	8
	21 September	264	F13	6 am & 6 pm	Terra (263) & Aqua (264)	16
	22 September	265	F15	6 am & 6 pm	Terra (265) & Aqua (264,266)	16
	24 September	267	F09	6 am & 6 pm	Terra (267) & Aqua (266,267,268)	24-32

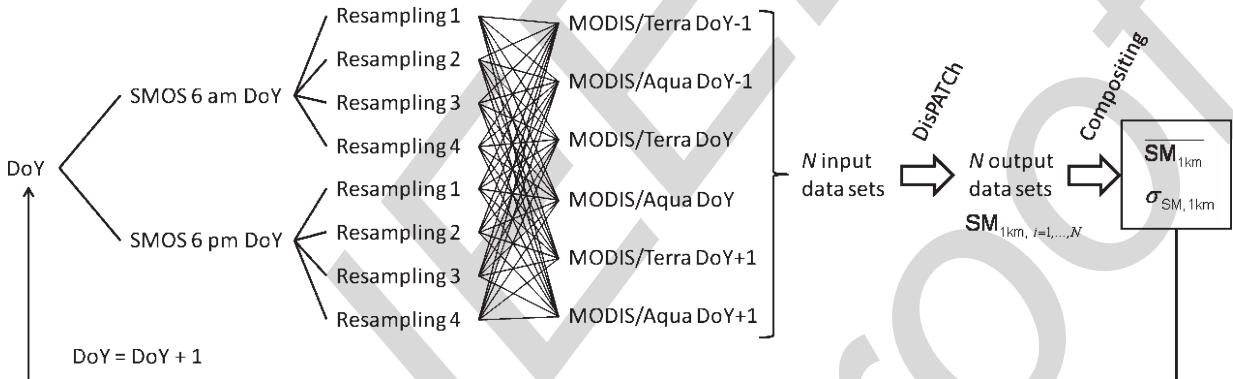


Fig. 2. Schematic diagram presenting the combination of SMOS and MODIS to generate an ensemble of input data to DisPATCH. The output data are composited at 1-km resolution by computing the average ( $\overline{SM}_{1\text{ km}}$ ) and standard deviation ( $\sigma_{SM, 1\text{ km}}$ ) of disaggregated SMOS soil moisture.

345 same bias in disaggregated data [30]. Consequently, although 346 the possible presence of a bias in SMOS data limits the accuracy 347 in the disaggregated soil moisture, it is not a limiting factor to 348 the applicability of DisPATCH. MODIS derived soil evaporative 349 efficiency is expressed as a linear function of soil temperature

$$SEE_{\text{MODIS}, 1\text{ km}} = \frac{T_{s,\text{max}} - T_{s,1\text{ km}}}{T_{s,\text{max}} - T_{s,\text{min}}} \quad (4)$$

350 with  $T_s$  being the MODIS-derived soil skin temperature, 351  $T_{s,\text{max}}$  the soil skin temperature at  $SEE = 0$  and  $T_{s,\text{min}}$  352 the soil skin temperature at  $SEE = 1$ . The linearity of the 353 relationship between soil evaporative efficiency and surface 354 soil temperature was verified using the physically based dual 355 source energy budget model in [31] using a synthetic data set 356 composed of a range of surface soil moisture values and differ- 357 ent atmospheric conditions (results not shown). End-members 358  $T_{s,\text{min}}$  and  $T_{s,\text{max}}$  are estimated from the polygons obtained

by plotting MODIS surface temperature against MODIS NDVI 359 and MODIS albedo as in [24]. Derivation of soil temperature is 360 based on a linear decomposition of the surface temperature into 361 its soil and vegetation components as a good approximation of 362 the relationship with fourth power for temperatures [32], [33] 363 and consistent with the triangle method. MODIS-derived soil 364 skin temperature is expressed as 365

$$T_{s,1\text{ km}} = \frac{T_{\text{MODIS}} - f_{v,1\text{ km}} T_{v,1\text{ km}}}{1 - f_{v,1\text{ km}}} \quad (5)$$

with  $T_{\text{MODIS}}$  being the 1-km resolution MODIS land sur- 366 face temperature,  $f_v$  the MODIS-derived fractional vegetation 367 cover, and  $T_v$  the vegetation temperature. In this study, vegeta- 368 tion temperature is estimated using the approach proposed by 369 [28]. In (5), fractional vegetation cover is written as 370

$$f_{v,1\text{ km}} = \frac{\text{NDVI}_{\text{MODIS}} - \text{NDVI}_s}{\text{NDVI}_v - \text{NDVI}_s} \quad (6)$$

371 with  $\text{NDVI}_{\text{MODIS}}$  being the 1-km resolution MODIS NDVI,  
 372  $\text{NDVI}_s$  the NDVI corresponding to bare soil, and  $\text{NDVI}_v$  the  
 373 NDVI corresponding to full-cover vegetation. Minimum and  
 374 maximum NDVI values are set to 0.15 and 0.90, respectively.

375 In [16], the accuracy and robustness of the disaggregation  
 376 methodology were tested using three different formulations of  
 377 soil evaporative efficiency [26], [34], [35]. Results based on the  
 378 NAFE'06 data set [36], which was collected over a 60 km by  
 379 40 km area in the AACES area, indicated that the model in  
 380 [26] was better adapted for conditions where soil properties are  
 381 unknown at high resolution. Consequently, the partial derivative  
 382 in (3) is computed using the soil evaporative efficiency model  
 383 in [26]

$$\text{SEE}_{\text{mod}} = \frac{1}{2} - \frac{1}{2} \cos(\pi \cdot \text{SM}/\text{SM}_p) \quad (7)$$

384 with  $\text{SM}_p$  being a soil parameter (in soil moisture unit). In  
 385 [26],  $\text{SM}_p$  was set to the soil moisture at field capacity. In  
 386 DisPATCH,  $\text{SM}_p$  is retrieved at 40-km resolution from SMOS  
 387 and aggregated MODIS data [16]. By inverting (7), one obtains

$$\text{SM}_{\text{mod}} = \frac{\text{SM}_p}{\pi} \cos^{-1}(1 - 2 \text{SEE}) \quad (8)$$

388 2) *Vegetation Temperature*: Vegetation temperature in (5) is  
 389 estimated at 1-km resolution with the “hourglass” approach in  
 390 [28]. By plotting the diagonals in the quadrilateral in Fig. 3,  
 391 four areas are distinguished in the space defined by surface  
 392 temperature and fractional vegetation cover. In zone A, land  
 393 surface temperature is mainly controlled by soil evaporation  
 394 leading to optimal sensitivity to surface soil moisture. In zone  
 395 D, land surface temperature is mainly controlled by vegetation  
 396 transpiration with no sensitivity to surface soil moisture. In  
 397 zones B and C, land surface temperature is controlled by both  
 398 soil evaporation and vegetation transpiration with intermediate  
 399 (average) sensitivity to surface soil moisture. Based on this un-  
 400 derstanding, vegetation temperature is estimated in a different  
 401 manner in each zone.

402 For a given data point located in Zone A, vegetation temper-  
 403 ature is

$$T_{v,1 \text{ km}} = (\text{T}_{v,\text{min}} + \text{T}_{v,\text{max}})/2 \quad (9)$$

404 with  $\text{T}_{v,\text{min}}$  and  $\text{T}_{v,\text{max}}$  being the vegetation temperature  
 405 at minimum and maximum water stress, respectively. End-  
 406 members  $\text{T}_{v,\text{min}}$  and  $\text{T}_{v,\text{max}}$  are estimated from the poly-  
 407 gons obtained by plotting MODIS surface temperature against  
 408 MODIS NDVI and MODIS albedo as in [24].

409 For a given data point located in Zone B, vegetation temper-  
 410 ature is

$$T_{v,1 \text{ km}} = (T_{v,\text{min},1 \text{ km}} + \text{T}_{v,\text{max}})/2 \quad (10)$$

411 with  $T_{v,\text{min},1 \text{ km}}$  being the vegetation temperature associated  
 412 with  $\text{SEE} = 0$  ( $\text{T}_s = \text{T}_{s,\text{max}}$ ).

413 For a given data point located in Zone C, vegetation temper-  
 414 ature is

$$T_{v,1 \text{ km}} = (\text{T}_{v,\text{min}} + T_{v,\text{max},1 \text{ km}})/2 \quad (11)$$

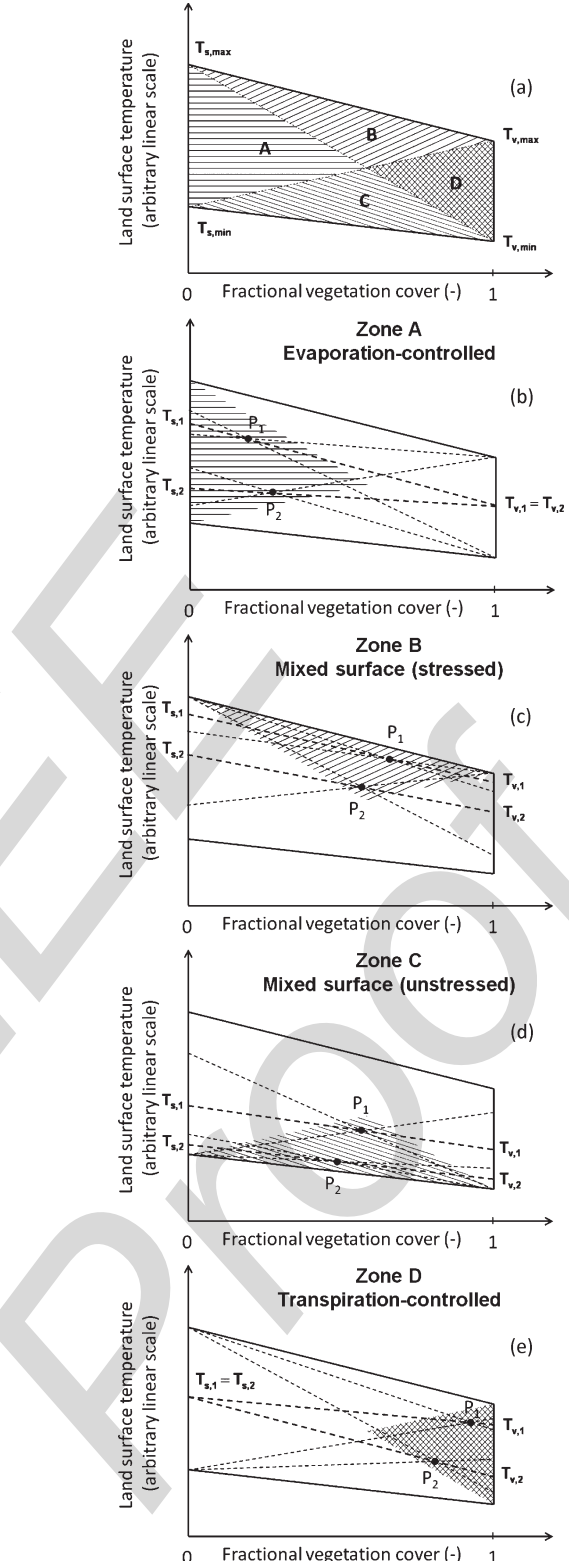


Fig. 3. Polygon defined in the land surface temperature-fractional vegetation cover space contains four distinct zones A, B, C, and D. In Zone A (soil-dominated area), the estimated vegetation temperature is constant leading to optimal sensitivity of estimated soil temperature to surface soil moisture. In Zone D, the estimated soil temperature is constant with no sensitivity to surface soil moisture. In Zone B and C (mixed surface), surface temperature is both controlled by soil evaporation and vegetation transpiration with intermediate (average) sensitivity of estimated soil temperature to surface soil moisture. DisPATCH can be run in the Zone A+B+C mode or in the Zone A only mode.

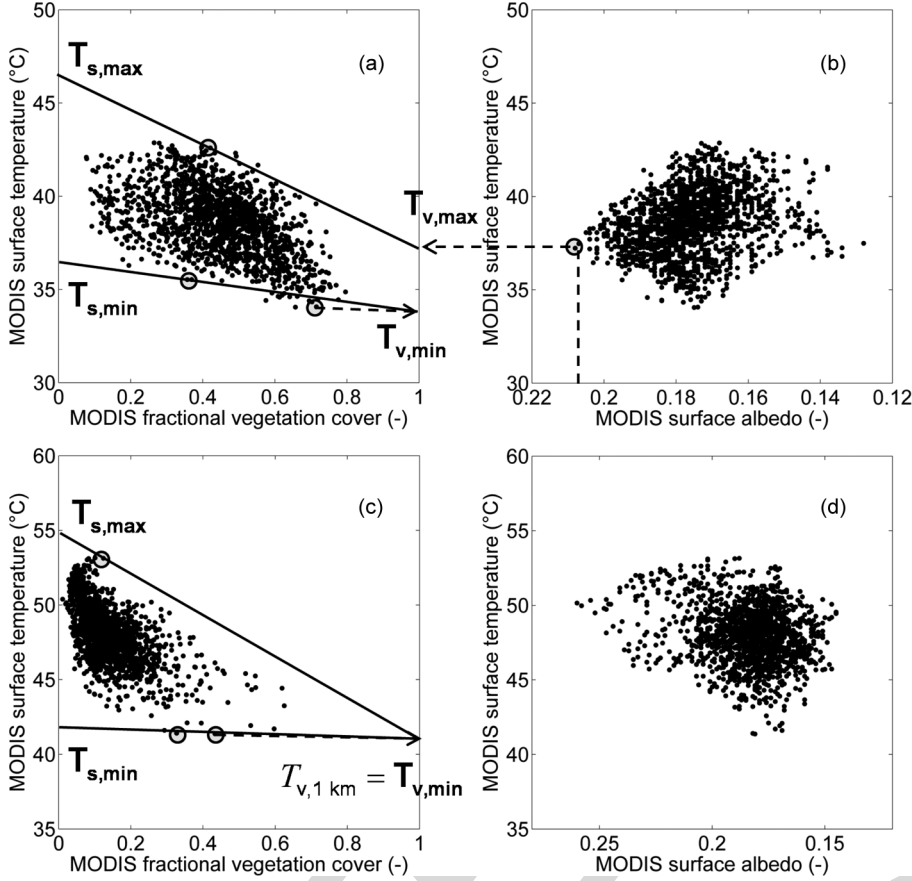


Fig. 4. Temperature end-members  $T_{s,\min}$ ,  $T_{s,\max}$ ,  $T_{v,\min}$  and  $T_{v,\max}$  are estimated from the surface temperature-fractional vegetation cover space and the surface temperature-surface albedo space within two given SMOS pixels. In (b), the pixel corresponding to the largest MODIS albedo has a fractional vegetation cover larger than 0.5, so that  $T_{v,\max}$  is set to its surface temperature. In (d), the pixel corresponding to the largest MODIS albedo has a fractional vegetation cover lower than 0.5, so that  $T_{v,\max}$  is set to  $T_{v,\min}$ .

415 with  $T_{v,\max,1 \text{ km}}$  being the vegetation temperature associated  
 416 with SEE = 1 ( $T_s = T_{s,\min}$ ).

417 For a given data point located in Zone D, vegetation temper-  
 418 ature is

$$T_{v,1 \text{ km}} = (T_{v,\min,1 \text{ km}} + T_{s,\max,1 \text{ km}})/2 \quad (12)$$

419 3) End-Members: End-members  $T_{s,\min}$ ,  $T_{s,\max}$ ,  $T_{v,\min}$   
 420 and  $T_{v,\max}$  are estimated by combining the spatial information  
 421 provided by the surface temperature-fractional vegetation cover  
 422 space and the surface temperature-albedo space plotted using  
 423 MODIS data collected in a 40-km resolution SMOS pixel. An  
 424 illustration is provided in Fig. 4 for two given SMOS pixels.

- 425 •  $T_{v,\min}$ : the vegetation temperature at minimum vegeta-  
 426 tion water stress is set to the minimum MODIS surface  
 427 temperature in the SMOS pixel [see Fig. 4(a) and (c)].
- 428 •  $T_{v,\max}$ : the vegetation temperature at maximum vegeta-  
 429 tion water stress is set to the MODIS surface temperature  
 430 of the pixel with the maximum value of MODIS albedo in  
 431 the SMOS pixel [see Fig. 4(b)]. If the fractional vegetation  
 432 cover of that pixel is lower than 0.5 [see Fig. 4(d)], the vege-  
 433 tation temperature at maximum vegetation water stress  
 434 is alternatively set to  $T_{v,\min}$ , meaning that vegetation is  
 435 unstressed within the SMOS pixel. The condition based  
 436 on fractional vegetation cover is lower than 0.5 aims to  
 437 increase the robustness of the determination approach of

438  $T_{v,\max}$ , particularly in the SMOS pixels where all surface  
 439 conditions are not met.

- 440 •  $T_{s,\min}$ : the soil temperature at SEE = 0 is extrapolated  
 441 along the wet soil edge at  $f_v = 0$ . The wet soil edge  
 442 is defined as the line passing through  $(1, T_{v,\min})$  and  
 443 through the data point such that all the data points with  
 444  $f_v < 0.5$  are located above the wet soil edge [see Fig. 4(a)  
 445 and (c)].
- 446 •  $T_{s,\max}$ : the soil temperature at SEE = 0 is extrapolated  
 447 along the dry soil edge at  $f_v = 0$ . The dry soil edge  
 448 is defined as the line passing through  $(1, T_{v,\max})$  and  
 449 through the data point such that all the data points with  
 450  $f_v < 0.5$  are located below the dry soil edge [see Fig. 4(a)  
 451 and (c)].

#### B. Atmospheric Correction

In MOD11A1 and MYD11A1 products, the land surface 453 temperature is derived from MODIS thermal radiances using 454 the split window algorithm [37]

$$T_{\text{MODIS}} = C + \left( A_1 + A_2 \frac{1 - \epsilon}{\epsilon} + A_3 \frac{\Delta\epsilon}{\epsilon^2} \right) \frac{Tb_{31} + Tb_{32}}{2} \\ + \left( B_1 + B_2 \frac{1 - \epsilon}{\epsilon} + B_3 \frac{\Delta\epsilon}{\epsilon^2} \right) \frac{Tb_{31} - Tb_{32}}{2} \quad (13)$$

456 with  $Tb_{31}$  and  $Tb_{32}$  being the brightness temperatures measured in the MODIS bands 31 and 32, respectively,  $\epsilon_{31}$  and  $\epsilon_{32}$  the surface emissivities estimated in the respective bands, and  $A_1, A_2, A_3, B_1, B_2, B_3$ , and  $C$  regression coefficients. These coefficients are available during algorithm execution via a look up table stratified by subranges of near surface air temperature and total column water vapor. These input field are obtained at 463 a 5-km resolution from the MODIS07\_L2 product.

464 Given that regression coefficients in (13) are provided at 465 5-km resolution, the atmospheric corrections on the MODIS 466 land surface temperature product are actually made at 5-km 467 resolution. To test whether atmospheric corrections on MODIS 468 temperature have an impact on disaggregation results, a different 469 procedure is proposed to obtain another temperature data set whose atmospheric corrections are operated at the scale 471 of a SMOS pixel, i.e., at 40-km resolution (instead of 5-km 472 resolution for the official MODIS temperature product). The 473 approach is to normalize the mean MODIS radiance-derived 474 brightness temperature at the SMOS resolution. Normalization 475 is done by adjusting the minimum and maximum mean MODIS 476 brightness temperature to the minimum and maximum value 477 of the official MODIS land surface temperature product within 478 the SMOS pixel, respectively. The new temperature noted 479  $T_{\text{MODIS}}^{\text{unif. corr.}}$  (uniform atmospheric corrections) is written

$$T_{\text{MODIS}}^{\text{unif. corr.}} = T_{\text{MODIS,min}} + \frac{(T_{\text{MODIS,max}} - T_{\text{MODIS,min}})}{\frac{Tb_{31} + Tb_{32} - \text{Min}(Tb_{31} + Tb_{32})}{\text{Max}(Tb_{31} + Tb_{32}) - \text{Min}(Tb_{31} + Tb_{32})}} \quad (14)$$

480 with  $T_{\text{MODIS,min}}$  and  $T_{\text{MODIS,max}}$  being the minimum and 481 maximum MODIS land surface temperature within the SMOS 482 pixel, and  $\text{Min}()$  and  $\text{Max}()$  the function that returns the 483 minimum and maximum value within the SMOS pixel, respectively. 484 Note that the underlying assumptions of (14) are:

- 485 • near surface air temperature and column water vapor vary 486 at scales larger than 40 km (size of a SMOS pixel).
- 487 • surface emissivity is close to 1.

### 488 C. Algorithm

489 The steps used in applying DisPATCH include: 1) selecting 490 the SMOS pixels with at least 90% (clear sky) MODIS 491 retrieved land surface temperature coverage; 2) computing 492 soil evaporative efficiency over nominal MODIS pixels with 493 (4); 3) estimating soil evaporative efficiency over non-nominal 494 MODIS pixels; 4) retrieving parameter  $SM_p$ ; 5) applying the 495 downscaling relationship of (3); 6) correcting disaggregated 496 soil moisture by the SMOS pixel weighting function; and 7) 497 compositing on a daily basis the disaggregation output ensemble 498 [21]. The input and output data and their link within 499 DisPATCH are summarized in Fig. 5.

500 1) *Selecting Clear Sky SMOS Pixels*: A threshold of 90% 501 cloud-free MODIS coverage is used to select the SMOS pixels 502 to be disaggregated. In the official MODIS land surface 503 temperature product (MOD11A1 for Terra and MYD11A1 for 504 Aqua), the data affected by the presence of clouds are already 505 masked. Hence, selection of the 90% clear sky SMOS pixels is

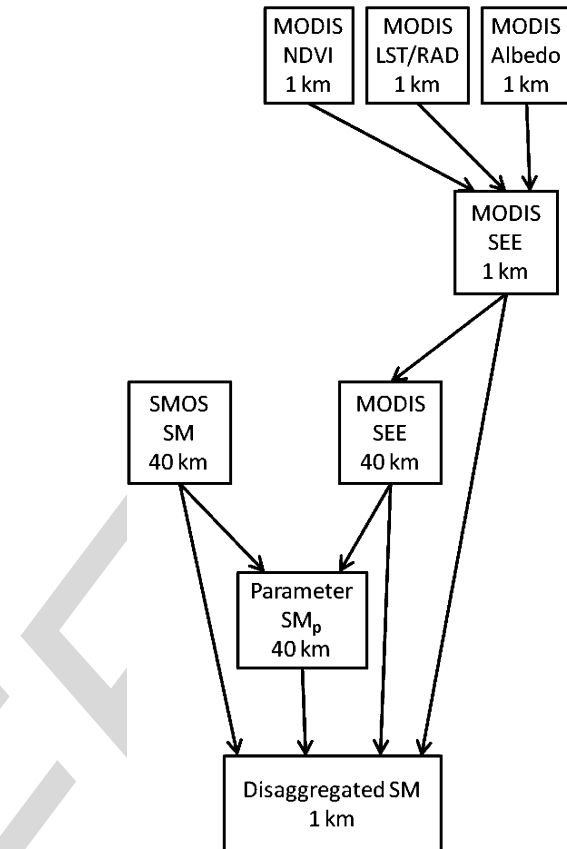


Fig. 5. Schematic diagram presenting the input and output data of DisPATCH.

directly based on the MODIS land surface temperature product 506 masking.

2) *Non-Nominal Pixels*: Nominal MODIS pixels are defined as the 1-km resolution pixels that do not include open water and where land surface temperature is actually retrieved. Open water pixels are flagged in the algorithm when MODIS NDVI retrievals yield negative values. The soil evaporative efficiency of open water pixels is set to 1. The emerged pixels where land surface temperature is not retrieved (due to the presence of some clouds within the SMOS pixel) are processed as pixels with mean surface conditions. In practice, the soil evaporative efficiency of cloudy pixels (which represent less than 10% of the surface area within the SMOS pixel) is set to the mean soil evaporative efficiency calculated over the clear sky MODIS pixels. Allocating a soil evaporative efficiency value to non-nominal pixels allows DisPATCH to be run over a wider range of SMOS pixels, including those partially covered by clouds. However, non-nominal 1-km resolution pixels are flagged and discarded from the disaggregation output ensemble.

3) *Forested Areas*: In this study, DisPATCH is applied to all the SMOS pixels where the soil moisture retrieval is successful, even those including forest class, as long as the 1 km MODIS pixels are in Zone A, B or C (see Fig. 3). This choice is relevant here because the AACLES extensive data were almost exclusively collected in agricultural areas (cropping/grazing), so forests for this study are not an issue. In the case of a mixed SMOS pixel including a significant fraction of forest, DisPATCH should be applied to the surface area of the dominant

534 class, thus excluding the surface area of the minority land cover  
535 classes.

536 4) *Calibration*: The soil moisture parameter  $\mathbf{SM}_p$  used to  
537 compute  $\partial\mathbf{SM}_{\text{mod}}/\partial\text{SEE}$  in (3) is estimated by inverting the  
538 SEE model in (7) at SMOS resolution

$$\mathbf{SM}_p = \frac{\pi \cdot \mathbf{SM}_{\text{SMOS}}}{\cos^{-1}(1 - 2\langle\text{SEE}_{\text{MODIS}, 1 \text{ km}}\rangle_{40 \text{ km}})} \quad (15)$$

539 A value of  $\mathbf{SM}_p$  is obtained for each SMOS pixel and each  
540 input data set. Note that the main assumption limiting validity  
541 of the calibration approach is the soil evaporative efficiency  
542 model [26] itself. The soil evaporative efficiency model in [26]  
543 was chosen for its simplicity (one parameter) and its ability  
544 to represent the general behavior of soil evaporative efficiency  
545 over the full range of soil moisture: particularly the null deriva-  
546 tive at zero and at maximum soil moisture, and an inflexion  
547 point in between [38]. However, it has some inconsistencies.  
548 In particular, [38] have indicated that 1) potential evaporation  
549 is physically reached at soil saturation and not at field capac-  
550 ity; therefore the model in [26] should be (strictly speaking)  
551 parameterized by the soil moisture at saturation and not by the  
552 soil moisture at field capacity, and 2) soil evaporative efficiency  
553 varies with potential evaporation, meaning that the soil moisture  
554 parameter (set to the soil moisture at field capacity in [26])  
555 should theoretically vary in time with atmospheric evaporative  
556 demand. Consequently, the  $\mathbf{SM}_p$  retrieved from SMOS and  
557 MODIS data using the model in [26] is definitely not the soil  
558 moisture at field capacity as in [26], although it could be in part  
559 related to it. In this study,  $\mathbf{SM}_p$  is therefore considered to be a  
560 fitting parameter self-estimated by DisPATCH.

561 5) *Weighting Function*: A SMOS pixel WEighting Function  
562 (WEF) is used to take into account the impact of soil mois-  
563 ture distribution on the SMOS scale soil moisture as seen by  
564 SMOS radiometer. A centrosymmetric analytical approxima-  
565 tion MEAN\_WEF is provided in [19], [20]

$$\text{MEAN\_WEF}(\rho) = C_{\text{MWEF}2} + \text{WEF}_A \left( \frac{\rho}{C_{\text{MWEF}1}} \cdot \frac{\pi}{C_{\text{WEF}1}} \right) \quad (16)$$

566 with  $\rho$  being the distance from the SMOS pixel center, and  
567  $C_{\text{MWEF}1} = 40 \text{ km}$ ,  $C_{\text{MWEF}2} = 0.027$ ,  $C_{\text{WEF}1} = 73.30$  and

$$\text{WEF}_A(\rho') = \frac{[\text{sinc}(C_{\text{WEF}1} \cdot \rho')]^{C_{\text{WEF}2}}}{1 + C_{\text{WEF}3} \cdot \rho'^{C_{\text{WEF}4}}} \quad (17)$$

568 with  $\rho'$  being the distance in the director cosines coordinates,  
569  $\text{sinc}(x) = \sin(x)/x$ , and  $C_{\text{WEF}2} = 1.4936$ ,  $C_{\text{WEF}3} = 524.5$   
570 and  $C_{\text{WEF}4} = 2.103$ .

571 A correction is applied to disaggregated soil moisture in (3)

$$\begin{aligned} \mathbf{SM}_{1 \text{ km}}^{\text{wef corr.}} &= \mathbf{SM}_{1 \text{ km}} + \frac{\sum \text{MEAN\_WEF}(\rho) \cdot \mathbf{SM}_{1 \text{ km}}(\rho)}{\sum \text{MEAN\_WEF}(\rho)} \\ &\quad - \mathbf{SM}_{\text{SMOS}} \end{aligned} \quad (18)$$

572 with  $\mathbf{SM}_{1 \text{ km}}^{\text{wef corr.}}$  being the WEF-corrected disaggregated  
573 soil moisture. Mathematically speaking, one should replace  
574  $\mathbf{SM}_{\text{SMOS}}$  with  $\sum \text{MEAN\_WEF} \cdot \mathbf{SM}_{1 \text{ km}} / \sum \text{MEAN\_WEF}$   
575 in (3) and (15) and run an iteration loop until convergence

576 of  $\mathbf{SM}_{1 \text{ km}}^{\text{wef corr.}}$  values. However, the impact of the WEF on 577 disaggregated soil moisture is expected to be low so that the 578 simple correction in (18) is considered to be sufficient for the 579 purpose of the study. 579

580 6) *Disaggregation Output*: The downscaling relationship in 580  
581 (3) is applied to each input data set, and the disaggregated soil 581  
582 moisture data ensemble is averaged on each 1-km resolution 582  
583 pixel within the study area. Averaging is a way to reduce 583  
584 random uncertainties in the disaggregation output. In [17], [27], 584  
585 disaggregated soil moisture was averaged in space (aggregated) 585  
586 at the expense of downscaling resolution. Herein, temporal 586  
587 averaging [30] is preferred to keep an optimal downscaling 587  
588 resolution. Note that a condition to average disaggregated soil 588  
589 moisture in time is the availability of thermal infrared data 589  
590 at high temporal frequency. Another significant advantage of 590  
591 applying DisPATCH to an input ensemble is to provide an 591  
592 estimate of the uncertainty in 1-km resolution disaggregated 592  
593 soil moisture, e.g., by computing the standard deviation within 593  
594 the output ensemble. 594

#### IV. APPLICATION

595 To test DisPATCH under various surface and atmospheric 596 conditions, the algorithm is run during AACES-1 and AACES- 597  
598 2 in different modes, by including (or not) a correction for 598  
599 vegetation and atmospheric effects. In each case, disaggregated 599  
600 SMOS soil moisture and HDAS measurements are compared 600  
601 at 1-km resolution for all date-farm units with overlapping 601  
602 HDAS/SMOS/MODIS data. 602

##### A. Null Hypothesis

603 In this study, the null hypothesis is defined as the application 604  
605 of DisPATCH with parameter  $\mathbf{SM}_p$  set to zero in (8). Hence, 605  
606 the downscaling relationship in (3) becomes 606

$$\mathbf{SM}_{1 \text{ km}} = \mathbf{SM}_{\text{SMOS}} \quad (19)$$

607 meaning that no 1-km information is used. Defining a null 608 hypothesis is useful to test whether DisPATCH is able to re- 608  
609 produce the subpixel variability within the  $\sim 10 \text{ km}^2$  sam- 609  
610 pling farms with better skill than simply assuming a uniform 610  
611 moisture condition. Statistical results in terms of root mean 611  
612 square difference, mean difference, correlation coefficient, and 612  
613 slope of the linear regression between the SMOS soil moisture 613  
614 disaggregated with (19) and *in situ* measurements are listed in 614  
615 Table III. One observes that the root mean square difference 615  
616 is generally explained by a (negative) bias in SMOS data and 616  
617 that none of the correlations evaluated at 1-km resolution for 617  
618 each farm separately is statistically significant (all calculated p- 618  
619 values are larger than 0.10). Thus, the rationale for developing 619  
620 DisPATCH is to improve the correlation at fine scale between 620  
621 SMOS and ground soil moisture and to reduce the bias in 621  
622 disaggregated SMOS data in the specific case where the bias 622  
623 in SMOS data at the farm scale is due to the heterogeneity of 623  
624 soil moisture within the SMOS pixel. 624

**TABLE III**  
**DISPATCH IS RUN WITH NO 1-km INFORMATION ( $\text{SM}_p$  SET TO ZERO) AND STATISTICAL RESULTS ARE LISTED IN TERMS OF ROOT MEAN SQUARE DIFFERENCE (RMSE), MEAN DIFFERENCE (BIAS), CORRELATION COEFFICIENT (R), AND SLOPE OF THE LINEAR REGRESSION BETWEEN 1-km RESOLUTION DISAGGREGATED SMOS SOIL MOISTURE AND 1-km AGGREGATED *In Situ* MEASUREMENTS. THE MEAN AND STANDARD DEVIATION OF GROUND MEASUREMENTS ( $\langle \text{SM}_{\text{HDAS}} \rangle$  AND  $\sigma_{\text{HDAS}}$ ), THE NUMBER OF CONSIDERED 1-km PIXELS, AND STATISTICAL SIGNIFICANCE (P-VALUE) ARE ALSO LISTED FOR EACH DATE-FARM UNIT**

DoY/Farm	$\langle \text{SM}_{\text{HDAS}} \rangle$ ( $\text{m}^3/\text{m}^3$ )	$\sigma_{\text{HDAS}}$ ( $\text{m}^3/\text{m}^3$ )	Number of 1 km pixels	RMSE ( $\text{m}^3/\text{m}^3$ )	Bias ( $\text{m}^3/\text{m}^3$ )	R <sup>†</sup> (-)	Slope <sup>†</sup> (-)	p-value (-)
28/F05	0.04	0.02	7	0.04	-0.04	-	-	1.0
30/F07	0.02	0.03	8	0.02	-0.02	-	-	1.0
30/F08	0.03	0.02	7	0.02	-0.02	-	-	0.69
46/F15	0.29	0.05	8	0.04	0.03	-	-	0.91
46/F16	0.34	0.06	8	0.09	-0.08	-	-	1.0
49/F17	0.21	0.06	8	0.04	-0.04	-	-	0.66
49/F18	0.25	0.07	6	0.08	-0.08	-	-	0.42
49/F20	0.20	0.09	4	0.02	-0.007	-	-	0.87
51/F19	0.24	0.08	6	0.13	-0.13	-	-	0.77
51/F20	0.20	0.10	6	0.09	-0.08	-	-	0.79
AACES-1 mean <sup>‡</sup>	-	-	-	-	-	-	-	>0.10
254/F09	0.33	0.07	9	0.13	-0.13	-	-	0.13
256/F07	0.36	0.10	8	0.19	-0.18	-	-	0.15
264/F13	0.30	0.07	8	0.18	-0.17	-	-	1.0
265/F15	0.25	0.06	7	0.05	-0.05	-	-	1.0
267/F09	0.21	0.07	9	0.14	-0.14	-	-	0.43
AACES-2 mean <sup>‡</sup>	-	-	-	-	-	-	-	>0.10

<sup>†</sup> R and slope values are reported if p-value<0.10.

<sup>‡</sup> the mean values computed for AACES-1 and AACES-2 include only statistically significant (p-value<0.10) results.

### 625 B. Visual Assessment of Disaggregation Images

626 As an example, DisPATCH is applied on DoY 49 over a 120  
627 km by 80 km subarea including the farms F16, F17, F18, F19,  
628 and F20. The images of 1-km resolution disaggregated SMOS  
629 soil moisture are presented in Fig. 6. DisPATCH is run with  
630  $\text{SM}_p$  set to zero (null hypothesis) and in four distinct modes  
631 corresponding to the combinations of the “LST” (the official  
632 MODIS land surface temperature product is used) and “RAD”  
633 [the land surface temperature is derived from MODIS radiances  
634 using (14)] modes and the “Zone A+B+C” (the vegetation-  
635 transpiration dominated 1-km pixels are discarded) and “Zone  
636 A only” (only the soil evaporation-dominated 1-km pixels are  
637 selected) modes.

638 In Fig. 6, the SMOS DGG nodes where level-2 soil moisture  
639 is successfully retrieved are overlaid on the image correspond-  
640 ing to the null hypothesis (resampled SMOS data with no 1-km  
641 information) for 6 am and 6 pm overpass times separately. The  
642 gaps in SMOS data in the lower middle part of the images  
643 are due to topography flagging over the Australian Alps. In  
644 the version-4 SMOS level-2 processor, soil moisture is not  
645 retrieved at the DGG nodes where the topography effects on  
646 simulated brightness temperatures exceed a certain threshold,  
647 so as to prevent large errors in soil moisture values. The appar-  
648 ent resolution of the null hypothesis image is 20 km because  
649 it is generated from the composition of four 40-km resolution  
650 resampled SMOS snapshot images, whose resampling grids are

separated by 20 km (the SMOS level-2 data resampling strategy 651  
was described in Section II-B.). 652

Note that the disaggregation products in the Zone A+B+C 653  
mode cover an area larger than the area sampled by SMOS 654  
data, because the SMOS resolution (about 40 km) is larger 655  
than the SMOS product sampling length (about 15 km), but 656  
does not provide disaggregated values at a distance larger than 657  
20 km from the successful retrieval nodes. Concerning the Zone 658  
A only mode, disaggregation products do not cover an area 659  
larger than the SMOS sampling area because the Australian 660  
Alps are surrounded by forests where the fraction of bare soil is 661  
less than elsewhere in the area, and which correspond to Zone 662  
B or C in the hourglass in Fig. 3. 663

When looking at the images obtained in the Zone A+B+C 664  
mode in Fig. 6, one observes that the spatial structures of 665  
1-km disaggregated SMOS soil moisture encompass, but does 666  
not seem to be correlated with, the SMOS data sampling 667  
length. However, a “boxy artifact” is still apparent at 20-km 668  
resolution, which is the separation length of the SMOS data 669  
resampling grids as explained in Section II-B. The notion of 670  
“boxy artifact” was introduced by [39] to analyze the quality of 671  
a disaggregation approach. The less apparent the low-resolution 672  
boxes, the better the disaggregation skill of the algorithm to 673  
spatially connect high-resolution disaggregated values between 674  
neighboring low-resolution pixels, and thus to derive a realistic 675  
high-resolution soil moisture field. When comparing the images 676  
obtained in the Zone A+B+C mode with those obtained in the 677

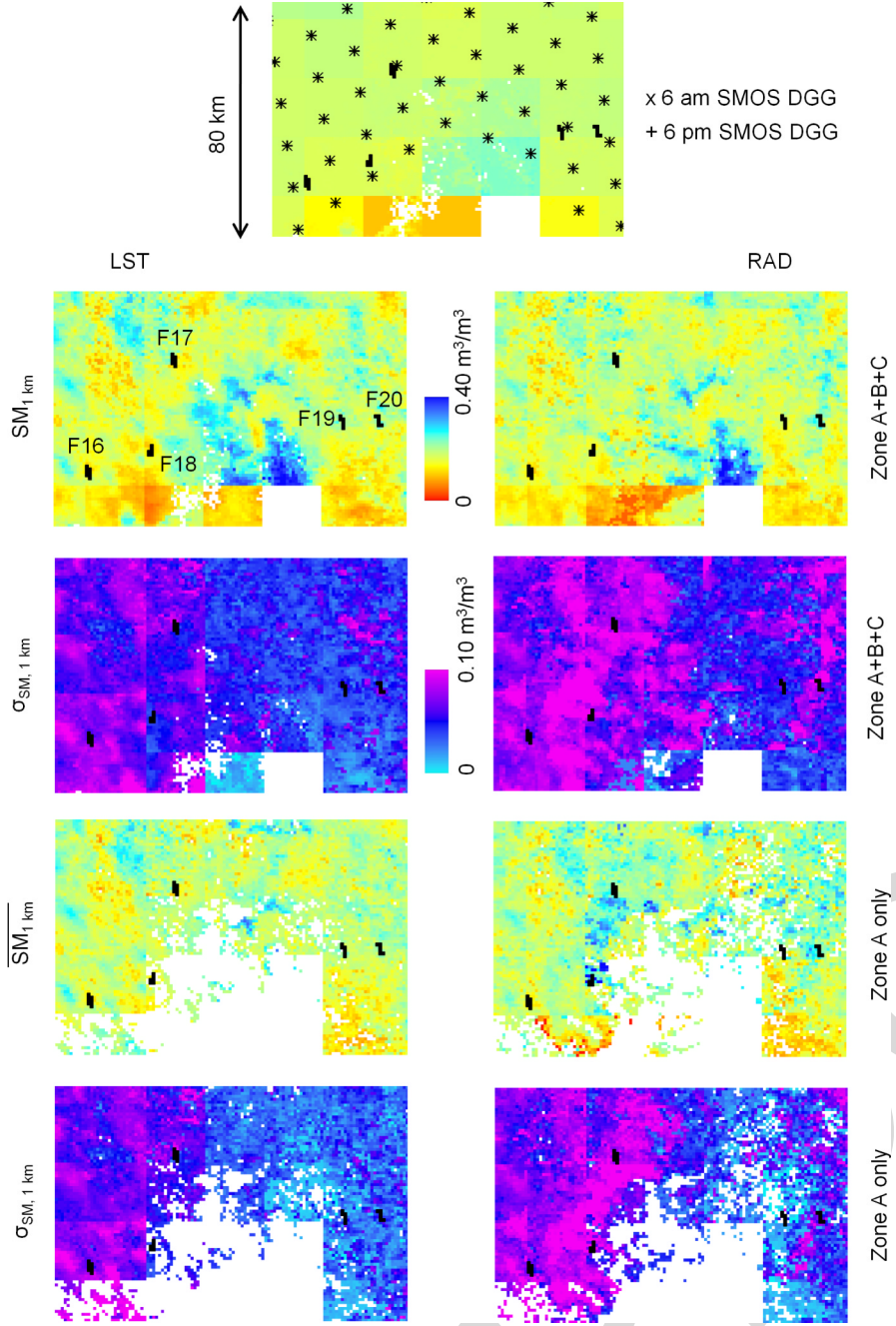


Fig. 6. Images of disaggregation results over a 120 km by 80 km subarea on DoY 49. The disaggregated soil moisture ( $\overline{SM}_{1 \text{ km}}$ ) and its estimated uncertainty ( $\sigma_{SM, 1 \text{ km}}$ ) are compared in the LST and RAD modes and in the Zone A+B+C and Zone A only modes. Sampling farms are overlaid on all images. SMOS DGG nodes are overlaid on the image corresponding to the null hypothesis (no 1-km resolution information) presented at top.

678 Zone A only mode, one observes that the 20-km resolution boxy  
 679 artifact is less apparent in the Zone A only mode, consistent  
 680 with the better sensitivity of MODIS-derived SEE with soil-  
 681 dominated pixels (Zone A) than with mixed-surface (Zone B  
 682 and C) pixels. In Fig. 6, the images obtained in the LST and  
 683 RAD mode highlight different spatial structures. In general,  
 684 there are less data gaps in the RAD than in the LST mode.  
 685 However, ground validation data are required to assess their  
 686 relative quality/accuracy.

687 As an assessment of the uncertainty in composited soil mois-  
 688 ture disaggregation, the standard deviation within the disaggre-  
 689 gation output ensemble is also reported for each disaggregation

690 product in Fig. 6. The same observations can be made as with  
 691 the soil moisture images: spatial structures are more visible, and  
 692 the boxy artifact is less apparent in the RAD than in the LST  
 693 mode. In general, the estimated uncertainty in disaggregated  
 694 products is larger in the RAD than in the LST mode, regardless  
 695 of the Zone (A+B+C or A only) mode.

### C. SMOS Weighting Function

696 To evaluate the impact of the SMOS instrument weighting  
 697 function on disaggregation results, DisPATCH is run with (and  
 698 without) the WEF correction in (18). The expected effect of the 699

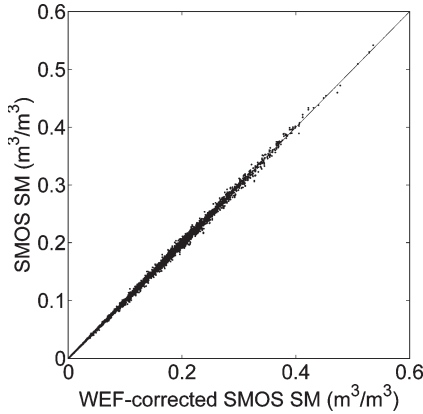


Fig. 7. Uncorrected versus WEF-corrected SMOS soil moisture for the entire data set.

WEF is a bias at 40 km resolution on disaggregated soil moisture. Fig. 7 plots the uncorrected against WEF-corrected SMOS soil moisture for the entire data set including both AACES-1 and AACES-2 experiments. The WEF correction has very little impact on disaggregated soil moisture with a maximum difference between uncorrected and WEF-corrected SMOS soil moisture of  $0.02 \text{ m}^3/\text{m}^3$ , a mean difference of approximately zero, and a standard deviation of  $0.003 \text{ m}^3/\text{m}^3$ . Although the difference is small with this data set, WEF-corrected products are expected to be more realistic. Therefore, the correction in (18) is used in all the DisPATCH runs that follow.

#### 711 D. Quantitative Comparison With In Situ Measurements

712 Fig. 8 presents the scatterplots of 1-km resolution disaggregated SMOS soil moisture versus 1-km resolution aggregated 713 *in situ* measurements for the ten date-farm units during 714 AACES-1. On each graph are plotted the soil moisture 715 aggregated in the Zone A+B+C mode (empty squares) and 716 the soil moisture disaggregated in the Zone A only mode 717 (black squares). At the beginning of AACES-1, conditions are 718 very dry so that SMOS retrievals are close to zero and the 719 variability of *in situ* measurements is low (about  $0.02 \text{ m}^3/\text{m}^3$ ). 720 In such conditions, no useful information is expected from the 721 application of DisPATCH, and the statistical results in terms of 722 spatial correlation are not meaningful for DoY 28/F05, DoY 723 30/F07 and DoY 30/F08. While wetter conditions occur after 724 DoY 30, cloud cover prevents DisPATCH to be run (MODIS 725 data are unavailable) until DoY 46. On DoY 46, the average 726 and standard deviation of *in situ* soil moisture measurements is 727  $0.32 \text{ m}^3/\text{m}^3$  and  $0.06 \text{ m}^3/\text{m}^3$ , respectively. The spatial variabil- 728 ity of 1-km soil moisture is nicely captured by DisPATCH notably 729 in the RAD mode. On DoY 49, the disaggregated SMOS 730 soil moisture is still correlated with the *in situ* measurements 731 made in three farms (F17, F18, and F20). On the last ground 732 sampling day, disaggregation results are significantly correlated 733 with *in situ* measurements in F19, but not in F20. The poor 734 results obtained with DoY 51/F20 is probably due to the time 735 gap (3 days) between ground sampling date (DoY 51) and 736 MODIS overpass day (DoY 54).

737 Statistical results in terms of root mean square difference, 738 mean difference, correlation coefficient, and slope of the linear

regression between the SMOS soil moisture disaggregated in 740 the Zone A+B+C mode and aggregated *in situ* measurements 741 are listed in Table IV. Statistical significance (p-value) is also 742 reported for each date-farm unit to select statistically significant 743 (p-value  $< 0.10$ ) results. Although the disaggregation of SMOS 744 data on extensively dry DoY 30 does not provide any additional 745 information (soil is uniformly dry), the observed correlation 746 between disaggregated (LST mode) and *in situ* soil moisture 747 is statistically significant, and the correlation coefficient value 748 is negative ( $-0.70$  and  $-0.95$  at F07 and F08, respectively). 749 One plausible explanation is the opposite effect of soil temper- 750 ature on HDAS soil moisture measurements and on MODIS- 751 derived soil evaporative efficiency: a slight undercorrection of 752 the temperature-corrected hydaprobe measurements at high 753 temperature [18] results in a slight increase of soil moisture 754 estimate with soil temperature, while an increase of soil temper- 755 ature makes soil evaporative efficiency decrease. Nevertheless, 756 the possible impact of soil temperature on HDAS measurements 757 is very low with a slope of the linear regression between 758 disaggregated SMOS and *in situ* soil moisture calculated as 759  $-0.08$  and  $-0.03$  for F07 and F08, respectively. When selecting 760 statistically significant results (p-value  $< 0.10$ ) and discarding 761 data for DoY 30, the mean correlation coefficient and slope in 762 RAD mode are  $0.75$  and  $0.58$ , respectively. 763

Fig. 9 presents the scatterplots of 1-km resolution disaggregated SMOS soil moisture versus 1-km resolution aggregated *in situ* measurements for the five date-farm units during AACES- 765 2. On each graph are plotted the soil moisture disaggregated in 766 the Zone A+B+C mode (empty squares) and the soil moisture 767 disaggregated in the Zone A only mode (black squares). The 768 surface conditions of AACES-2 were relatively wet with a mean 769 soil moisture value estimated as  $0.29 \text{ m}^3/\text{m}^3$ . The disaggre- 770 gated SMOS soil moisture does not correlate well with *in situ* 771 measurements with a p-value larger than 0.10 for all sampling 772 days, except for DoY 256/F07 in LST mode (see Table IV). The 773 negative correlation coefficient ( $-0.73$ ) obtained on DoY 256 is 774 discussed when comparing the Zone A+B+C and Zone A only 775 modes in Section IV-F. In general, statistical results in Table IV 776 indicate that DisPATCH does not succeed in representing the 777 variability of soil moisture at 1-km resolution during AACES- 779 2. In fact, DisPATCH is based on the tight coupling that occurs 780 between soil moisture and evaporation under high evaporative 781 demand conditions [40]. This coupling seems to be weak in 782 September over the study area so that the disaggregation results 783 at 1-km resolution are not reliable. 784

For DoY 264/F13, however, an interesting feature is ob- 785 served on the graph corresponding to the RAD and Zone A 786 only modes. When removing the (three) black squares with 787 the largest errorbars, the correlation coefficient and the slope 788 of the linear regression between disaggregated and *in situ* 789 observations becomes  $0.9$  and  $0.7$ , respectively. This suggests 790 that: 1) the standard deviation within the disaggregation output 791 ensemble can be a good estimate of the uncertainty in the 792 composited disaggregation product; and 2) the applicability of 793 DisPATCH is greatly dependent on the quality of MODIS land 794 surface temperature. Note that in this study, a choice was made 795 to maximize the number of data points used in the comparison 796 with *in situ* measurements. Consequently, all the cloud-free 797

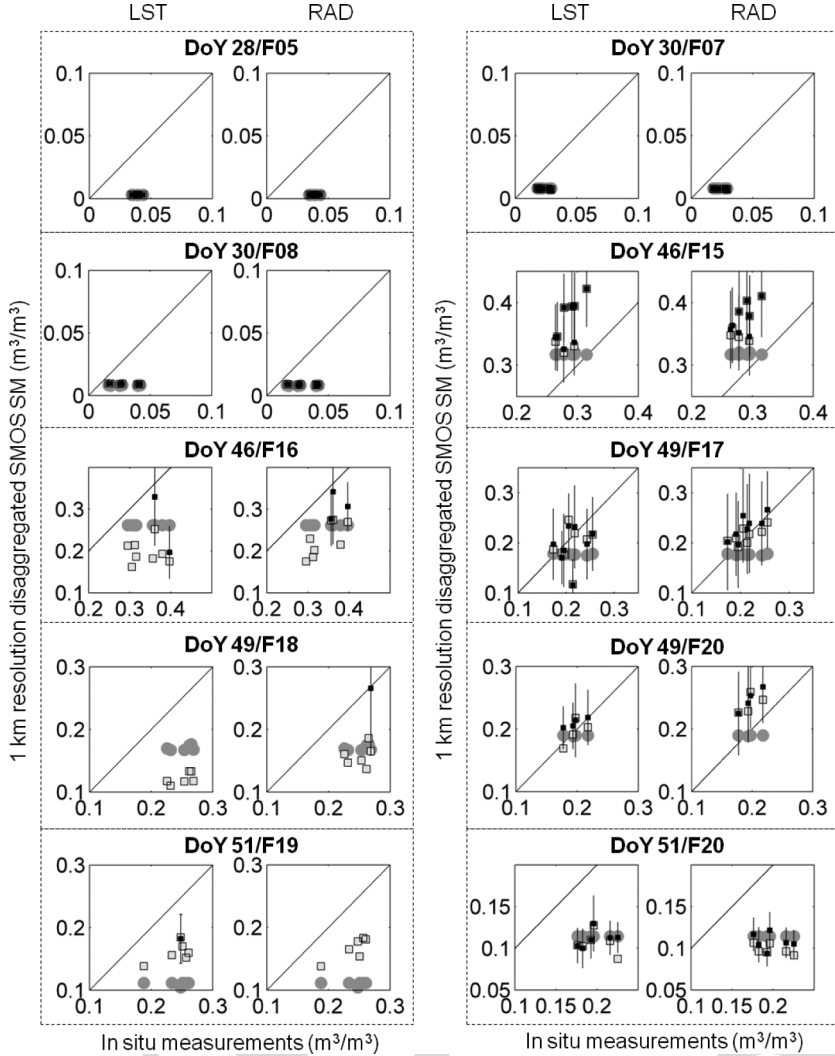


Fig. 8. Scatterplots of 1-km resolution disaggregated SMOS soil moisture versus 1-km resolution aggregated *in situ* measurements for each of the ten date-farm data sets during AACES-1. The filled circles correspond to disaggregation with no 1-km information, empty squares to Zone A+B+C mode and black squares to Zone A only mode. For the Zone A only mode, the uncertainty in disaggregated soil moisture is represented by vertical errorbars.

798 MODIS land surface temperature data were used regardless  
 799 of the MODIS land surface temperature quality index. Further  
 800 research should be conducted to assess whether selecting the  
 801 MODIS pixel with the best MODIS land surface temperature  
 802 quality index would improve the disaggregation results. This  
 803 would be possible using the AACES airborne data, which cover  
 804 a much larger area than *in situ* measurements.

#### 805 E. Atmospheric Corrections

806 The impact of atmospheric corrections on DisPATCh output  
 807 is analyzed by comparing the disaggregation results obtained  
 808 in the LST and RAD mode. Quantitative comparison between  
 809 LST and RAD modes is provided in Table IV in terms of root  
 810 mean square difference, mean difference, correlation coeffi-  
 811 cient, and slope of the linear regression between disaggregated  
 812 SMOS soil moisture and aggregated *in situ* measurements.  
 813 Correlation coefficient and slope values are reported only if  
 814 the p-value (statistical significance) is lower than 0.10. It is  
 815 apparent that statistical results are better in the RAD than in

the LST mode. When including all dates, the mean bias is 816 decreased from  $-0.05 \text{ m}^3/\text{m}^3$  in LST mode to  $-0.03 \text{ m}^3/\text{m}^3$  817 in RAD mode during AACES-1. When selecting statistically 818 significant results ( $p\text{-value} < 0.10$ ) and discarding data for 819 DoY 30, the mean correlation coefficient and slope is 0.75 and 820 0.58 in RAD mode, and 0.65 and 1.5 in LST mode, respectively. 821 Note that the improvement is very significant for DoY 46/F16 822 with a correlation coefficient and slope increasing from about 823 zero to 0.7 and 0.8, respectively. 824

The fact that the results obtained in RAD mode are superior 825 to those obtained in LST mode indicates that the atmospheric 826 corrections of the official MODIS land surface temperature 827 add significant uncertainties in the disaggregation products. 828 One rationale may be that the information used in atmospheric 829 corrections (notably air temperature and water vapor profile 830 data) are subjected to large uncertainties at 5-km resolution. 831 As DisPATCh is based on the spatial variations of MODIS 832 temperature relative to the 40 km scale mean, the atmospheric 833 corrections on the land surface temperature data are not nec- 834 essary at 5 km (as it is done in the MODIS temperature 835

TABLE IV  
DisPATCH IS RUN IN THE ZONE A+B+C MODE AND STATISTICAL RESULTS ARE LISTED IN TERMS OF ROOT MEAN SQUARE DIFFERENCE (RMSD), MEAN DIFFERENCE (BIAS), CORRELATION COEFFICIENT (R), AND SLOPE OF THE LINEAR REGRESSION BETWEEN 1-km RESOLUTION DISAGGREGATED SMOS SOIL MOISTURE AND 1-km AGGREGATED *In Situ* MEASUREMENTS. THE RESULTS OBTAINED USING THE RADIANCE-DERIVED LAND SURFACE TEMPERATURE DATA (RAD MODE) AND USING THE OFFICIAL MODIS LAND SURFACE TEMPERATURE DATA (LST MODE IN PARENTHESIS) ARE COMPARED. THE MEAN AND STANDARD DEVIATION OF GROUND MEASUREMENTS ( $\langle \text{SM}_{\text{HDAS}} \rangle$  AND  $\sigma_{\text{HDAS}}$ ), THE NUMBER OF CONSIDERED 1-km PIXELS AND STATISTICAL SIGNIFICANCE (P-VALUE) ARE ALSO LISTED FOR EACH DATE-FARM UNIT

DoY/Farm	$\langle \text{SM}_{\text{HDAS}} \rangle$ ( $\text{m}^3/\text{m}^3$ )	$\sigma_{\text{HDAS}}$ ( $\text{m}^3/\text{m}^3$ )	Number of 1 km pixels	RMSD ( $\text{m}^3/\text{m}^3$ )	Bias ( $\text{m}^3/\text{m}^3$ )	R <sup>†</sup> (-)	Slope <sup>†</sup> (-)	p-value (-)
28/F05	0.04	0.02	7 (7)	0.04 (0.04)	-0.04 (-0.04)	- (-)	- (-)	0.72 (0.80)
30/F07	0.02	0.03	8 (8)	0.02 (0.02)	-0.02 (-0.02)	- (-0.70)	- (-0.08)	0.20 (0.05)
30/F08	0.03	0.02	7 (7)	0.02 (0.02)	-0.02 (-0.02)	- (-0.95)	- (-0.03)	0.11 (0.001)
46/F15	0.29	0.05	8 (8)	0.09 (0.09)	0.09 (0.08)	- (0.65)	- (1.5)	0.12 (0.08)
46/F16	0.34	0.06	8 (8)	0.12 (0.15)	-0.11 (-0.14)	0.72 (-)	0.76 (-)	0.04 (0.95)
49/F17	0.21	0.06	8 (8)	0.02 (0.04)	0.00 (-0.02)	0.70 (-)	0.42 (-)	0.05 (0.54)
49/F18	0.25	0.07	6 (6)	0.10 (0.13)	-0.09 (-0.13)	- (-)	- (-)	0.60 (0.20)
49/F20	0.20	0.09	4 (4)	0.05 (0.01)	0.04 (0.00)	- (-)	- (-)	0.41 (0.32)
51/F19	0.24	0.08	6 (6)	0.07 (0.08)	-0.07 (-0.08)	0.84 (-)	0.56 (-)	0.04 (0.19)
51/F20	0.20	0.10	6 (6)	0.10 (0.09)	-0.10 (-0.09)	- (-)	- (-)	0.17 (0.51)
AACES-1 mean <sup>‡</sup>	0.26 (0.29)	0.07 (0.05)	7 (8)	0.07 (0.09)	-0.06 (-0.08)	0.75 (0.65)	0.58 (1.5)	0.04 (0.08)
254/F09	0.33	0.07	9 (9)	0.18 (0.14)	-0.16 (-0.11)	- (-)	- (-)	0.17 (0.74)
256/F07	0.36	0.10	8 (9)	0.12 (0.19)	-0.10 (-0.18)	- (-0.73)	- (-0.47)	0.12 (0.04)
264/F13	0.30	0.07	8 (8)	0.16 (0.19)	-0.14 (-0.16)	- (-)	- (-)	0.59 (0.47)
265/F15	0.25	0.06	7 (7)	0.16 (0.18)	0.01 (0.03)	- (-)	- (-)	0.32 (0.34)
267/F09	0.21	0.07	9 (9)	0.16 (0.15)	-0.15 (-0.15)	- (-)	- (-)	0.90 (0.86)
AACES-2 mean <sup>‡</sup>	0.36	0.10	- (9)	- (0.19)	- (-0.18)	- (-0.73)	- (-0.47)	>0.10 (0.04)

<sup>†</sup> R and slope values are reported if p-value<0.10.

<sup>‡</sup> the mean values computed for AACES-1 and AACES-2 include only statistically significant (p-value<0.10) results and discard extensive dry days DoY 28-30.

836 algorithm). An atmospheric correction at 40-km resolution is  
837 sufficient and provides even better disaggregation results than  
838 applying an atmospheric correction at 5-km resolution.

### 839 F. Vegetation Cover

840 The impact of vegetation cover on DisPATCH output during  
841 AACES-1 is analyzed by comparing the disaggregation results  
842 obtained in the Zone A+B+C and Zone A only mode. Quan-  
843 titative comparison between Zone A+B+C and Zone A only  
844 modes is provided in Tables IV and V in terms of root mean  
845 square difference, mean difference, correlation coefficient, and  
846 slope of the linear regression between disaggregated SMOS soil  
847 moisture and aggregated *in situ* measurements. It is apparent  
848 that statistical results are generally better in the Zone A only  
849 than in the Zone A+B+C mode for both LST and RAD modes.  
850 In the RAD mode for instance, the mean correlation coefficient  
851 is increased from 0.75 in the Zone A+B+C mode (Table IV) to  
852 0.89 in the Zone A only mode (Table V). Also the mean slope  
853 is closer to 1 as it switches from 0.58 in the Zone A+B+C mode  
854 (Table IV) to 0.91 in the Zone A only mode (Table V). Con-  
855 sequently, results are consistent with the hourglass approach in  
856 Fig. 3 that predicts a lower sensitivity of MODIS-derived soil  
857 temperature to soil moisture in Zone B and C, Zone A having

the highest potential for estimating soil moisture variability 858 from MODIS temperature. 859

On DoY 256, the negative correlation appearing in Zone 860 A+B+C mode (Table IV) is not significant in Zone A only mode 861 (Table V), suggesting that the contradictory result obtained on 862 DoY 256 is probably an artifact due to the small sample size. 863

Note that one drawback of the Zone A only mode is the larger 864 amount of data gaps in the soil moisture images. Therefore, 865 the use of both modes is a compromise between application 866 coverage and accuracy in the disaggregation output. 867

### 868 G. Distinguishing Between SMOS and DisPATCH Errors

By solving the extent mismatch between 40-km resolution 869 remote sensing observation and localized *in situ* measurements, 870 DisPATCH could be used as a tool to help improve the validation 871 strategies of SMOS data in low-vegetated semi-arid regions. It 872 also would reduce the coverage requirements identified by [41] 873 for airborne validation campaigns. However, such a validation 874 approach requires separating the different error sources that 875 may be attributed to SMOS soil moisture and to DisPATCH. 876 One solution is to estimate the errors attributed to DisPATCH 877 and then deduce the errors attributed to SMOS soil moisture. To 878 estimate the errors that are associated with the disaggregation 879

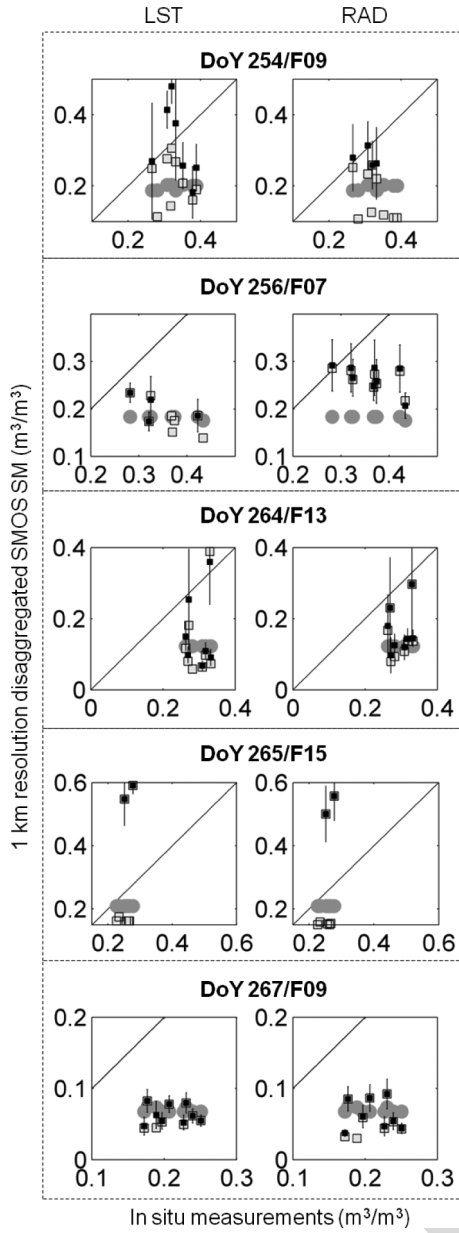


Fig. 9. Scatterplots of 1-km resolution disaggregated SMOS soil moisture versus 1-km resolution aggregated *in situ* measurements for each of the five date-farm data sets during AACES-2. The filled circles correspond to disaggregation with no 1-km information, empty squares to Zone A+B+C mode and black squares to Zone A only mode. For the Zone A only mode, the uncertainty in disaggregated soil moisture is represented by vertical errorbars.

methodology, it is suggested to analyze the spatial correlation between 1-km disaggregated SMOS soil moisture and 881 *in situ* measurements. If the correlation is significant, then the 882 disaggregation product is likely to be sufficiently accurate for 883 validating SMOS data.

Note that the errors in DisPATCH are in part coupled with 885 the errors in SMOS soil moisture, particularly because SMOS 886 is an input to DisPATCH. However, any uncertainties in SMOS 887 soil moisture should not impact the disaggregation results at a 888 distance shorter than the SMOS data sampling length (15 km). 889 This is the reason why such a validation strategy should be 890 conducted with ground measurements made within a distance 891 radius of 15 km.

In this study case, five date-farm units including DoY 893 46/F15, DoY 46/F16, DoY 49/F17, DoY 49/F18, and DoY 894 49/F20 indicate a significant correlation between disaggregated 895 SMOS soil moisture and *in situ* measurements. For these units, 896 the root mean square error in disaggregated SMOS soil mois- 897 ture is mainly explained by a bias in disaggregated soil moisture 898 (see Table IV). However, no conclusion can be drawn from 899 these data because: 1) the bias is sometimes positive (DoY 900 46/F15, DoY 49/F20), and sometimes negative (DoY 46/F16, 901 DoY 49/F17, DoY 49/F18); and 2) the comparison is made only 902 once for each farm, which does not allow analyzing the tempo- 903 ral behavior. Such a validation approach could be undertaken 904 in the near future using the OzNet (<http://www.oznet.org.au/>, 905 [42]) soil moisture monitoring network, providing continuous 906 measurements at 68 sites within the Murrumbidgee catchment 907 area.

#### H. Subpixel Variability and Assimilation Perspectives

909

DisPATCH is successively run in LST or RAD mode and in 910 Zone A+B+C or Zone A only mode during AACES-1. Fig. 10 911 plots for each case the estimated uncertainty in disaggregated 912 soil moisture (computed as the standard deviation of the disag- 913 gregation output ensemble) against the subpixel variability of 914 1-km resolution *in situ* measurements (computed as the stan- 915 dard deviation of the *in situ* measurements made within 916 1-km pixels). The data corresponding to DoY 51 are plotted 917 separately because of the time gap between HDAS/SMOS 918 (DoY 51) and MODIS (DoY 54) collection time. It is interest- 919 ing to observe that the estimated uncertainty in disaggregated 920 soil moisture is closely related to the observed subpixel vari- 921 ability of *in situ* measurements. Hence,  $\sigma_{SM, 1 \text{ km}}$  could be used 922 as a proxy for representing the soil moisture variability at scales 923 finer than 1-km resolution. Concerning the data on DoY 51, the 924 linear regression is clearly off the 1:1 line. This is consistent 925 with a decrease of the spatial variability in soil moisture during 926 a dry down period [43]. In particular, the spatial variability 927 in soil moisture is expected to be lower on DoY 54 than on 928 DoY 51.

929

The correlation between the estimated uncertainty in disag- 930 ggregated soil moisture and the subpixel soil moisture variability 931 makes an additional link between DisPATCH output and assim- 932 ilation schemes into hydrological models. A number of optimal 933 assimilation methodologies have been developed to combine 934 model predictions with remote sensing observations. However, 935 any so-called optimal assimilation technique stops being opti- 936 mal if the uncertainty in remotely sensed data is unknown or 937 estimated with a large uncertainty. In the perspective of assim- 938 ilating disaggregated SMOS data into land surface models, one 939 should keep in mind that the error information on observable 940 variables is as crucial as the observations themselves, e.g., [44]. 941

## V. SUMMARY AND CONCLUSION

942

DisPATCH is an algorithm dedicated to the disaggregation of 943 soil moisture observations using high-resolution soil tempera- 944 ture data. It converts soil temperature fields into soil moisture 945 fields given a semi-empirical soil evaporative efficiency model 946

TABLE V  
 DisPATCH IS RUN IN THE ZONE A ONLY MODE, AND STATISTICAL RESULTS ARE LISTED IN TERMS OF ROOT MEAN SQUARE DIFFERENCE (RMSD), MEAN DIFFERENCE (BIAS), CORRELATION COEFFICIENT (R), AND SLOPE OF THE LINEAR REGRESSION BETWEEN 1-km RESOLUTION DISAGGREGATED SMOS SOIL MOISTURE AND 1-km AGGREGATED *In Situ* MEASUREMENTS. THE RESULTS OBTAINED USING THE RADIANCE-DERIVED LAND SURFACE TEMPERATURE DATA (RAD MODE) AND USING THE OFFICIAL MODIS LAND SURFACE TEMPERATURE DATA (LST MODE IN PARENTHESIS) ARE COMPARED. THE MEAN AND STANDARD DEVIATION OF GROUND MEASUREMENTS ( $\langle SM_{HDAS} \rangle$  AND  $\sigma_{HDAS}$ ), THE NUMBER OF CONSIDERED 1-km PIXELS AND STATISTICAL SIGNIFICANCE (P-VALUE) ARE ALSO LISTED FOR EACH DATE-FARM UNIT

DoY/Farm	$\langle SM_{HDAS} \rangle$ ( $m^3/m^3$ )	$\sigma_{HDAS}$ ( $m^3/m^3$ )	Number of 1 km pixels	RMSD*	Bias*	R†	Slope†	p-value
28/F05	0.04	0.02	7 (7)	0.04 (0.04)	-0.04 (-0.04)	- (-)	- (-)	0.72 (0.80)
30/F07	0.02	0.03	8 (8)	0.02 (0.02)	-0.02 (-0.02)	- (-0.70)	- (-0.08)	0.20 (0.05)
30/F08	0.03	0.02	7 (7)	0.02 (0.02)	-0.02 (-0.02)	- (-0.95)	- (-0.03)	0.11 (0.001)
46/F15	0.29	0.05	8 (8)	0.09 (0.09)	0.09 (0.08)	- (0.66)	- (1.4)	0.13 (0.07)
46/F16	0.34	0.06	3 (2)	0.07 (0.14)	-0.06 (-0.12)	- (-)	- (-)	0.96 (-)
49/F17	0.21	0.06	8 (8)	0.02 (0.04)	0.02 (-0.02)	0.79 (-)	0.71 (-)	0.02 (0.64)
49/F18	0.25	0.07	1 (0)	- (-)	- (-)	- (-)	- (-)	0.20 (0.20)
49/F20	0.20	0.09	4 (4)	0.05 (0.02)	0.05 (0.01)	0.98 (0.92)	1.1 (0.42)	0.02 (0.08)
51/F19	0.24	0.08	0 (1)	- (-)	- (-)	- (-)	- (-)	0.19 (0.19)
51/F20	0.20	0.10	6 (6)	0.09 (0.09)	-0.09 (-0.09)	- (-)	- (-)	0.70 (0.45)
AACES-1 mean‡	0.21 (0.25)	0.08 (0.07)	6 (6)	0.04 (0.06)	0.04 (0.05)	0.89 (0.79)	0.91 (0.91)	0.02 (0.08)
254/F09	0.33	0.07	4 (7)	0.05 (0.12)	-0.03 (-0.02)	- (-)	- (-)	0.70 (0.30)
256/F07	0.36	0.10	8 (4)	0.12 (0.15)	-0.10 (-0.13)	- (-)	- (-)	0.13 (0.43)
264/F13	0.30	0.07	8 (7)	0.14 (0.17)	-0.13 (-0.14)	- (-)	- (-)	0.64 (0.86)
265/F15	0.25	0.06	2 (2)	0.26 (0.30)	0.26 (0.30)	- (-)	- (-)	- (-)
267/F09	0.21	0.07	8 (9)	0.15 (0.15)	-0.15 (-0.15)	- (-)	- (-)	0.77 (0.85)
AACES-2 mean‡	-	-	- (-)	- (-)	- (-)	- (-)	- (-)	>0.10 (>0.10)

\* RMSD and bias values are computed if the number of 1 km pixels>1.

† R and slope values are reported if p-value<0.10.

‡ the mean values computed for AACES-1 and AACES-2 include only statistically significant (p-value<0.10) results and discard extensive dry days DoY 28-30.

947 and a first-order Taylor series expansion around the field-mean  
 948 soil moisture. In this study, the disaggregation approach is ap-  
 949 plied to 40-km resolution version-4 SMOS level-2 soil moisture  
 950 using 1-km resolution MODIS data. The objective is to test  
 951 DisPATCh under different surface and atmospheric conditions  
 952 using the very intensive ground measurements collected in  
 953 southeastern Australia during the 2010 summer and winter  
 954 AACES campaigns. Those measurements are aggregated at  
 955 the downscaling resolution (1 km) and subsequently compared  
 956 to the disaggregated SMOS soil moisture. Over the study  
 957 area, climatic (evaporative demand), meteorologic (presence  
 958 of clouds), and vegetation (cover and water status) conditions  
 959 are strong constraints on disaggregation results. The quality  
 960 of disaggregation products varies greatly according to season:  
 961 while the correlation coefficient between disaggregated and  
 962 *in situ* soil moisture is 0.7 during the summer AACES, it  
 963 is about zero during the winter AACES, consistent with a  
 964 weaker coupling between evaporation and surface moisture  
 965 in temperate than in semi-arid climate. Moreover, vegetation  
 966 cover prevents the soil temperature to be retrieved from thermal  
 967 infrared data and the vegetation water stress may increase the  
 968 remotely sensed land surface temperature independent of near-  
 969 surface soil moisture. By separating the 1-km pixels where  
 970 MODIS temperature is mainly controlled by soil evaporation,

from those where MODIS temperature is controlled by both  
 971 soil evaporation and vegetation transpiration, the correlation  
 972 coefficient between disaggregated and *in situ* soil moisture is  
 973 increased from 0.70 to 0.85 during the summer AACES cam-  
 974 paign. Also, cloud cover totally obscures the surface during rain  
 975 events, and on clear sky days, the water vapor in the atmosphere  
 976 significantly affects the quality of land surface temperature  
 977 data. It is found that the 5-km resolution atmospheric correction  
 978 of the official MODIS temperature data has significant impact  
 979 on DisPATCh output. An alternative atmospheric correction at  
 980 40-km resolution increases the correlation coefficient between  
 981 disaggregated and *in situ* soil moisture from 0.72 to 0.82 during  
 982 the summer AACES.  
 983

The above limitations must be kept in mind when using  
 984 DisPATCh as a tool for validating SMOS soil moisture. Over  
 985 semi-arid areas, disaggregation can solve the extent mismatch  
 986 between the 40-km resolution SMOS data and localized *in situ*  
 987 measurements. However, the validation of SMOS using Dis-  
 988 PATCh requires separation of the errors associated with SMOS  
 989 data and the errors associated with DisPATCh. As SMOS data  
 990 are an input to DisPATCh, the errors in DisPATCh are also  
 991 linked to the uncertainty in SMOS soil moisture. Nevertheless,  
 992 one way to identify the error sources specifically attributed  
 993 to DisPATCh is to analyze the spatial correlation between  
 994

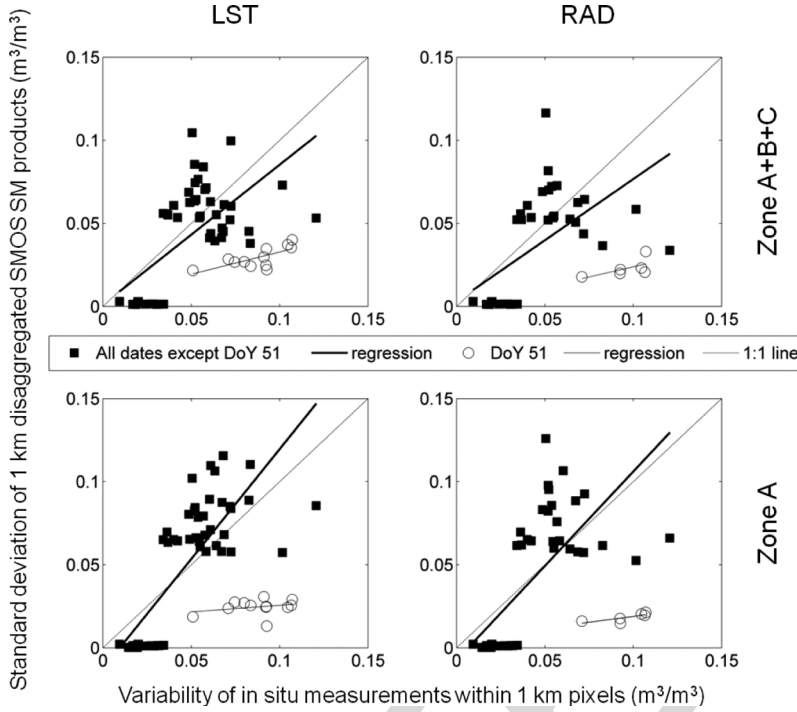


Fig. 10. Estimated uncertainty in disaggregated soil moisture ( $\sigma_{SM}$ , 1 km) versus subpixel variability of 1 km resolution *in situ* measurements for DisPATCH run in LST or RAD mode and Zone A+B+C or Zone A only mode.

995 disaggregated SMOS data and the *in situ* measurements made  
996 at a distance larger than the downscaling resolution (1 km with  
997 MODIS data) and smaller than the SMOS data sampling length  
998 (15 km).

999 Based on the results obtained using the AACES *in situ*  
1000 measurements, several improvements of DisPATCH can be  
1001 suggested:

- 1002 • Use of the MODIS land surface temperature quality index  
1003 to select the SMOS pixels with the highest MODIS data  
1004 quality.
- 1005 • Correcting the MODIS land surface temperature for  
1006 topography and illumination effects [45]. Within a 40-km  
1007 SMOS resolution pixel, the elevation range may be very  
1008 significant and thus induce a variability in land sur-  
1009 face temperature that is not attributed to surface soil  
1010 moisture.
- 1011 • Use of ancillary air temperature data to constrain the  
1012 estimation of end-members. The unstressed vegetation  
1013 temperature  $T_{v,min}$  could be set to the air temperature  
1014 instead of the minimum MODIS land surface temperature.  
1015 This would make the estimation of  $T_{v,min}$  less dependent  
1016 on the representativeness of the surface conditions met  
1017 within the SMOS pixel [24].
- 1018 • Accounting for the dependency of soil evaporative effi-  
1019 ciency to potential evaporation, by replacing the model in  
1020 [26] with the model in [38].
- 1021 • Estimating an optimal downscaling resolution for each  
1022 season: as the sensitivity of soil evaporative efficiency to  
1023 soil moisture is lower in the winter months than in the sum-  
1024 mer months, aggregating DisPATCH output may improve  
1025 the quality of disaggregation products at the expense of  
1026 spatial resolution [17].

A robust disaggregation methodology of SMOS soil moisture 1027 at 1-km resolution, which would provide both disaggregated 1028 soil moisture and its uncertainty at 1-km resolution is a crucial 1029 step toward the application of SMOS data to hydrological 1030 studies.

## REFERENCES

- [1] E. G. Njoku and L. Li, "Retrieval of land surface parameters using passive 1033 microwave measurements at 6–18 GHz," *IEEE Trans. Geosci. Remote 1034 Sens.*, vol. 37, no. 1, pp. 79–93, Jan. 1999. 1035
- [2] C. S. Draper, J. P. Walker, P. J. Steinle, R. A. M. D. Jeu, and 1036 T. R. H. Holmes, "An evaluation of AMSR-E derived soil moisture 1037 over Australia," *Remote Sens. Environ.*, vol. 113, no. 4, pp. 703–710, 1038 Apr. 2009. doi:10.1016/j.rse.2008.11.011. 1039
- [3] C. Kummerow, W. S. Olson, and L. Giglio, "A simplified scheme for 1040 obtaining precipitation and vertical hydrometeor profiles from passive 1041 microwave sensors," *IEEE Trans. Geosci. Remote Sens.*, vol. 34, no. 5, 1042 pp. 1213–1232, Sep. 1996. 1043
- [4] M. Grecu and E. N. Anagnostou, "Overland precipitation estimation from 1044 TRMM passive microwave observations," *J. Appl. Meteor.*, vol. 40, no. 8, 1045 pp. 1367–1380, Aug. 2001. 1046
- [5] T. J. Jackson, M. H. Cosh, R. Bindlish, P. J. Starks, D. D. Bosch, 1047 M. Seyfried, D. C. Goodrich, M. S. Moran, and J. Du, "Validation of 1048 advanced microwave scanning radiometer soil moisture products," *IEEE 1049 Trans. Geosci. Remote Sens.*, vol. 48, no. 12, pp. 4256–4272, Dec. 2010. 1050 doi:10.1109/TGRS.2010.2051035. 1051
- [6] Y. H. Kerr, P. Waldteufel, J.-P. Wigneron, S. Delwart, F. Cabot, 1052 J. Boutin, M. J. Escorihuela, J. Font, N. Reul, C. Gruhier, S. E. Juglea, 1053 M. R. Drinkwater, A. Hahne, M. Martin-Neira, and S. Mecklenburg, 1054 "The SMOS mission: New tool for monitoring key elements of the 1055 global water cycle," *Proc. IEEE*, vol. 98, no. 5, pp. 666–687, May 2010. 1056 doi:10.1109/JPROC.2010.2043032. 1057
- [7] P. Matos, A. Gutiérrez, and F. Moreira, *SMOS LI Processor Discrete 1058 Global Grids Document*, vol. SMOS-DMS-TN-5200. Lisboa, Portugal: 1059 DEIMOS Engenharia, 2004, V1.4. 1060
- [8] S. Bircher, J. E. Balling, N. Skou, and Y. Kerr, "SMOS validation by 1061 means of an airborne campaign in the Skjern river catchment, Western 1062 Denmark," *IEEE Trans. Geosci. Remote Sens.*, 2011, to be published. 1063 AQ11
- [9] C. Gruhier, P. de Rosnay, S. Hasenauer, T. Holmes, R. de Jeu, 1064 Y. Kerr, E. Mougin, E. Njoku, F. Timouk, W. Wagner, and M. Zribi 1065

- 1066 (2010, Jan.). Soil moisture active and passive microwave products:  
1067 Intercomparison and evaluation over a Sahelian site. *Hydrol. Earth Syst.*  
1068 *Sci. [Online]*, 14(1), pp. 141–156. Available: www.hydrol-earth-syst-  
1069 sci.net/14/141/2010/
- 1070 [10] J.-C. Calvet, N. Fritz, F. Froissard, D. Suquia, A. Petipia, and B. Piguet,  
1071 “In situ soil moisture observations for the CAL/VAL of SMOS: The  
1072 SMOSMANIA network,” in *Proc. IGARSS*, Barcelona, Spain, 2007,  
1073 pp. 1196–1199.
- 1074 [11] S. Peischl, J. P. Walker, M. Allahmoradi, D. Barrett, R. Gurney, Y. Kerr,  
1075 E. Kim, J. Le Marshall, C. Rüdiger, D. Ryu, and N. Ye, “Towards vali-  
1076 dation of SMOS using airborne and ground data over the Murrumbidgee  
1077 catchment,” in *Proc. MODSIM*, Cairns, Australia, 2009, pp. 3733–3739.
- 1078 [12] M. H. Cosh, T. J. Jackson, S. M. Moran, and R. Bindlish, “Temporal  
1079 persistence and stability of surface soil moisture in a semi-arid water-  
1080 shed,” *Remote Sens. Environ.*, vol. 112, no. 2, pp. 304–313, Feb. 2008.  
1081 doi:10.1016/j.rse.2007.07.001.
- 1082 [13] P. de Rosnay, C. Gruhier, F. Timouk, F. Baup, E. Mougin, P. Hiernaux,  
1083 L. Kergoat, and V. Le Dantec, “Multi-scale soil moisture measurements  
1084 at the Gourma meso-scale site in Mali,” *J. Hydrol.*, vol. 375, no. 1/2,  
1085 pp. 241–252, Aug. 2009. doi:10.1016/j.jhydrol.2009.01.015.
- 1086 [14] N. S. Chauhan, S. Miller, and P. Ardanuy, “Spaceborne soil moisture esti-  
1087 mation at high resolution: A microwave-optical/IR synergistic approach,”  
1088 *Int. J. Remote Sens.*, vol. 24, no. 22, pp. 4599–4622, Nov. 2003.
- 1089 [15] M. Piles, A. Camps, M. Vall-llossera, I. Corbella, R. Panciera, C. Rüdiger,  
1090 Y. H. Kerr, and J. P. Walker, “Downscaling SMOS-derived soil moisture  
1091 using MODIS visible/infrared data,” *IEEE Trans. Geosci. Remote Sens.*,  
1092 vol. 49, no. 9, pp. 3156–3166, Sep. 2011.
- 1093 [16] O. Merlin, A. Al Bitar, J. P. Walker, and Y. Kerr, “An improved algorithm  
1094 for disaggregating microwave-derived soil moisture based on red, near-  
1095 infrared and thermal-infrared data,” *Remote Sens. Environ.*, vol. 114,  
1096 no. 10, pp. 2305–2316, Oct. 2010. doi:10.1016/j.rse.2010.05.007.
- 1097 [17] O. Merlin, A. Al Bitar, J. P. Walker, and Y. Kerr, “A sequential model  
1098 for disaggregating near-surface soil moisture observations using multi-  
1099 resolution thermal sensors,” *Remote Sens. Environ.*, vol. 113, no. 10,  
1100 pp. 2275–2284, Oct. 2009. doi:10.1016/j.rse.2009.06.012.
- 1101 [18] O. Merlin, J. Walker, R. Panciera, R. Young, J. Kalma, and  
1102 E. Kim, “Soil moisture measurement in heterogeneous terrain,” in *Proc.*  
1103 *MODSIM—International Congress Modelling Simulation Modelling*  
1104 *Simulation Society Australia New Zealand*, Dec. 2007, pp. 2604–2610.
- 1105 [19] Y. H. Kerr, P. Waldteufel, P. Richaume, P. Ferrazzoli, and J.-P. Wigneron,  
1106 *SMOS Level 2 Processor Soil Moisture Algorithm Theoretical Basis*  
1107 *Document (ATBD)*, vol. SO-TN-ESL-SM-GS-0001. Toulouse, France:  
1108 CESBIO, May 2011, V3.f.
- 1109 [20] Y. H. Kerr, P. Waldteufel, P. Richaume, J. P. Wigneron, P. Ferrazzoli,  
1110 A. Mahmoodi, A. Al Bitar, F. Cabot, C. Gruhier, D. Leroux, A. Mialon,  
1111 and S. Delwart, “The SMOS soil moisture retrieval algorithm,” *IEEE*  
1112 *Trans. Geosci. Remote Sens.*, 2011.
- 1113 [21] O. Merlin, C. Rüdiger, P. Richaume, A. Al Bitar, A. Mialon, J. P. Walker,  
1114 and Y. Kerr, “Disaggregation as a top-down approach for evaluating  
1115 40 km resolution SMOS data using point-scale measurements: Application  
1116 to AACES-1,” in *Proc. SPIE, Remote Sens. Agriculture, Ecosystems,*  
1117 *Hydrol. XII*, Toulouse, France, 2010, pp. 782.401-1–782.401-8.
- 1118 [22] K. Nishida, R. R. Nemani, J. M. Glassy, and S. W. Running, “Develop-  
1119 ment of an evapotranspiration index from Aqua/MODIS for monitoring  
1120 surface moisture status,” *IEEE Trans. Geosci. Remote Sens.*, vol. 41, no. 2,  
1121 pp. 493–501, Feb. 2003.
- 1122 [23] G. Gutman and A. Ignatov, “The derivation of the green vegetation fraction  
1123 from NOAA/AVHRR data for use in numerical weather prediction  
1124 models,” *Int. J. Remote Sens.*, vol. 19, pp. 1533–1543, 1998.
- 1125 [24] O. Merlin, B. Duchemin, O. Hagolle, F. Jacob, B. Coudert, G. Chehbouni,  
1126 G. Dedieu, J. Garatza, and Y. Kerr, “Disaggregation of MODIS surface  
1127 temperature over an agricultural area using a time series of Formosat-2  
1128 images,” *Remote Sens. Environ.*, vol. 114, no. 11, pp. 2500–2512,  
1129 Nov. 2010. doi:10.1016/j.rse.2010.05.025.
- 1130 [25] A. C. T. Pinheiro, J. Descloitres, J. L. Privette, J. Susskind, L. Iredell, and  
1131 J. Schmaltz, “Near-real time retrievals of land surface temperature within  
1132 the MODIS rapid response system,” *Remote Sens. Environ.*, vol. 106,  
1133 no. 3, pp. 326–336, Feb. 2007. doi:10.1016/j.rse.2006.09.006.
- 1134 [26] J. Noilhan and S. Planton, “A simple parameterization of land surface  
1135 processes for meteorological models,” *Monthly Weather Rev.*, vol. 117,  
1136 no. 3, pp. 536–549, 1989.
- 1137 [27] O. Merlin, J. P. Walker, A. Chehbouni, and Y. Kerr, “Towards deter-  
1138 ministic downscaling of SMOS soil moisture using MODIS derived soil  
1139 evaporative efficiency,” *Remote Sens. Environ.*, vol. 112, no. 10, pp. 3935–  
1140 3946, Oct. 2008. doi:10.1016/j.rse.2008.06.012.
- 1141 [28] M. S. Moran, T. R. Clarke, Y. Inoue, and A. Vidal, “Estimating crop water  
1142 deficit using the relation between surface-air temperature and spectral  
1143 vegetation index,” *Remote Sens. Environ.*, vol. 49, no. 3, pp. 246–263, 1994.  
1144
- [29] T. N. Carlson, R. R. Gillies, and E. M. Perry, “A method to make use of thermal infrared temperature and NDVI measurements to infer soil water content and fractional vegetation cover,” *Remote Sens. Rev.*, vol. 52, pp. 45–49, 1994.
- [30] O. Merlin, G. Chehbouni, J. P. Walker, R. Panciera, and Y. Kerr, “A simple method to disaggregate passive microwave based soil moisture,” *IEEE Trans. Geosci. Remote Sens.—SMOS Special Issue*, vol. 46, no. 3, pp. 786–796, Mar. 2008. doi:10.1109/TGRS.2007.914807.
- [31] W. P. Kustas and J. M. Norman, “Evaluation of soil and vegetation heat flux predictions using a simple two-source model with radiometric temperatures for partial canopy cover,” *Agricultural Forest Meteorol.*, vol. 94, no. 1, pp. 13–29, 1999.
- [32] M. C. Anderson, J. M. Norman, G. R. Diak, W. P. Kustas, and J. R. Mecikalski, “A two-source time-integrated model for estimating surface fluxes using thermal infrared remote sensing,” *Remote Sens. Environ.*, vol. 60, no. 2, pp. 195–216, May 1997.
- [33] O. Merlin and G. Chehbouni, “Different approaches in estimating heat flux using dual angle observations of radiative surface temperature,” *Int. J. Remote Sens.*, vol. 25, no. 1, pp. 275–289, 2004.
- [34] T. J. Lee and R. A. Pielke, “Estimating the soil surface specific humidity,” *J. Appl. Meteorol.*, vol. 31, no. 5, pp. 480–484, 1992.
- [35] T. S. Komatsu, “Towards a robust phenomenological expression of evaporation efficiency for unsaturated soil surfaces,” *J. Appl. Meteorol.*, vol. 42, no. 9, pp. 1330–1334, Sep. 2003.
- [36] O. Merlin, J. P. Walker, J. D. Kalma, E. J. Kim, J. Hacker, R. Panciera, R. Young, G. Summerell, J. Hornbuckle, M. Hafeez, and T. J. Jackson, “The NAFe’06 data set: Towards soil moisture retrieval at intermediate resolution,” *Adv. Water Resour.*, vol. 31, pp. 1444–1455, 2008. doi:10.1016/j.advwatres.2008.01.018.
- [37] Z. Wan and J. Dozier, “A generalized split-window algorithm for retrieving land-surface temperature from space,” *IEEE Trans. Geosci. Remote Sens.*, vol. 34, no. 4, pp. 892–905, Jul. 1996.
- [38] O. Merlin, A. Al Bitar, V. Rivalland, P. Béziat, E. Ceschia, and G. Dedieu, “An analytical model of evaporation efficiency for unsaturated soil surfaces with an arbitrary thickness,” *J. Appl. Meteorol. Climatol.*, vol. 50, no. 2, pp. 457–471, Feb. 2011. doi:10.1175/2010JAMC2418.1.
- [39] N. Agam, W. P. Kustas, M. C. Anderson, F. Li, and C. M. U. Neale, “A vegetation index based technique for spatial sharpening of thermal imagery,” *Remote Sens. Environ.*, vol. 107, no. 4, pp. 545–558, 2007.
- [40] E. E. Small and S. A. Kure, “Tight coupling between soil moisture and the surface radiation budget in semiarid environments: Implications for land-atmosphere interactions,” *Water Resour. Res.*, vol. 39, no. 10, p. 1278, Oct. 2003. doi:10.1029/2002WR001297.
- [41] C. Rüdiger, J. P. Walker, and Y. H. Kerr, “On the airborne spatial coverage requirement for microwave satellite validation,” *IEEE Geosci. Remote Sens. Lett.*, vol. 8, no. 4, pp. 824–828, Jul. 2011.
- [42] R. Young, J. Walker, N. Yeoh, A. Smith, K. Ellett, O. Merlin, and A. Western, *Soil Moisture and Meteorological Observations from the Murrumbidgee Catchment*. Melbourne, Australia: Dept. Civil Environ. Eng., Univ. Melbourne, 2008.
- [43] A. J. Teuling, R. Uijlenhoet, R. Hurkmans, O. Merlin, R. Panciera, J. Walker, and P. A. Troch, “Dry-end surface soil moisture variability during NAFe’06,” *Geophys. Res. Lett.*, vol. 34, no. L17402, Sep. 2007.
- [44] W. T. Crow and E. F. Wood, “The assimilation of remotely sensed soil brightness temperature imagery into a land surface model using Ensemble Kalman filtering: A case study based on ESTAR measurements during SGP97,” *Adv. Water Resour.*, vol. 26, pp. 137–149, 2003.
- [45] Q. K. Hassan, C. P.-A. Bourque, F.-R. Meng, and R. M. Cox, “A wetness index using terrain-corrected surface temperature and normalized difference vegetation index derived from standard MODIS products: An evaluation of its use in a humid forest-dominated region of eastern Canada,” *Sensors*, vol. 7, no. 10, pp. 2028–2048, 2007.

**Olivier Merlin**, photograph and biography not available at the time of publication.

**Christoph Rüdiger**, photograph and biography not available at the time of publication.

1211 **Ahmad Al Bitar**, photograph and biography not available at the time of  
1212 publication.

Jeffrey P. Walker, photograph and biography not available at the time of 1215  
1216 publication.

1213 **Philippe Richaume**, photograph and biography not available at the time of  
1214 publication.

Yann H. Kerr, photograph and biography not available at the time of 1217  
1218 publication.

IEEE  
Proof

## AUTHOR QUERIES

AUTHOR PLEASE ANSWER ALL QUERIES

Please be aware that the authors are required to pay overlength page charges (\$200 per page) if the paper is longer than 6 pages. If you cannot pay any or all of these charges please let us know.

AQ1 = Please provide publication update in Ref. [8].

AQ2 = Please provide volume, issue number, page range and month of publication in [20].

END OF ALL QUERIES

IEEE Proof

# Disaggregation of SMOS Soil Moisture in Southeastern Australia

Olivier Merlin, Christoph Rüdiger, Ahmad Al Bitar, Philippe Richaume, Jeffrey P. Walker, and Yann H. Kerr

**Abstract**—Disaggregation based on Physical And Theoretical scale Change (DisPATCh) is an algorithm dedicated to the disaggregation of soil moisture observations using high-resolution soil temperature data. DisPATCh converts soil temperature fields into soil moisture fields given a semi-empirical soil evaporative efficiency model and a first-order Taylor series expansion around the field-mean soil moisture. In this study, the disaggregation approach is applied to soil moisture and ocean salinity (SMOS) data over the 500 km by 100 km AACES (Australian Airborne Calibration/validation Experiments for SMOS) area. The 40-km resolution SMOS surface soil moisture pixels are disaggregated at 1-km resolution using the soil skin temperature derived from moderate resolution imaging spectroradiometer (MODIS) data, and subsequently compared with the AACES intensive ground measurements aggregated at 1-km resolution. The objective is to test DisPATCh under various surface and atmospheric conditions. It is found that the accuracy of disaggregation products varies greatly according to season: while the correlation coefficient between disaggregated and *in situ* soil moisture is about 0.7 during the summer AACES, it is approximately zero during the winter AACES, consistent with a weaker coupling between evaporation and surface soil moisture in temperate than in semi-arid climate. Moreover, during the summer AACES, the correlation coefficient between disaggregated and *in situ* soil moisture is increased from 0.70 to 0.85, by separating the 1-km pixels where MODIS temperature is mainly controlled by soil evaporation, from those where MODIS temperature is controlled by both soil evaporation and vegetation transpiration. It is also found that the 5-km resolution atmospheric correction of the official MODIS temperature data has a significant impact on DisPATCh output. An alternative atmospheric correction at 40-km resolution increases the correlation coefficient between disaggregated and *in situ* soil moisture from 0.72 to 0.82 during the summer AACES. Results indicate that

DisPATCh has a strong potential in low-vegetated semi-arid areas where it can be used as a tool to evaluate SMOS data (by reducing the mismatch in spatial extent between SMOS observations and localized *in situ* measurements), and as a further step, to derive a 1-km resolution soil moisture product adapted for large-scale hydrological studies.

**Index Terms**—AACES, calibration/validation, disaggregation, Disaggregation based on Physical And Theoretical scale Change (DisPATCh), field campaign, moderate resolution imaging spectroradiometer (MODIS), soil moisture and ocean salinity (SMOS).

## I. INTRODUCTION

PASSIVE MICROWAVE remote sensing has the capability to provide key elements of the terrestrial hydrological cycle such as surface soil moisture [1], [2] and overland precipitation [3], [4]. Nevertheless, due to the large discrepancy between the observation scale (several tens of km) and the scale of physical interactions with the land surface (one wavelength or several cm), the radiative transfer models applied to passive microwave remote sensing data are only semiphysically based. Consequently, the retrieval process of land surface parameters from microwave brightness temperatures requires ancillary data for calibration and validation purposes [5]. It also requires a strategy to use such ancillary data since ground-based sampling is often made over a small area/point, which constrains with the large integrated extent of spaceborne passive microwave observations.

The soil moisture and ocean salinity (SMOS), [6] satellite was launched on November 2, 2009. Over land, the SMOS mission aims at providing  $\sim 5$  cm surface soil moisture data at a spatial resolution better than 50 km and a repeat cycle of less than 3 days. The payload is a 2-D interferometer equipped with 69 individual L-band antennas regularly spaced along Y-shaped arms. This new concept allows observing all pixels in the 1000 km wide field of view at a range of incidence angles. It also allows reconstructing brightness temperatures on a fixed sampling grid [7].

Since the SMOS launch, various field experiments (the HOBE site in Denmark [8], the Mali site in Western Africa [9], the SMOSMANIA site in Southwestern France [10] just to name a few) have been undertaken to validate SMOS reconstructed brightness temperatures and soil moisture retrievals. The AACES (Australian Airborne Calibration/validation Experiment for SMOS, [11]) is one of the most comprehensive campaigns worldwide dedicated to SMOS calibration/validation. A series of two experiments were undertaken in 2010, AACES-1 in January–February (Austral summer) and

Manuscript received March 31, 2011; revised September 1, 2011; accepted October 30, 2011. The AACES participants are gratefully acknowledged for their participation in collecting this extensive data set. The Australian Airborne Calibration/validation Experiments for SMOS have been made possible through infrastructure (LE0453434) and research (DP0879212) funding from the Australian Research Council, and the collaboration of a large number of scientists from throughout Australia, United States and Europe. Initial setup and maintenance of the study catchments was funded by two research Grants (DP0343778, DP0557543) from the Australian Research Council and by the CRC for Catchment Hydrology. This work was funded by the CNES TOSCA (Terre solide, Océan, Surfaces Continentales et Atmosphère) program and the Centre National de la Recherche Scientifique.

O. Merlin is with the Centre d'Etudes Spatiales de la Biosphère (CESBIO), 31401 Toulouse, France (e-mail: olivier.merlin@cesbio.cnes.fr).

C. Rüdiger (e-mail: chris.rudiger@monash.edu).

A. Al Bitar (e-mail: ahmad.albitar@cesbio.cnes.fr).

P. Richaume (e-mail: philippe.richaume@cesbio.cnes.fr).

J. P. Walker (e-mail: jeff.walker@monash.edu).

Y. H. Kerr (e-mail: yann.kerr@cesbio.cnes.fr).

Color versions of one or more of the figures in this paper are available online at <http://ieeexplore.ieee.org>.

Digital Object Identifier 10.1109/TGRS.2011.2175000

83 AACES-2 in September (Austral winter). The data collected  
 84 in AACES include 1-km resolution airborne L-band brightness  
 85 temperature mapped over a 500 km by 100 km area, 20 days  
 86 of very intensive ground measurements and 20 5 km by 2 km  
 87 ground sampling areas.

88 Even though the AACES ground measurements are very  
 89 extensive, it is not feasible to cover the whole extent of a  
 90 SMOS pixel by ground sampling alone. This is the reason why  
 91 most validation strategies of spaceborne passive microwave  
 92 data using *in situ* measurements have been based on the as-  
 93 sumption that local observations are representative of a much  
 94 larger spatial extent (i.e., the size of a microwave pixel). In the  
 95 heterogeneous case where this assumption does not hold, up-  
 96 scaling approaches [12], [13] have been developed to relate the  
 97 available ground observations to satellite scale soil moisture.  
 98 Such approaches are very useful over sites which have been  
 99 monitored for a long time and where extensive measurements  
 100 have been made over a range of spatial scales. However, aggrega-  
 101 tion rules are difficult to build over sites which have been set  
 102 up recently, or where no extensive field campaigns have been  
 103 undertaken.

104 This study develops a methodology to facilitate the cali-  
 105 bration and validation of SMOS data using localized ground  
 106 measurements, such as those collected during AACES. The  
 107 methodology combines upscaling (aggregation) and downscal-  
 108 ing (disaggregation) approaches to make remote sensing and  
 109 *in situ* observations match at an intermediate spatial resolution  
 110 of 1 km. The key step in the procedure is a disaggregation  
 111 algorithm of passive microwave soil moisture using kilometric  
 112 optical data [14]–[16]. Disaggregating SMOS soil moisture can  
 113 solve the disparity of spatial scales between satellite and *in situ*  
 114 observations. However, the validation of spaceborne data by  
 115 means of a disaggregation approach requires the uncertainties  
 116 and potential error sources in downscaled data to be assessed.  
 117 Generally speaking, disaggregation is a compromise between  
 118 downscaling resolution and accuracy. The higher downscaling  
 119 resolution, the more disaggregated values are spatially repre-  
 120 sentative of ground observations, but typically have a lower  
 121 accuracy and vice versa [17]. In this context, a disaggrega-  
 122 tion algorithm named Disaggregation based on Physical And  
 123 Theoretical scale Change (DisPATCH) is applied to 40-km  
 124 resolution SMOS soil moisture over the AACES area using 1-  
 125 km resolution Moderate resolution Imaging Spectroradiometer  
 126 (MODIS) data. The objective is to test DisPATCH under various  
 127 surface and atmospheric conditions. Specifically, the impact  
 128 of climatic (evaporative demand), meteorologic (presence of  
 129 clouds), and vegetation (cover and water status) conditions on  
 130 1-km resolution disaggregated soil moisture is evaluated both  
 131 qualitatively by visual assessment of disaggregation images and  
 132 quantitatively by comparing DisPATCH output with AACES  
 133 intensive ground measurements.

134 The AACES, SMOS, and MODIS data used in this study  
 135 are first described. Next, the disaggregation methodology is  
 136 presented followed by a step-by-step description of the Dis-  
 137 PATCH algorithm. Results of the comparison between disag-  
 138 ggregated SMOS soil moisture and *in situ* measurements are  
 139 then reported. To test DisPATCH under various surface and  
 140 atmospheric conditions, the algorithm is run during AACES-1

and AACES-2 in different modes, by including (or not) a 141  
 correction for vegetation and atmospheric effects. Finally, some 142  
 perspectives in the use of DisPATCH for validating SMOS data 143  
 using ground-based sampling are given. 144

## II. DATA COLLECTION AND PREPROCESSING 145

The AACES experiments were planned to provide ground 146  
 and airborne soil moisture data over an area of approximately 147  
 500 km by 100 km during the two main seasons in the 148  
 Murrumbidgee river catchment, in southeastern Australia. The 149  
 first AACES campaign (AACES-1) was undertaken in summer 150  
 2010 from January 18 to February 21, and the second campaign 151  
 (AACES-2) was undertaken in the following Austral winter 152  
 from September 11 to September 24 [11]. Fig. 1 presents the 153  
 study area including the 20 5 km by 2 km ground sampling 154  
 focus areas. The background image is the MODIS 250-m res- 155  
 olution 16-day normalized difference vegetation index (NDVI) 156  
 product of February 2, 2010. The climate of the Murrumbidgee 157  
 catchment area ranges from semi-arid in the west to alpine in 158  
 the east, with a strong rainfall and potential evapotranspiration 159  
 gradient in the west-east direction. Land use is extensive graz- 160  
 ing in the west, cropping in the center, and mostly grazing/forest 161  
 in the east (refer to [11] for a detailed account of AACES). 162

### A. HDAS 163

During both AACES-1 and AACES-2, a spatially enabled 164  
 platform (Hydraprobe Data Acquisition System, HDAS) was 165  
 used to collect extensive measurements of near-surface soil 166  
 moisture. HDAS is a handheld system combining a soil dielec- 167  
 tric sensor (Hydraprobe) and a pocket PC with GPS receiver, 168  
 allowing for direct storage of location and measurement within 169  
 the GIS software. HDAS measurements were calibrated using 170  
 the approach presented in [18] with a root mean square error 171  
 of point estimate of about  $0.03 \text{ m}^3/\text{m}^3$ . The sampling coverage 172  
 was two 5 km by 2 km farms per day during AACES-1 and one 173  
 5 km by 2 km farm per day during AACES-2. Within each farm, 174  
 a total of six adjacent 5 km long transects separated by 330 m 175  
 were walked to cover each area of  $10 \text{ km}^2$ , and three separate 176  
 HDAS measurements were made along transects every 50 m. 177

In this study, HDAS soil moisture data are aggregated at 178  
 1-km resolution by averaging all measurements made within 179  
 each pixel of the MODIS resolution grid. Out of concern for 180  
 spatial representativeness of *in situ* observations, only the 1-km 181  
 pixels whose ground sampling covers more than two third of 182  
 its surface area are kept for comparison with disaggregation 183  
 results. The 1-km average of HDAS measurements is denoted 184  
 $\langle \text{SM}_{\text{HDAS}} \rangle$  and the standard deviation of *in situ* measurements 185  
 (denoted  $\sigma_{\text{HDAS}}$ ) computed to estimate the subpixel variability 186  
 at 1-km resolution. 187

### B. SMOS 188

The version-4 SMOS level-2 soil moisture product is used. 189  
 This product (released on March 24, 2011) was produced from 190  
 the reprocessed level 1C data, and the version-4 level-2 soil 191  
 moisture algorithm. SMOS has a 6 am (ascending) and 6 pm 192

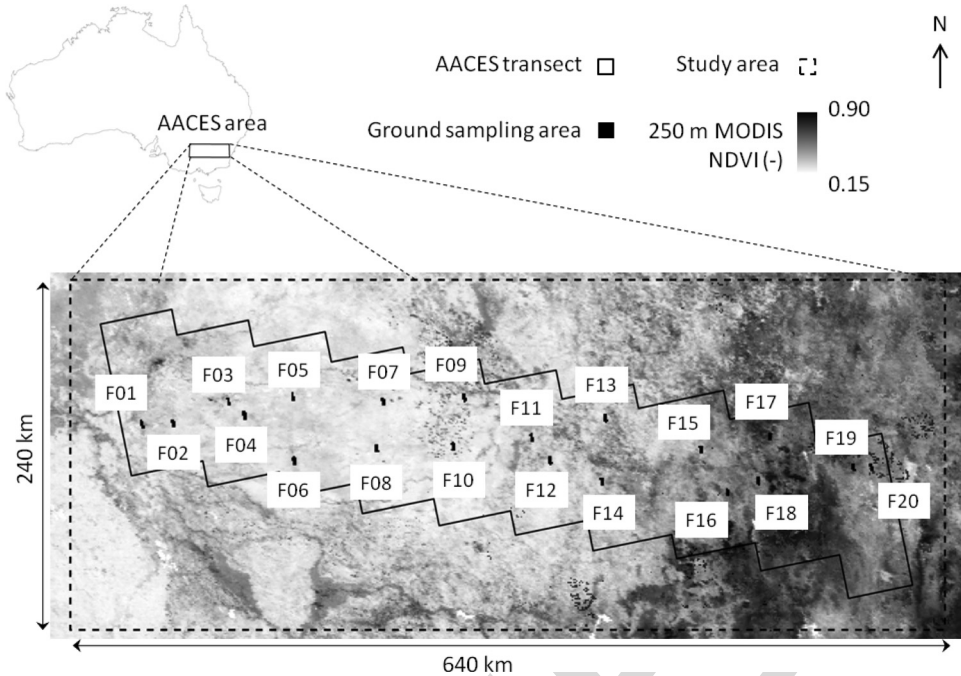


Fig. 1. Overview of the study area. During AACES, ten 100 km by 50 km patches were overflown by an airborne L-band radiometer. Within each patch, two 5 km by 2 km subareas were sampled to collect spatial soil moisture measurements. In this study, DisPATCH is run over a 640 by 240 km area including the whole AACES area, and disaggregation results are evaluated over the ground sampling areas.

193 (descending) equator crossing time. The sampling grid of the  
 194 SMOS level-2 soil moisture product is called DGG or discrete  
 195 global grid [19], [20] and has a node separation of about  
 196 15 km. The DGG provides a discretization that is higher than  
 197 the SMOS natural pixel size, which is 40 km on average,  
 198 ranging from 30 km at boresight to 90 km at high incidence  
 199 angles. In this study, the disaggregation procedure takes advan-  
 200 tage of the oversampling of SMOS data to potentially reduce  
 201 (and provide an estimate of) random errors in disaggregated  
 202 SMOS data. Instead of using a single snapshot SMOS im-  
 203 age, DisPATCH uses four (overlapping) independent snapshots,  
 204 which are generated by: 1) sliding a 40-km resolution grid; and  
 205 2) extracting the DGG nodes approximately centered on each  
 206 40 km pixel. The extraction of SMOS DGG nodes is presented  
 207 in [21]. The DGG node(s) that fall(s) near the center of the  
 208 40-km resolution pixels with a  $\pm 10$ -km tolerance are se-  
 209 lected. If more than one DGG is selected, the associated soil  
 210 moisture values are averaged to produce a single value for each  
 211 40-km resolution pixel. The 40-km resolution grid that fits the  
 212 study area corresponds to what is termed here Resampling 1.  
 213 Similarly, Resampling 2, 3, and 4 are performed by sliding the  
 214 40-km resolution grid to coordinates  $(+20 \text{ km}, 0)$ ,  $(0, -20 \text{ km})$ ,  
 215 and  $(+20 \text{ km}, -20 \text{ km})$ , respectively. The four 40-km resolu-  
 216 tion SMOS data sets are then used independently as input to  
 217 DisPATCH.

### 218 C. MODIS

219 The MODIS data used in this paper are composed of:

- 220 • Version-5 MODIS/Terra land surface temperature and  
 221 emissivity daily level-3 global 1-km grid product  
 222 (MOD11A1) and version-5 MODIS/Aqua land surface

temperature and emissivity daily level-3 global 1-km grid 223  
 product (MYD11A1). The land surface temperature data 224  
 set is the main component of DisPATCH. It is used to 225  
 estimate 1-km resolution soil evaporative efficiency at 226  
 10 am (Terra data) and 1 pm (Aqua data) [22]. 227

- Version-5 MODIS/Terra vegetation indices 16-day level-3 228  
 global 1-km grid product (MOD13A2). The NDVI data set 229  
 is used in DisPATCH to estimate the fractional vegetation 230  
 cover at 1-km resolution [23]. 231
- Version-5 MODIS/Terra+Aqua albedo 16-day level-3 232  
 global 1-km grid product (MCD43B3). The surface albedo 233  
 data set is used in DisPATCH to estimate the vegetation 234  
 temperature at maximum water stress from the space land 235  
 surface temperature albedo [24]. The MCD43B3 product 236  
 provides 1-km data describing both directional hemispher- 237  
 ical reflectance (black-sky albedo) at local solar noon 238  
 and bihemispherical reflectance (white-sky albedo). In this 239  
 study, surface albedo refers to the MODIS shortwave white 240  
 sky albedo. 241
- MODIS/Terra level-1B calibrated radiances swath 1-km 242  
 grid product (MOD021KM) and MODIS/Aqua level- 243  
 1B calibrated radiances swath 1-km grid product 244  
 (MYD021KM). The radiance data set is used to derive 245  
 a land surface temperature data set that differs from the 246  
 official MOD11A1 and MYD11A1 products with respect 247  
 to atmospheric correction. 248

Products MOD11A1, MYD11A1, MOD13A2, and 249  
 MCD43B3 were downloaded through the NASA Warehouse 250  
 Inventory Search Tool (WIST <http://wist.echo.nasa.gov/>) and 251  
 products MOD021KM and MYD021KM were downloaded 252  
 through the NASA Level 1 and Atmosphere Archive and Dis- 253  
 tribution System (LAADS <http://ladsweb.nascom.nasa.gov>). 254

TABLE I  
SCALE AND OFFSET VALUES USED TO CONVERT TERRA (AND AQUA)  
MODIS RADIANCE DATA TO PHYSICAL RADIANCE  
VALUES OVER THE AACES AREA

Thermal band	Scale ( $\text{W m}^{-2} \text{ sr}^{-1}$ )	Offset (-)
31	$8.4002 \cdot 10^{-4}$ ( $6.5081 \cdot 10^{-4}$ )	1577 (2036)
32	$7.2970 \cdot 10^{-4}$ ( $5.7100 \cdot 10^{-4}$ )	1658 (2119)

255 All products were projected in UTM 55 South with a sampling  
256 interval of 1000 m using the MODIS reprojection tool.

257 The level-1B calibrated radiance data ( $R_{31}$  and  $R_{32}$  for bands  
258 31 and 32, respectively) were converted from digital number  
259 (DN) to radiance in  $\text{W m}^{-2} \text{ sr}^{-1}$  using the radiance scales and  
260 offsets provided with each MODIS granule as listed in Table I

$$R_\lambda = \text{Scale}_\lambda \times (\text{DN}_\lambda - \text{Offset}_\lambda) \quad (1)$$

261 The radiance values were then converted to brightness temper-  
262 ature in K using the inverse of the Planck function [25]

$$Tb_\lambda = \frac{c_2}{\lambda \ln \left( 1 + \frac{c_1}{R_\lambda \lambda^5} \right)} \quad (2)$$

263 with  $c_1 = 1.19107 \times 10^8 \mu\text{m}^5 \text{ W m}^{-2} \text{ sr}^{-1}$  and  $c_2 =$   
264  $1.43883 \times 10^4 \mu\text{m K}$ , for center wavelength of the given band  
265 (11.0186  $\mu\text{m}$  and 12.0325  $\mu\text{m}$  for 31 and 32 band, respectively).

#### 266 D. Overlapping HDAS, SMOS, and MODIS Data and 267 Generating an Input Data Set

268 As indicated in Table II, HDAS soil moisture, SMOS soil  
269 moisture, and cloud-free MODIS land surface temperature data  
270 have overlapped on five days during AACES-1 (on January  
271 28 and 30 and February 15, 18, and 20) and on five days  
272 during AACES-2 (on September 11, 13, 21, 22, and 24). On  
273 each sampling day, two farms were sampled during AACES-1  
274 (except on February 18 when three farms were sampled), and  
275 one farm was sampled during AACES-2, so that disaggregation  
276 results can be evaluated for ten date-farm units during AACES-  
277 1 and five date-farm units during AACES-2.

278 DisPATCh is applied to an input ensemble composed of the  
279 different combinations of available SMOS (ascending orbit at  
280 6 am and/or descending orbit at 6 pm) and MODIS (onboard  
281 Terra platform at 10 am and/or Aqua platform at 1 pm) data. To  
282 increase the quantity of input data sets, the MODIS data col-  
283 lected on the day before and the day after the SMOS overpass  
284 date are also included. For SMOS data on day of year (DoY)  
285 51, the clear sky MODIS data collected on DoY 54 are used.  
286 Note that one implicitly assumes that no rainfall occurs between  
287 MODIS and SMOS overpasses, and that the spatial variability  
288 captured by MODIS is relatively similar to the actual variabil-  
289 ity of surface soil moisture at the time of SMOS overpass.  
290 Moreover, the SMOS data oversampling is used to generate  
291 four (overlapping) 40-km resolution SMOS grids on which  
292 DisPATCh is run independently, thus increasing the number  
293 of downscaled data that could be used in the validation. It is  
294 reminded that the spacing (about 15 km) between neighboring  
295 SMOS DGG nodes is smaller than the SMOS resolution (about

40 km). By combining the four SMOS grids, the two potential 296 SMOS data sets (two orbits in one day) and the six potential 297 MODIS data sets (three days including two overpasses each), 298 the maximum number of input data sets is 48. The generation 299 of input data sets is shown in Fig. 2 and the number of daily 300 input data sets is indicated for each date-farm unit in Table II. 301

### III. DISAGGREGATION ALGORITHM

DisPATCh converts 1-km resolution MODIS-derived soil 303 temperature fields into 1-km resolution surface soil moisture 304 fields given a semi-empirical soil evaporative efficiency model 305 [26] and a first-order Taylor series expansion around the 306 40-km resolution SMOS observation. DisPATCh is an im- 307 proved version of the algorithms in [16] and [27], and mainly 308 differs with regard to the representation of the vegetation water 309 status. In previous versions [16], [27], the soil temperature was 310 derived from MODIS land surface temperature by assuming 311 that vegetation was unstressed so that vegetation temperature 312 was uniformly set to the minimum surface temperature ob- 313 served within the SMOS pixel. In this study, the approach in 314 [28] is implemented to take into account vegetation water status 315 in the estimation of soil temperature. 316

#### A. Disaggregation Methodology

The disaggregation procedure decouples the soil evaporation 318 from the 0–5 cm soil layer and the vegetation transpiration 319 from the root-zone soil layer by separating MODIS surface 320 temperature into its soil and vegetation components as in the 321 triangle or trapezoidal method [28], [29]. MODIS-derived soil 322 temperature is then used to estimate soil evaporative efficiency, 323 which is known to be relatively constant during the day on clear 324 sky conditions. MODIS-derived soil evaporative efficiency is 325 finally used as a proxy for surface (0–5 cm) soil moisture 326 variability within the SMOS pixel. The link between surface 327 soil moisture and soil evaporative efficiency at different scales 328 is ensured by a downscaling relationship and a soil evapo- 329 rative efficiency model, as described below in more detail. 330 The originality of DisPATCh relies on a dynamical land cover 331 classification (based on the hourglass approach in [28]) that 332 takes into account the subpixel variability of the sensitivity of 333 soil evaporative efficiency to surface soil moisture. 334

1) Downscaling Relationship: The downscaling relation- 335 ship can be written as 336

$$\text{SM}_{1 \text{ km}} = \text{SM}_{\text{SMOS}} + \frac{\partial \text{SM}_{\text{mod}}}{\partial \text{SEE}} \times (\text{SEE}_{\text{MODIS}, 1 \text{ km}} - \langle \text{SEE}_{\text{MODIS}, 1 \text{ km}} \rangle_{40 \text{ km}}) \quad (3)$$

with  $\text{SM}_{\text{SMOS}}$  being the SMOS soil moisture (for clarity, 337 the variables defined at SMOS scale are written in bold), 338  $\text{SEE}_{\text{MODIS}}$  the MODIS-derived soil evaporative efficiency (ra- 339 tio of actual to potential evaporation),  $\langle \text{SEE}_{\text{MODIS}} \rangle_{40 \text{ km}}$  its 340 average within a SMOS pixel and  $\partial \text{SM}_{\text{mod}} / \partial \text{SEE}$  the partial 341 derivative evaluated at SMOS scale of soil moisture with re- 342 spect to soil evaporative efficiency. Note that the linearity of (3) 343 implies that a possible bias in SMOS data would produce the 344

TABLE II  
LIST OF OVERLAPPING HDAS, SMOS, AND MODIS (MOD11A1 AND MYD11A1) DATA DURING AACES-1 AND AACES-2. ONLY THE SMOS DATA COLLECTED ON THE SAME DAY AS GROUND SAMPLING HAVE BEEN CONSIDERED. THE MODIS DATA CONSIDERED AS INPUT TO DisPATCH HAVE BEEN COLLECTED WITHIN PLUS OR MINUS ONE DAY EITHER SIDE THE GROUND SAMPLING (AND SMOS OVERPASS) DATE. ON EACH SAMPLING DATE, THE RESULTANT NUMBER OF INPUT DATA SETS TO DisPATCH IS ALSO INDICATED

Experiment	Sampling date	DoY	Farm	SMOS overpass time	Cloud free MODIS data (DoY)	Number of input data sets to DisPATCH
AACES-1	28 January	28	F05	6 am	Terra (27,29) & Aqua (29)	3
	30 January	30	F07	6 am	Terra (29,30) & Aqua (29)	12
	,	,	F08	6 am	Terra (29,30) & Aqua (29)	9-12
	15 February	46	F15	6 am & 6 pm	Terra (46) & Aqua (47)	8-14
	,	,	F16	6 am & 6 pm	Terra (46) & Aqua (47)	8-10
	18 February	49	F17	6 am & 6 pm	Terra (48,50) & Aqua (48,49,50)	30-38
	,	,	F18	6 am & 6 pm	Terra (48,50) & Aqua (48,49,50)	24-30
	,	,	F20	6 am & 6 pm	Terra (48,50) & Aqua (48,49,50)	34-40
	20 February	51	F19	6 am & 6 pm	Terra (54) & Aqua (54)	6-8
	,	,	F20	6 am & 6 pm	Terra (54) & Aqua (54)	16
AACES-2	11 September	254	F09	6 am & 6 pm	Terra (253,254) & Aqua (254)	6-14
	13 September	256	F07	6 am & 6 pm	Terra (256)	8
	21 September	264	F13	6 am & 6 pm	Terra (263) & Aqua (264)	16
	22 September	265	F15	6 am & 6 pm	Terra (265) & Aqua (264,266)	16
	24 September	267	F09	6 am & 6 pm	Terra (267) & Aqua (266,267,268)	24-32

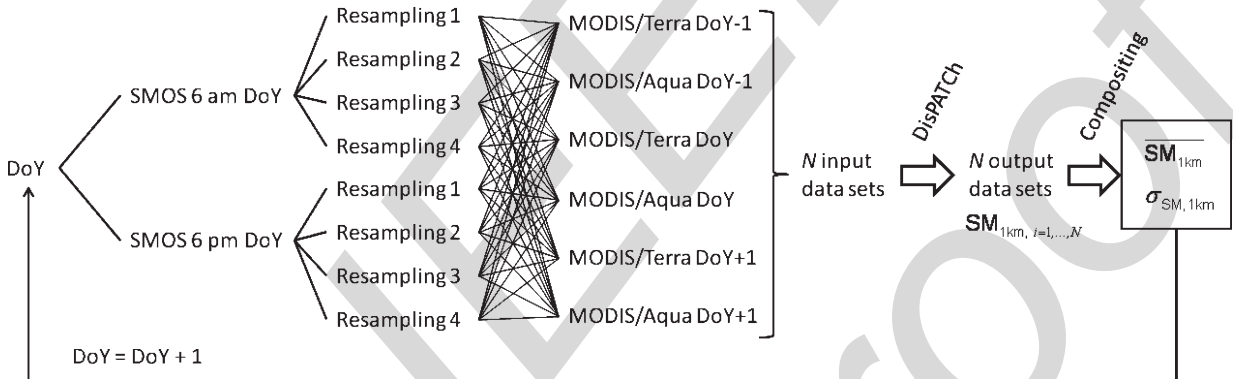


Fig. 2. Schematic diagram presenting the combination of SMOS and MODIS to generate an ensemble of input data to DisPATCH. The output data are composited at 1-km resolution by computing the average ( $\overline{SM}_{1\text{ km}}$ ) and standard deviation ( $\sigma_{SM,1\text{ km}}$ ) of disaggregated SMOS soil moisture.

345 same bias in disaggregated data [30]. Consequently, although 346 the possible presence of a bias in SMOS data limits the accuracy 347 in the disaggregated soil moisture, it is not a limiting factor to 348 the applicability of DisPATCH. MODIS derived soil evaporative 349 efficiency is expressed as a linear function of soil temperature

$$SEE_{\text{MODIS},1\text{ km}} = \frac{T_{s,\text{max}} - T_{s,1\text{ km}}}{T_{s,\text{max}} - T_{s,\text{min}}} \quad (4)$$

350 with  $T_s$  being the MODIS-derived soil skin temperature, 351  $T_{s,\text{max}}$  the soil skin temperature at  $SEE = 0$  and  $T_{s,\text{min}}$  352 the soil skin temperature at  $SEE = 1$ . The linearity of the 353 relationship between soil evaporative efficiency and surface 354 soil temperature was verified using the physically based dual 355 source energy budget model in [31] using a synthetic data set 356 composed of a range of surface soil moisture values and differ- 357 ent atmospheric conditions (results not shown). End-members 358  $T_{s,\text{min}}$  and  $T_{s,\text{max}}$  are estimated from the polygons obtained

by plotting MODIS surface temperature against MODIS NDVI 359 and MODIS albedo as in [24]. Derivation of soil temperature is 360 based on a linear decomposition of the surface temperature into 361 its soil and vegetation components as a good approximation of 362 the relationship with fourth power for temperatures [32], [33] 363 and consistent with the triangle method. MODIS-derived soil 364 skin temperature is expressed as 365

$$T_{s,1\text{ km}} = \frac{T_{\text{MODIS}} - f_{v,1\text{ km}} T_{v,1\text{ km}}}{1 - f_{v,1\text{ km}}} \quad (5)$$

with  $T_{\text{MODIS}}$  being the 1-km resolution MODIS land sur- 366 face temperature,  $f_v$  the MODIS-derived fractional vegetation 367 cover, and  $T_v$  the vegetation temperature. In this study, vegeta- 368 tion temperature is estimated using the approach proposed by 369 [28]. In (5), fractional vegetation cover is written as 370

$$f_{v,1\text{ km}} = \frac{\text{NDVI}_{\text{MODIS}} - \text{NDVI}_s}{\text{NDVI}_v - \text{NDVI}_s} \quad (6)$$

371 with  $\text{NDVI}_{\text{MODIS}}$  being the 1-km resolution MODIS NDVI,  
 372  $\text{NDVI}_s$  the NDVI corresponding to bare soil, and  $\text{NDVI}_v$  the  
 373 NDVI corresponding to full-cover vegetation. Minimum and  
 374 maximum NDVI values are set to 0.15 and 0.90, respectively.

375 In [16], the accuracy and robustness of the disaggregation  
 376 methodology were tested using three different formulations of  
 377 soil evaporative efficiency [26], [34], [35]. Results based on the  
 378 NAFE'06 data set [36], which was collected over a 60 km by  
 379 40 km area in the AACES area, indicated that the model in  
 380 [26] was better adapted for conditions where soil properties are  
 381 unknown at high resolution. Consequently, the partial derivative  
 382 in (3) is computed using the soil evaporative efficiency model  
 383 in [26]

$$\text{SEE}_{\text{mod}} = \frac{1}{2} - \frac{1}{2} \cos(\pi \cdot \text{SM}/\text{SM}_p) \quad (7)$$

384 with  $\text{SM}_p$  being a soil parameter (in soil moisture unit). In  
 385 [26],  $\text{SM}_p$  was set to the soil moisture at field capacity. In  
 386 DisPATCH,  $\text{SM}_p$  is retrieved at 40-km resolution from SMOS  
 387 and aggregated MODIS data [16]. By inverting (7), one obtains

$$\text{SM}_{\text{mod}} = \frac{\text{SM}_p}{\pi} \cos^{-1}(1 - 2 \text{SEE}) \quad (8)$$

388 2) *Vegetation Temperature*: Vegetation temperature in (5) is  
 389 estimated at 1-km resolution with the “hourglass” approach in  
 390 [28]. By plotting the diagonals in the quadrilateral in Fig. 3,  
 391 four areas are distinguished in the space defined by surface  
 392 temperature and fractional vegetation cover. In zone A, land  
 393 surface temperature is mainly controlled by soil evaporation  
 394 leading to optimal sensitivity to surface soil moisture. In zone  
 395 D, land surface temperature is mainly controlled by vegetation  
 396 transpiration with no sensitivity to surface soil moisture. In  
 397 zones B and C, land surface temperature is controlled by both  
 398 soil evaporation and vegetation transpiration with intermediate  
 399 (average) sensitivity to surface soil moisture. Based on this un-  
 400 derstanding, vegetation temperature is estimated in a different  
 401 manner in each zone.

402 For a given data point located in Zone A, vegetation temper-  
 403 ature is

$$T_{v,1 \text{ km}} = (\text{T}_{v,\text{min}} + \text{T}_{v,\text{max}})/2 \quad (9)$$

404 with  $\text{T}_{v,\text{min}}$  and  $\text{T}_{v,\text{max}}$  being the vegetation temperature  
 405 at minimum and maximum water stress, respectively. End-  
 406 members  $\text{T}_{v,\text{min}}$  and  $\text{T}_{v,\text{max}}$  are estimated from the poly-  
 407 gons obtained by plotting MODIS surface temperature against  
 408 MODIS NDVI and MODIS albedo as in [24].

409 For a given data point located in Zone B, vegetation temper-  
 410 ature is

$$T_{v,1 \text{ km}} = (T_{v,\text{min},1 \text{ km}} + \text{T}_{v,\text{max}})/2 \quad (10)$$

411 with  $T_{v,\text{min},1 \text{ km}}$  being the vegetation temperature associated  
 412 with  $\text{SEE} = 0$  ( $\text{T}_s = \text{T}_{s,\text{max}}$ ).

413 For a given data point located in Zone C, vegetation temper-  
 414 ature is

$$T_{v,1 \text{ km}} = (\text{T}_{v,\text{min}} + T_{v,\text{max},1 \text{ km}})/2 \quad (11)$$

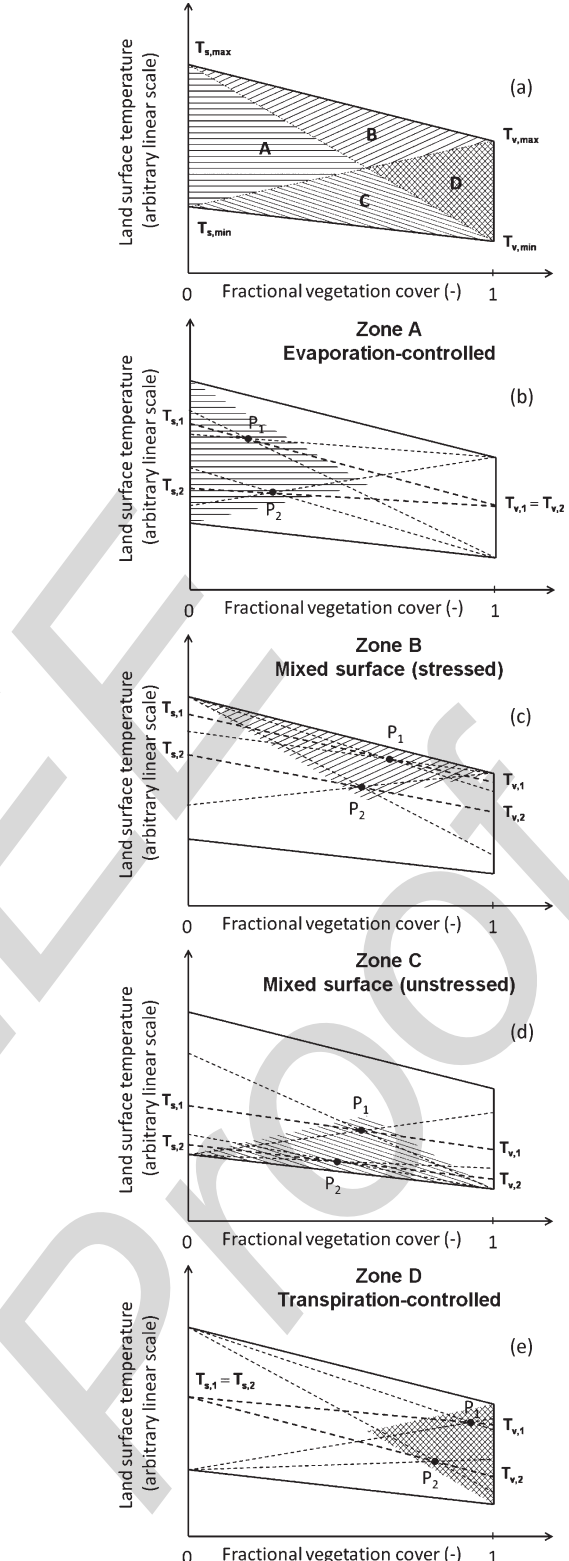


Fig. 3. Polygon defined in the land surface temperature-fractional vegetation cover space contains four distinct zones A, B, C, and D. In Zone A (soil-dominated area), the estimated vegetation temperature is constant leading to optimal sensitivity of estimated soil temperature to surface soil moisture. In Zone D, the estimated soil temperature is constant with no sensitivity to surface soil moisture. In Zone B and C (mixed surface), surface temperature is both controlled by soil evaporation and vegetation transpiration with intermediate (average) sensitivity of estimated soil temperature to surface soil moisture. DisPATCH can be run in the Zone A+B+C mode or in the Zone A only mode.

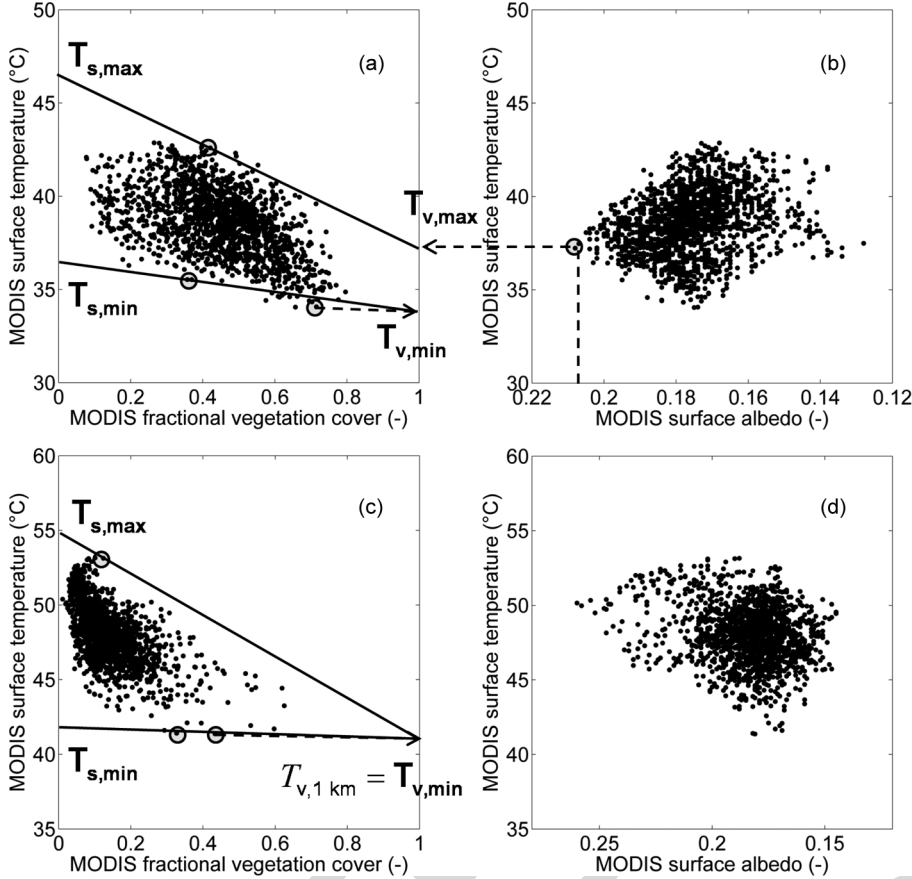


Fig. 4. Temperature end-members  $T_{s,\min}$ ,  $T_{s,\max}$ ,  $T_{v,\min}$  and  $T_{v,\max}$  are estimated from the surface temperature-fractional vegetation cover space and the surface temperature-surface albedo space within two given SMOS pixels. In (b), the pixel corresponding to the largest MODIS albedo has a fractional vegetation cover larger than 0.5, so that  $T_{v,\max}$  is set to its surface temperature. In (d), the pixel corresponding to the largest MODIS albedo has a fractional vegetation cover lower than 0.5, so that  $T_{v,\max}$  is set to  $T_{v,\min}$ .

415 with  $T_{v,\max,1\text{ km}}$  being the vegetation temperature associated  
 416 with SEE = 1 ( $T_s = T_{s,\min}$ ).

417 For a given data point located in Zone D, vegetation temper-  
 418 ature is

$$T_{v,1\text{ km}} = (T_{v,\min,1\text{ km}} + T_{s,\max,1\text{ km}})/2 \quad (12)$$

419 3) End-Members: End-members  $T_{s,\min}$ ,  $T_{s,\max}$ ,  $T_{v,\min}$   
 420 and  $T_{v,\max}$  are estimated by combining the spatial information  
 421 provided by the surface temperature-fractional vegetation cover  
 422 space and the surface temperature-albedo space plotted using  
 423 MODIS data collected in a 40-km resolution SMOS pixel. An  
 424 illustration is provided in Fig. 4 for two given SMOS pixels.

- 425 •  $T_{v,\min}$ : the vegetation temperature at minimum vegeta-  
 426 tion water stress is set to the minimum MODIS surface  
 427 temperature in the SMOS pixel [see Fig. 4(a) and (c)].  
 428 •  $T_{v,\max}$ : the vegetation temperature at maximum vegeta-  
 429 tion water stress is set to the MODIS surface temperature  
 430 of the pixel with the maximum value of MODIS albedo in  
 431 the SMOS pixel [see Fig. 4(b)]. If the fractional vegeta-  
 432 tion cover of that pixel is lower than 0.5 [see Fig. 4(d)], the  
 433 vegetation temperature at maximum vegetation water stress  
 434 is alternatively set to  $T_{v,\min}$ , meaning that vegetation is  
 435 unstressed within the SMOS pixel. The condition based  
 436 on fractional vegetation cover is lower than 0.5 aims to  
 437 increase the robustness of the determination approach of

438  $T_{v,\max}$ , particularly in the SMOS pixels where all surface  
 439 conditions are not met.

- 440 •  $T_{s,\min}$ : the soil temperature at SEE = 0 is extrapolated  
 441 along the wet soil edge at  $f_v = 0$ . The wet soil edge  
 442 is defined as the line passing through  $(1, T_{v,\min})$  and  
 443 through the data point such that all the data points with  
 444  $f_v < 0.5$  are located above the wet soil edge [see Fig. 4(a)  
 445 and (c)].
- 446 •  $T_{s,\max}$ : the soil temperature at SEE = 0 is extrapolated  
 447 along the dry soil edge at  $f_v = 0$ . The dry soil edge  
 448 is defined as the line passing through  $(1, T_{v,\max})$  and  
 449 through the data point such that all the data points with  
 450  $f_v < 0.5$  are located below the dry soil edge [see Fig. 4(a)  
 451 and (c)].

#### B. Atmospheric Correction

452 In MOD11A1 and MYD11A1 products, the land surface  
 453 temperature is derived from MODIS thermal radiances using  
 454 the split window algorithm [37].

$$T_{\text{MODIS}} = C + \left( A_1 + A_2 \frac{1 - \epsilon}{\epsilon} + A_3 \frac{\Delta\epsilon}{\epsilon^2} \right) \frac{Tb_{31} + Tb_{32}}{2} \\ + \left( B_1 + B_2 \frac{1 - \epsilon}{\epsilon} + B_3 \frac{\Delta\epsilon}{\epsilon^2} \right) \frac{Tb_{31} - Tb_{32}}{2} \quad (13)$$

456 with  $T_{b31}$  and  $T_{b32}$  being the brightness temperatures measured in the MODIS bands 31 and 32, respectively,  $\epsilon_{31}$  and  $\epsilon_{32}$  the surface emissivities estimated in the respective bands, and  $A_1, A_2, A_3, B_1, B_2, B_3$ , and  $C$  regression coefficients. These coefficients are available during algorithm execution via a look up table stratified by subranges of near surface air temperature and total column water vapor. These input field are obtained at 463 a 5-km resolution from the MODIS07\_L2 product.

464 Given that regression coefficients in (13) are provided at 465 5-km resolution, the atmospheric corrections on the MODIS 466 land surface temperature product are actually made at 5-km 467 resolution. To test whether atmospheric corrections on MODIS 468 temperature have an impact on disaggregation results, a different 469 procedure is proposed to obtain another temperature data set whose atmospheric corrections are operated at the scale 471 of a SMOS pixel, i.e., at 40-km resolution (instead of 5-km 472 resolution for the official MODIS temperature product). The 473 approach is to normalize the mean MODIS radiance-derived 474 brightness temperature at the SMOS resolution. Normalization 475 is done by adjusting the minimum and maximum mean MODIS 476 brightness temperature to the minimum and maximum value 477 of the official MODIS land surface temperature product within 478 the SMOS pixel, respectively. The new temperature noted 479  $T_{\text{MODIS}}^{\text{unif. corr.}}$  (uniform atmospheric corrections) is written

$$T_{\text{MODIS}}^{\text{unif. corr.}} = T_{\text{MODIS,min}} + \frac{(T_{\text{MODIS,max}} - T_{\text{MODIS,min}})}{\frac{T_{b31} + T_{b32} - \text{Min}(T_{b31} + T_{b32})}{\text{Max}(T_{b31} + T_{b32}) - \text{Min}(T_{b31} + T_{b32})}} \quad (14)$$

480 with  $T_{\text{MODIS,min}}$  and  $T_{\text{MODIS,max}}$  being the minimum and 481 maximum MODIS land surface temperature within the SMOS 482 pixel, and  $\text{Min}()$  and  $\text{Max}()$  the function that returns the 483 minimum and maximum value within the SMOS pixel, respectively. 484 Note that the underlying assumptions of (14) are:

- 485 • near surface air temperature and column water vapor vary 486 at scales larger than 40 km (size of a SMOS pixel).
- 487 • surface emissivity is close to 1.

### 488 C. Algorithm

489 The steps used in applying DisPATCH include: 1) selecting 490 the SMOS pixels with at least 90% (clear sky) MODIS 491 retrieved land surface temperature coverage; 2) computing 492 soil evaporative efficiency over nominal MODIS pixels with 493 (4); 3) estimating soil evaporative efficiency over non-nominal 494 MODIS pixels; 4) retrieving parameter  $SM_p$ ; 5) applying the 495 downscaling relationship of (3); 6) correcting disaggregated 496 soil moisture by the SMOS pixel weighting function; and 7) 497 compositing on a daily basis the disaggregation output ensemble 498 [21]. The input and output data and their link within 499 DisPATCH are summarized in Fig. 5.

500 1) *Selecting Clear Sky SMOS Pixels*: A threshold of 90% 501 cloud-free MODIS coverage is used to select the SMOS pixels 502 to be disaggregated. In the official MODIS land surface 503 temperature product (MOD11A1 for Terra and MYD11A1 for 504 Aqua), the data affected by the presence of clouds are already 505 masked. Hence, selection of the 90% clear sky SMOS pixels is

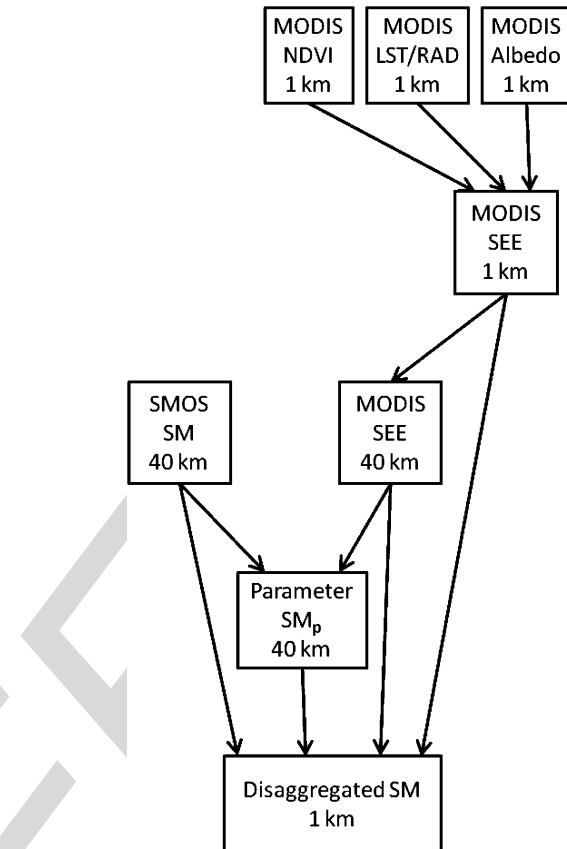


Fig. 5. Schematic diagram presenting the input and output data of DisPATCH.

directly based on the MODIS land surface temperature product 506 masking.

2) *Non-Nominal Pixels*: Nominal MODIS pixels are defined as the 1-km resolution pixels that do not include open water and where land surface temperature is actually retrieved. Open water pixels are flagged in the algorithm when MODIS NDVI retrievals yield negative values. The soil evaporative efficiency of open water pixels is set to 1. The emerged pixels where land surface temperature is not retrieved (due to the presence of some clouds within the SMOS pixel) are processed as pixels with mean surface conditions. In practice, the soil evaporative efficiency of cloudy pixels (which represent less than 10% of the surface area within the SMOS pixel) is set to the mean soil evaporative efficiency calculated over the clear sky MODIS pixels. Allocating a soil evaporative efficiency value to non-nominal pixels allows DisPATCH to be run over a wider range of SMOS pixels, including those partially covered by clouds. However, non-nominal 1-km resolution pixels are flagged and discarded from the disaggregation output ensemble.

3) *Forested Areas*: In this study, DisPATCH is applied to all the SMOS pixels where the soil moisture retrieval is successful, even those including forest class, as long as the 1 km MODIS pixels are in Zone A, B or C (see Fig. 3). This choice is relevant here because the AACLES extensive data were almost exclusively collected in agricultural areas (cropping/grazing), so forests for this study are not an issue. In the case of a mixed SMOS pixel including a significant fraction of forest, DisPATCH should be applied to the surface area of the dominant

534 class, thus excluding the surface area of the minority land cover  
535 classes.

536 4) *Calibration*: The soil moisture parameter  $\mathbf{SM}_p$  used to  
537 compute  $\partial\mathbf{SM}_{\text{mod}}/\partial\text{SEE}$  in (3) is estimated by inverting the  
538 SEE model in (7) at SMOS resolution

$$\mathbf{SM}_p = \frac{\pi \cdot \mathbf{SM}_{\text{SMOS}}}{\cos^{-1}(1 - 2\langle\text{SEE}_{\text{MODIS}, 1 \text{ km}}\rangle_{40 \text{ km}})} \quad (15)$$

539 A value of  $\mathbf{SM}_p$  is obtained for each SMOS pixel and each  
540 input data set. Note that the main assumption limiting validity  
541 of the calibration approach is the soil evaporative efficiency  
542 model [26] itself. The soil evaporative efficiency model in [26]  
543 was chosen for its simplicity (one parameter) and its ability  
544 to represent the general behavior of soil evaporative efficiency  
545 over the full range of soil moisture: particularly the null deriva-  
546 tive at zero and at maximum soil moisture, and an inflexion  
547 point in between [38]. However, it has some inconsistencies.  
548 In particular, [38] have indicated that 1) potential evaporation  
549 is physically reached at soil saturation and not at field capac-  
550 ity; therefore the model in [26] should be (strictly speaking)  
551 parameterized by the soil moisture at saturation and not by the  
552 soil moisture at field capacity, and 2) soil evaporative efficiency  
553 varies with potential evaporation, meaning that the soil moisture  
554 parameter (set to the soil moisture at field capacity in [26])  
555 should theoretically vary in time with atmospheric evaporative  
556 demand. Consequently, the  $\mathbf{SM}_p$  retrieved from SMOS and  
557 MODIS data using the model in [26] is definitely not the soil  
558 moisture at field capacity as in [26], although it could be in part  
559 related to it. In this study,  $\mathbf{SM}_p$  is therefore considered to be a  
560 fitting parameter self-estimated by DisPATCH.

561 5) *Weighting Function*: A SMOS pixel WEighting Function  
562 (WEF) is used to take into account the impact of soil mois-  
563 ture distribution on the SMOS scale soil moisture as seen by  
564 SMOS radiometer. A centrosymmetric analytical approxima-  
565 tion MEAN\_WEF is provided in [19], [20]

$$\text{MEAN\_WEF}(\rho) = C_{\text{MWEF}2} + \text{WEF}_A \left( \frac{\rho}{C_{\text{MWEF}1}} \cdot \frac{\pi}{C_{\text{WEF}1}} \right) \quad (16)$$

566 with  $\rho$  being the distance from the SMOS pixel center, and  
567  $C_{\text{MWEF}1} = 40 \text{ km}$ ,  $C_{\text{MWEF}2} = 0.027$ ,  $C_{\text{WEF}1} = 73.30$  and

$$\text{WEF}_A(\rho') = \frac{[\text{sinc}(C_{\text{WEF}1} \cdot \rho')]^{C_{\text{WEF}2}}}{1 + C_{\text{WEF}3} \cdot \rho'^{C_{\text{WEF}4}}} \quad (17)$$

568 with  $\rho'$  being the distance in the director cosines coordinates,  
569  $\text{sinc}(x) = \sin(x)/x$ , and  $C_{\text{WEF}2} = 1.4936$ ,  $C_{\text{WEF}3} = 524.5$   
570 and  $C_{\text{WEF}4} = 2.103$ .

571 A correction is applied to disaggregated soil moisture in (3)

$$\begin{aligned} \mathbf{SM}_{1 \text{ km}}^{\text{wef corr.}} &= \mathbf{SM}_{1 \text{ km}} + \frac{\sum \text{MEAN\_WEF}(\rho) \cdot \mathbf{SM}_{1 \text{ km}}(\rho)}{\sum \text{MEAN\_WEF}(\rho)} \\ &\quad - \mathbf{SM}_{\text{SMOS}} \end{aligned} \quad (18)$$

572 with  $\mathbf{SM}_{1 \text{ km}}^{\text{wef corr.}}$  being the WEF-corrected disaggregated  
573 soil moisture. Mathematically speaking, one should replace  
574  $\mathbf{SM}_{\text{SMOS}}$  with  $\sum \text{MEAN\_WEF} \cdot \mathbf{SM}_{1 \text{ km}} / \sum \text{MEAN\_WEF}$   
575 in (3) and (15) and run an iteration loop until convergence

576 of  $\mathbf{SM}_{1 \text{ km}}^{\text{wef corr.}}$  values. However, the impact of the WEF on 577 disaggregated soil moisture is expected to be low so that the 578 simple correction in (18) is considered to be sufficient for the 579 purpose of the study. 579

580 6) *Disaggregation Output*: The downscaling relationship in 580  
581 (3) is applied to each input data set, and the disaggregated soil 581  
582 moisture data ensemble is averaged on each 1-km resolution 582  
583 pixel within the study area. Averaging is a way to reduce 583  
584 random uncertainties in the disaggregation output. In [17], [27], 584  
585 disaggregated soil moisture was averaged in space (aggregated) 585  
586 at the expense of downscaling resolution. Herein, temporal 586  
587 averaging [30] is preferred to keep an optimal downscaling 587  
588 resolution. Note that a condition to average disaggregated soil 588  
589 moisture in time is the availability of thermal infrared data 589  
590 at high temporal frequency. Another significant advantage of 590  
591 applying DisPATCH to an input ensemble is to provide an 591  
592 estimate of the uncertainty in 1-km resolution disaggregated 592  
593 soil moisture, e.g., by computing the standard deviation within 593  
594 the output ensemble. 594

#### IV. APPLICATION

595 To test DisPATCH under various surface and atmospheric 596 conditions, the algorithm is run during AACES-1 and AACES- 597  
598 2 in different modes, by including (or not) a correction for 598  
599 vegetation and atmospheric effects. In each case, disaggregated 599  
600 SMOS soil moisture and HDAS measurements are compared 600  
601 at 1-km resolution for all date-farm units with overlapping 601  
602 HDAS/SMOS/MODIS data. 602

##### A. Null Hypothesis

603 In this study, the null hypothesis is defined as the application 604  
605 of DisPATCH with parameter  $\mathbf{SM}_p$  set to zero in (8). Hence, 605  
606 the downscaling relationship in (3) becomes 606

$$\mathbf{SM}_{1 \text{ km}} = \mathbf{SM}_{\text{SMOS}} \quad (19)$$

607 meaning that no 1-km information is used. Defining a null 608 hypothesis is useful to test whether DisPATCH is able to re- 608  
609 produce the subpixel variability within the  $\sim 10 \text{ km}^2$  sam- 609  
610 pling farms with better skill than simply assuming a uniform 610  
611 moisture condition. Statistical results in terms of root mean 611  
612 square difference, mean difference, correlation coefficient, and 612  
613 slope of the linear regression between the SMOS soil moisture 613  
614 disaggregated with (19) and *in situ* measurements are listed in 614  
615 Table III. One observes that the root mean square difference 615  
616 is generally explained by a (negative) bias in SMOS data and 616  
617 that none of the correlations evaluated at 1-km resolution for 617  
618 each farm separately is statistically significant (all calculated p- 618  
619 values are larger than 0.10). Thus, the rationale for developing 619  
620 DisPATCH is to improve the correlation at fine scale between 620  
621 SMOS and ground soil moisture and to reduce the bias in 621  
622 disaggregated SMOS data in the specific case where the bias 622  
623 in SMOS data at the farm scale is due to the heterogeneity of 623  
624 soil moisture within the SMOS pixel. 624

**TABLE III**  
**DISPATCH IS RUN WITH NO 1-km INFORMATION ( $\text{SM}_p$  SET TO ZERO) AND STATISTICAL RESULTS ARE LISTED IN TERMS OF ROOT MEAN SQUARE DIFFERENCE (RMSE), MEAN DIFFERENCE (BIAS), CORRELATION COEFFICIENT (R), AND SLOPE OF THE LINEAR REGRESSION BETWEEN 1-km RESOLUTION DISAGGREGATED SMOS SOIL MOISTURE AND 1-km AGGREGATED *In Situ* MEASUREMENTS. THE MEAN AND STANDARD DEVIATION OF GROUND MEASUREMENTS ( $\langle \text{SM}_{\text{HDAS}} \rangle$  AND  $\sigma_{\text{HDAS}}$ ), THE NUMBER OF CONSIDERED 1-km PIXELS, AND STATISTICAL SIGNIFICANCE (P-VALUE) ARE ALSO LISTED FOR EACH DATE-FARM UNIT**

DoY/Farm	$\langle \text{SM}_{\text{HDAS}} \rangle$ ( $\text{m}^3/\text{m}^3$ )	$\sigma_{\text{HDAS}}$ ( $\text{m}^3/\text{m}^3$ )	Number of 1 km pixels	RMSE ( $\text{m}^3/\text{m}^3$ )	Bias ( $\text{m}^3/\text{m}^3$ )	R <sup>†</sup> (-)	Slope <sup>†</sup> (-)	p-value (-)
28/F05	0.04	0.02	7	0.04	-0.04	-	-	1.0
30/F07	0.02	0.03	8	0.02	-0.02	-	-	1.0
30/F08	0.03	0.02	7	0.02	-0.02	-	-	0.69
46/F15	0.29	0.05	8	0.04	0.03	-	-	0.91
46/F16	0.34	0.06	8	0.09	-0.08	-	-	1.0
49/F17	0.21	0.06	8	0.04	-0.04	-	-	0.66
49/F18	0.25	0.07	6	0.08	-0.08	-	-	0.42
49/F20	0.20	0.09	4	0.02	-0.007	-	-	0.87
51/F19	0.24	0.08	6	0.13	-0.13	-	-	0.77
51/F20	0.20	0.10	6	0.09	-0.08	-	-	0.79
AACES-1 mean <sup>‡</sup>	-	-	-	-	-	-	-	>0.10
254/F09	0.33	0.07	9	0.13	-0.13	-	-	0.13
256/F07	0.36	0.10	8	0.19	-0.18	-	-	0.15
264/F13	0.30	0.07	8	0.18	-0.17	-	-	1.0
265/F15	0.25	0.06	7	0.05	-0.05	-	-	1.0
267/F09	0.21	0.07	9	0.14	-0.14	-	-	0.43
AACES-2 mean <sup>‡</sup>	-	-	-	-	-	-	-	>0.10

<sup>†</sup> R and slope values are reported if p-value<0.10.

<sup>‡</sup> the mean values computed for AACES-1 and AACES-2 include only statistically significant (p-value<0.10) results.

### 625 B. Visual Assessment of Disaggregation Images

626 As an example, DisPATCH is applied on DoY 49 over a 120  
627 km by 80 km subarea including the farms F16, F17, F18, F19,  
628 and F20. The images of 1-km resolution disaggregated SMOS  
629 soil moisture are presented in Fig. 6. DisPATCH is run with  
630  $\text{SM}_p$  set to zero (null hypothesis) and in four distinct modes  
631 corresponding to the combinations of the “LST” (the official  
632 MODIS land surface temperature product is used) and “RAD”  
633 [the land surface temperature is derived from MODIS radiances  
634 using (14)] modes and the “Zone A+B+C” (the vegetation-  
635 transpiration dominated 1-km pixels are discarded) and “Zone  
636 A only” (only the soil evaporation-dominated 1-km pixels are  
637 selected) modes.

638 In Fig. 6, the SMOS DGG nodes where level-2 soil moisture  
639 is successfully retrieved are overlaid on the image correspond-  
640 ing to the null hypothesis (resampled SMOS data with no 1-km  
641 information) for 6 am and 6 pm overpass times separately. The  
642 gaps in SMOS data in the lower middle part of the images  
643 are due to topography flagging over the Australian Alps. In  
644 the version-4 SMOS level-2 processor, soil moisture is not  
645 retrieved at the DGG nodes where the topography effects on  
646 simulated brightness temperatures exceed a certain threshold,  
647 so as to prevent large errors in soil moisture values. The appar-  
648 ent resolution of the null hypothesis image is 20 km because  
649 it is generated from the composition of four 40-km resolution  
650 resampled SMOS snapshot images, whose resampling grids are

separated by 20 km (the SMOS level-2 data resampling strategy 651  
was described in Section II-B.). 652

Note that the disaggregation products in the Zone A+B+C 653  
mode cover an area larger than the area sampled by SMOS 654  
data, because the SMOS resolution (about 40 km) is larger 655  
than the SMOS product sampling length (about 15 km), but 656  
does not provide disaggregated values at a distance larger than 657  
20 km from the successful retrieval nodes. Concerning the Zone 658  
A only mode, disaggregation products do not cover an area 659  
larger than the SMOS sampling area because the Australian 660  
Alps are surrounded by forests where the fraction of bare soil is 661  
less than elsewhere in the area, and which correspond to Zone 662  
B or C in the hourglass in Fig. 3. 663

When looking at the images obtained in the Zone A+B+C 664  
mode in Fig. 6, one observes that the spatial structures of 665  
1-km disaggregated SMOS soil moisture encompass, but does 666  
not seem to be correlated with, the SMOS data sampling 667  
length. However, a “boxy artifact” is still apparent at 20-km 668  
resolution, which is the separation length of the SMOS data 669  
resampling grids as explained in Section II-B. The notion of 670  
“boxy artifact” was introduced by [39] to analyze the quality of 671  
a disaggregation approach. The less apparent the low-resolution 672  
boxes, the better the disaggregation skill of the algorithm to 673  
spatially connect high-resolution disaggregated values between 674  
neighboring low-resolution pixels, and thus to derive a realistic 675  
high-resolution soil moisture field. When comparing the images 676  
obtained in the Zone A+B+C mode with those obtained in the 677

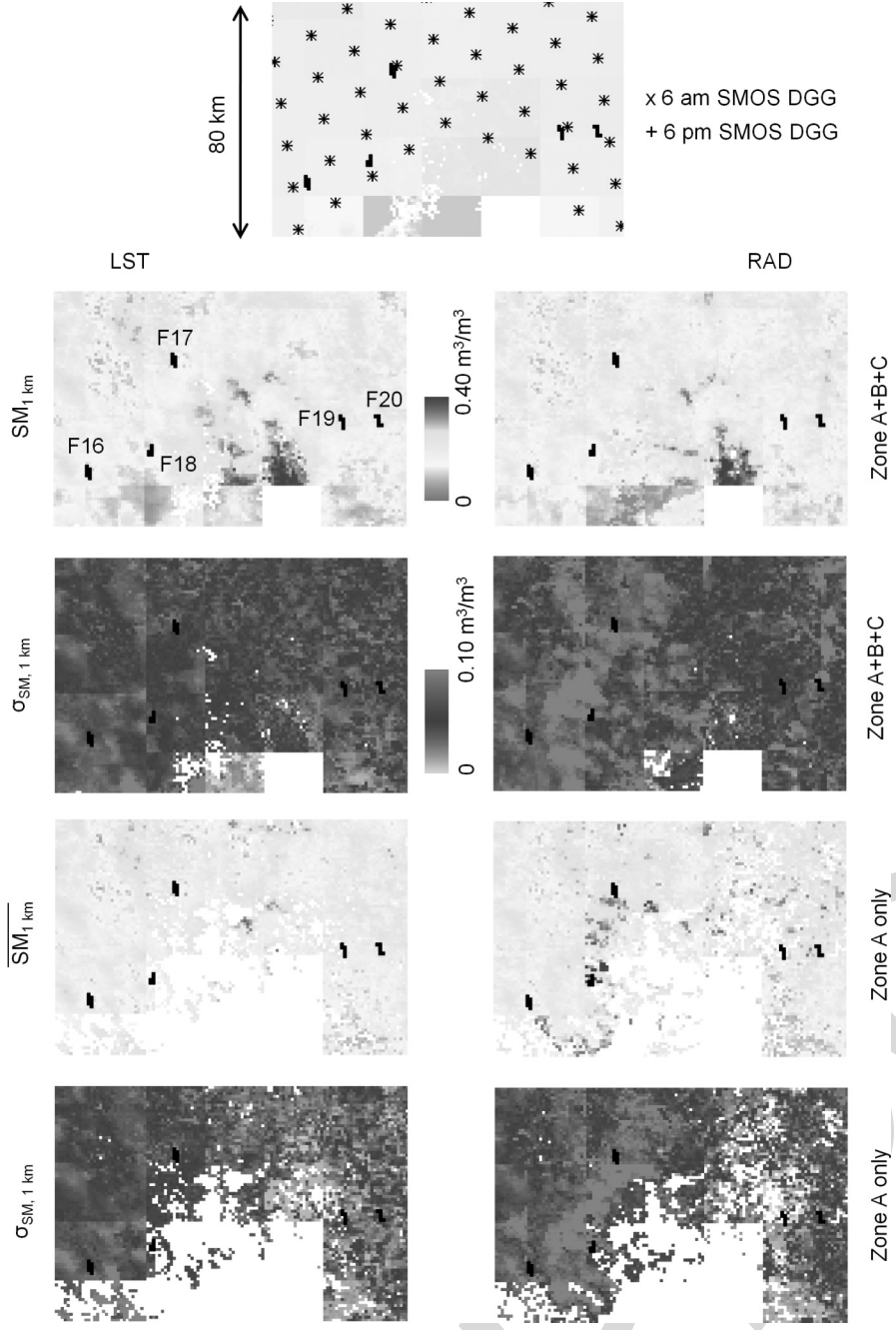


Fig. 6. Images of disaggregation results over a 120 km by 80 km subarea on DoY 49. The disaggregated soil moisture ( $\overline{SM}_{1\text{ km}}$ ) and its estimated uncertainty ( $\sigma_{SM, 1\text{ km}}$ ) are compared in the LST and RAD modes and in the Zone A+B+C and Zone A only modes. Sampling farms are overlaid on all images. SMOS DGG nodes are overlaid on the image corresponding to the null hypothesis (no 1-km resolution information) presented at top.

678 Zone A only mode, one observes that the 20-km resolution boxy  
 679 artifact is less apparent in the Zone A only mode, consistent  
 680 with the better sensitivity of MODIS-derived SEE with soil-  
 681 dominated pixels (Zone A) than with mixed-surface (Zone B  
 682 and C) pixels. In Fig. 6, the images obtained in the LST and  
 683 RAD mode highlight different spatial structures. In general,  
 684 there are less data gaps in the RAD than in the LST mode.  
 685 However, ground validation data are required to assess their  
 686 relative quality/accuracy.

687 As an assessment of the uncertainty in composited soil mois-  
 688 ture disaggregation, the standard deviation within the disaggre-  
 689 gation output ensemble is also reported for each disaggregation

690 product in Fig. 6. The same observations can be made as with  
 691 the soil moisture images: spatial structures are more visible, and  
 692 the boxy artifact is less apparent in the RAD than in the LST  
 693 mode. In general, the estimated uncertainty in disaggregated  
 694 products is larger in the RAD than in the LST mode, regardless  
 695 of the Zone (A+B+C or A only) mode.

#### C. SMOS Weighting Function

696 To evaluate the impact of the SMOS instrument weighting  
 697 function on disaggregation results, DisPATCH is run with (and  
 698 without) the WEF correction in (18). The expected effect of the 699

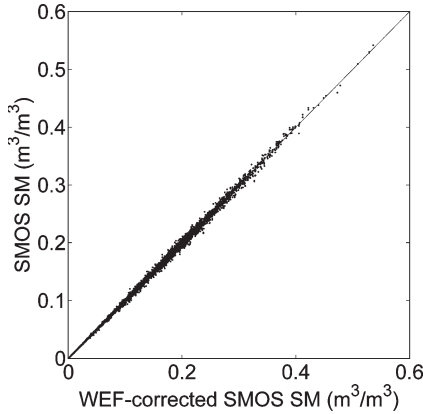


Fig. 7. Uncorrected versus WEF-corrected SMOS soil moisture for the entire data set.

WEF is a bias at 40 km resolution on disaggregated soil moisture. Fig. 7 plots the uncorrected against WEF-corrected SMOS soil moisture for the entire data set including both AACES-1 and AACES-2 experiments. The WEF correction has very little impact on disaggregated soil moisture with a maximum difference between uncorrected and WEF-corrected SMOS soil moisture of  $0.02 \text{ m}^3/\text{m}^3$ , a mean difference of approximately zero, and a standard deviation of  $0.003 \text{ m}^3/\text{m}^3$ . Although the difference is small with this data set, WEF-corrected products are expected to be more realistic. Therefore, the correction in (18) is used in all the DisPATCH runs that follow.

#### 711 D. Quantitative Comparison With In Situ Measurements

Fig. 8 presents the scatterplots of 1-km resolution disaggregated SMOS soil moisture versus 1-km resolution aggregated *in situ* measurements for the ten date-farm units during AACES-1. On each graph are plotted the soil moisture disaggregated in the Zone A+B+C mode (empty squares) and the soil moisture disaggregated in the Zone A only mode (black squares). At the beginning of AACES-1, conditions are very dry so that SMOS retrievals are close to zero and the variability of *in situ* measurements is low (about  $0.02 \text{ m}^3/\text{m}^3$ ). In such conditions, no useful information is expected from the application of DisPATCH, and the statistical results in terms of spatial correlation are not meaningful for DoY 28/F05, DoY 30/F07 and DoY 30/F08. While wetter conditions occur after DoY 30, cloud cover prevents DisPATCH to be run (MODIS data are unavailable) until DoY 46. On DoY 46, the average and standard deviation of *in situ* soil moisture measurements is  $0.32 \text{ m}^3/\text{m}^3$  and  $0.06 \text{ m}^3/\text{m}^3$ , respectively. The spatial variability of 1-km soil moisture is nicely captured by DisPATCH notably in the RAD mode. On DoY 49, the disaggregated SMOS soil moisture is still correlated with the *in situ* measurements made in three farms (F17, F18, and F20). On the last ground sampling day, disaggregation results are significantly correlated with *in situ* measurements in F19, but not in F20. The poor results obtained with DoY 51/F20 is probably due to the time gap (3 days) between ground sampling date (DoY 51) and MODIS overpass day (DoY 54).

Statistical results in terms of root mean square difference, mean difference, correlation coefficient, and slope of the linear

regression between the SMOS soil moisture disaggregated in the Zone A+B+C mode and aggregated *in situ* measurements are listed in Table IV. Statistical significance (*p*-value) is also reported for each date-farm unit to select statistically significant (*p*-value  $< 0.10$ ) results. Although the disaggregation of SMOS data on extensively dry DoY 30 does not provide any additional information (soil is uniformly dry), the observed correlation between disaggregated (LST mode) and *in situ* soil moisture is statistically significant, and the correlation coefficient value is negative ( $-0.70$  and  $-0.95$  at F07 and F08, respectively). One plausible explanation is the opposite effect of soil temperature on HDAS soil moisture measurements and on MODIS-derived soil evaporative efficiency: a slight undercorrection of the temperature-corrected hydaprobe measurements at high temperature [18] results in a slight increase of soil moisture estimate with soil temperature, while an increase of soil temperature makes soil evaporative efficiency decrease. Nevertheless, the possible impact of soil temperature on HDAS measurements is very low with a slope of the linear regression between disaggregated SMOS and *in situ* soil moisture calculated as  $-0.08$  and  $-0.03$  for F07 and F08, respectively. When selecting statistically significant results (*p*-value  $< 0.10$ ) and discarding data for DoY 30, the mean correlation coefficient and slope in RAD mode are  $0.75$  and  $0.58$ , respectively.

Fig. 9 presents the scatterplots of 1-km resolution disaggregated SMOS soil moisture versus 1-km resolution aggregated *in situ* measurements for the five date-farm units during AACES-2. On each graph are plotted the soil moisture disaggregated in the Zone A+B+C mode (empty squares) and the soil moisture disaggregated in the Zone A only mode (black squares). The surface conditions of AACES-2 were relatively wet with a mean soil moisture value estimated as  $0.29 \text{ m}^3/\text{m}^3$ . The disaggregated SMOS soil moisture does not correlate well with *in situ* measurements with a *p*-value larger than  $0.10$  for all sampling days, except for DoY 256/F07 in LST mode (see Table IV). The negative correlation coefficient ( $-0.73$ ) obtained on DoY 256 is discussed when comparing the Zone A+B+C and Zone A only modes in Section IV-F. In general, statistical results in Table IV indicate that DisPATCH does not succeed in representing the variability of soil moisture at 1-km resolution during AACES-2. In fact, DisPATCH is based on the tight coupling that occurs between soil moisture and evaporation under high evaporative demand conditions [40]. This coupling seems to be weak in September over the study area so that the disaggregation results at 1-km resolution are not reliable.

For DoY 264/F13, however, an interesting feature is observed on the graph corresponding to the RAD and Zone A only modes. When removing the (three) black squares with the largest errorbars, the correlation coefficient and the slope of the linear regression between disaggregated and *in situ* observations becomes  $0.9$  and  $0.7$ , respectively. This suggests that: 1) the standard deviation within the disaggregation output ensemble can be a good estimate of the uncertainty in the composited disaggregation product; and 2) the applicability of DisPATCH is greatly dependent on the quality of MODIS land surface temperature. Note that in this study, a choice was made to maximize the number of data points used in the comparison with *in situ* measurements. Consequently, all the cloud-free

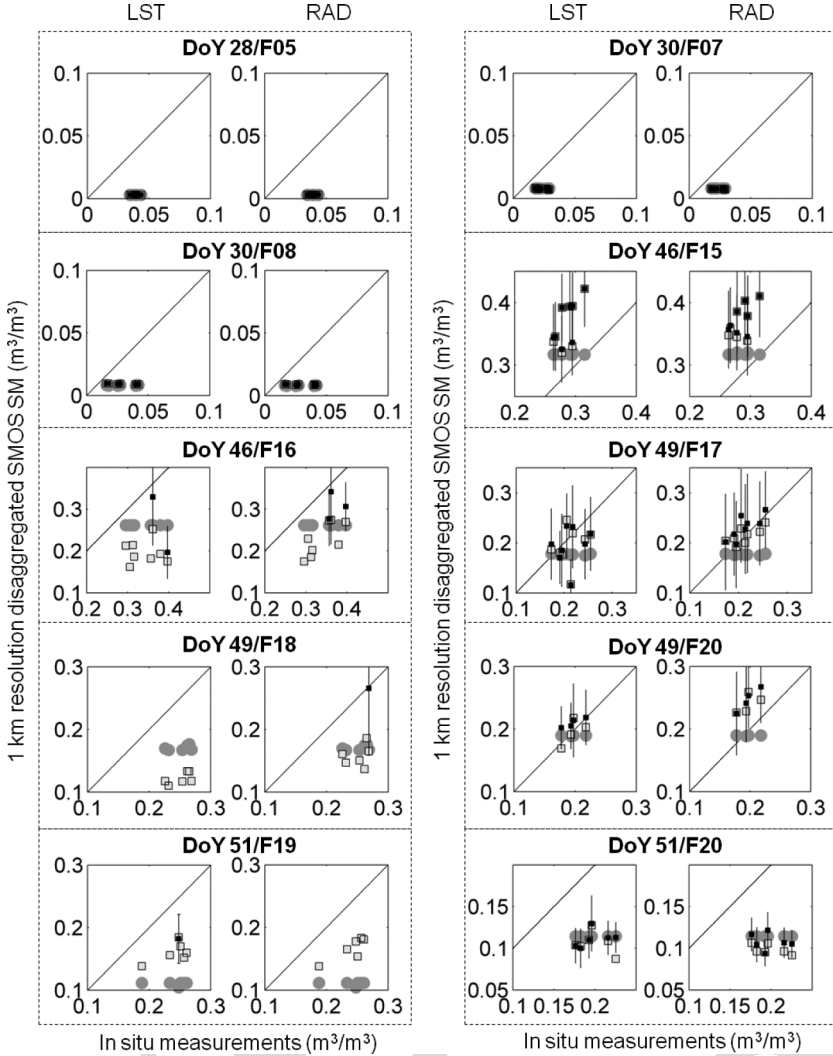


Fig. 8. Scatterplots of 1-km resolution disaggregated SMOS soil moisture versus 1-km resolution aggregated *in situ* measurements for each of the ten date-farm data sets during AACES-1. The filled circles correspond to disaggregation with no 1-km information, empty squares to Zone A+B+C mode and black squares to Zone A only mode. For the Zone A only mode, the uncertainty in disaggregated soil moisture is represented by vertical errorbars.

798 MODIS land surface temperature data were used regardless  
 799 of the MODIS land surface temperature quality index. Further  
 800 research should be conducted to assess whether selecting the  
 801 MODIS pixel with the best MODIS land surface temperature  
 802 quality index would improve the disaggregation results. This  
 803 would be possible using the AACES airborne data, which cover  
 804 a much larger area than *in situ* measurements.

#### 805 E. Atmospheric Corrections

806 The impact of atmospheric corrections on DisPATCh output  
 807 is analyzed by comparing the disaggregation results obtained  
 808 in the LST and RAD mode. Quantitative comparison between  
 809 LST and RAD modes is provided in Table IV in terms of root  
 810 mean square difference, mean difference, correlation coeffi-  
 811 cient, and slope of the linear regression between disaggregated  
 812 SMOS soil moisture and aggregated *in situ* measurements.  
 813 Correlation coefficient and slope values are reported only if  
 814 the p-value (statistical significance) is lower than 0.10. It is  
 815 apparent that statistical results are better in the RAD than in

the LST mode. When including all dates, the mean bias is 816 decreased from  $-0.05 \text{ m}^3/\text{m}^3$  in LST mode to  $-0.03 \text{ m}^3/\text{m}^3$  817 in RAD mode during AACES-1. When selecting statistically 818 significant results ( $p\text{-value} < 0.10$ ) and discarding data for 819 DoY 30, the mean correlation coefficient and slope is 0.75 and 820 0.58 in RAD mode, and 0.65 and 1.5 in LST mode, respectively. 821 Note that the improvement is very significant for DoY 46/F16 822 with a correlation coefficient and slope increasing from about 823 zero to 0.7 and 0.8, respectively. 824

The fact that the results obtained in RAD mode are superior 825 to those obtained in LST mode indicates that the atmospheric 826 corrections of the official MODIS land surface temperature 827 add significant uncertainties in the disaggregation products. 828 One rationale may be that the information used in atmospheric 829 corrections (notably air temperature and water vapor profile 830 data) are subjected to large uncertainties at 5-km resolution. 831 As DisPATCh is based on the spatial variations of MODIS 832 temperature relative to the 40 km scale mean, the atmospheric 833 corrections on the land surface temperature data are not nec- 834 essary at 5 km (as it is done in the MODIS temperature 835

TABLE IV  
DisPATCH IS RUN IN THE ZONE A+B+C MODE AND STATISTICAL RESULTS ARE LISTED IN TERMS OF ROOT MEAN SQUARE DIFFERENCE (RMSD), MEAN DIFFERENCE (BIAS), CORRELATION COEFFICIENT (R), AND SLOPE OF THE LINEAR REGRESSION BETWEEN 1-km RESOLUTION DISAGGREGATED SMOS SOIL MOISTURE AND 1-km AGGREGATED *In Situ* MEASUREMENTS. THE RESULTS OBTAINED USING THE RADIANCE-DERIVED LAND SURFACE TEMPERATURE DATA (RAD MODE) AND USING THE OFFICIAL MODIS LAND SURFACE TEMPERATURE DATA (LST MODE IN PARENTHESIS) ARE COMPARED. THE MEAN AND STANDARD DEVIATION OF GROUND MEASUREMENTS ( $\langle \text{SM}_{\text{HDAS}} \rangle$  AND  $\sigma_{\text{HDAS}}$ ), THE NUMBER OF CONSIDERED 1-km PIXELS AND STATISTICAL SIGNIFICANCE (P-VALUE) ARE ALSO LISTED FOR EACH DATE-FARM UNIT

DoY/Farm	$\langle \text{SM}_{\text{HDAS}} \rangle$ ( $\text{m}^3/\text{m}^3$ )	$\sigma_{\text{HDAS}}$ ( $\text{m}^3/\text{m}^3$ )	Number of 1 km pixels	RMSD ( $\text{m}^3/\text{m}^3$ )	Bias ( $\text{m}^3/\text{m}^3$ )	R <sup>†</sup> (-)	Slope <sup>†</sup> (-)	p-value (-)
28/F05	0.04	0.02	7 (7)	0.04 (0.04)	-0.04 (-0.04)	- (-)	- (-)	0.72 (0.80)
30/F07	0.02	0.03	8 (8)	0.02 (0.02)	-0.02 (-0.02)	- (-0.70)	- (-0.08)	0.20 (0.05)
30/F08	0.03	0.02	7 (7)	0.02 (0.02)	-0.02 (-0.02)	- (-0.95)	- (-0.03)	0.11 (0.001)
46/F15	0.29	0.05	8 (8)	0.09 (0.09)	0.09 (0.08)	- (0.65)	- (1.5)	0.12 (0.08)
46/F16	0.34	0.06	8 (8)	0.12 (0.15)	-0.11 (-0.14)	0.72 (-)	0.76 (-)	0.04 (0.95)
49/F17	0.21	0.06	8 (8)	0.02 (0.04)	0.00 (-0.02)	0.70 (-)	0.42 (-)	0.05 (0.54)
49/F18	0.25	0.07	6 (6)	0.10 (0.13)	-0.09 (-0.13)	- (-)	- (-)	0.60 (0.20)
49/F20	0.20	0.09	4 (4)	0.05 (0.01)	0.04 (0.00)	- (-)	- (-)	0.41 (0.32)
51/F19	0.24	0.08	6 (6)	0.07 (0.08)	-0.07 (-0.08)	0.84 (-)	0.56 (-)	0.04 (0.19)
51/F20	0.20	0.10	6 (6)	0.10 (0.09)	-0.10 (-0.09)	- (-)	- (-)	0.17 (0.51)
AACES-1 mean <sup>‡</sup>	0.26 (0.29)	0.07 (0.05)	7 (8)	0.07 (0.09)	-0.06 (-0.08)	0.75 (0.65)	0.58 (1.5)	0.04 (0.08)
254/F09	0.33	0.07	9 (9)	0.18 (0.14)	-0.16 (-0.11)	- (-)	- (-)	0.17 (0.74)
256/F07	0.36	0.10	8 (9)	0.12 (0.19)	-0.10 (-0.18)	- (-0.73)	- (-0.47)	0.12 (0.04)
264/F13	0.30	0.07	8 (8)	0.16 (0.19)	-0.14 (-0.16)	- (-)	- (-)	0.59 (0.47)
265/F15	0.25	0.06	7 (7)	0.16 (0.18)	0.01 (0.03)	- (-)	- (-)	0.32 (0.34)
267/F09	0.21	0.07	9 (9)	0.16 (0.15)	-0.15 (-0.15)	- (-)	- (-)	0.90 (0.86)
AACES-2 mean <sup>‡</sup>	0.36	0.10	- (9)	- (0.19)	- (-0.18)	- (-0.73)	- (-0.47)	>0.10 (0.04)

<sup>†</sup> R and slope values are reported if p-value<0.10.

<sup>‡</sup> the mean values computed for AACES-1 and AACES-2 include only statistically significant (p-value<0.10) results and discard extensive dry days DoY 28-30.

836 algorithm). An atmospheric correction at 40-km resolution is  
837 sufficient and provides even better disaggregation results than  
838 applying an atmospheric correction at 5-km resolution.

### 839 F. Vegetation Cover

840 The impact of vegetation cover on DisPATCH output during  
841 AACES-1 is analyzed by comparing the disaggregation results  
842 obtained in the Zone A+B+C and Zone A only mode. Quan-  
843 titative comparison between Zone A+B+C and Zone A only  
844 modes is provided in Tables IV and V in terms of root mean  
845 square difference, mean difference, correlation coefficient, and  
846 slope of the linear regression between disaggregated SMOS soil  
847 moisture and aggregated *in situ* measurements. It is apparent  
848 that statistical results are generally better in the Zone A only  
849 than in the Zone A+B+C mode for both LST and RAD modes.  
850 In the RAD mode for instance, the mean correlation coefficient  
851 is increased from 0.75 in the Zone A+B+C mode (Table IV) to  
852 0.89 in the Zone A only mode (Table V). Also the mean slope  
853 is closer to 1 as it switches from 0.58 in the Zone A+B+C mode  
854 (Table IV) to 0.91 in the Zone A only mode (Table V). Con-  
855 sequently, results are consistent with the hourglass approach in  
856 Fig. 3 that predicts a lower sensitivity of MODIS-derived soil  
857 temperature to soil moisture in Zone B and C, Zone A having

the highest potential for estimating soil moisture variability 858 from MODIS temperature. 859

On DoY 256, the negative correlation appearing in Zone 860 A+B+C mode (Table IV) is not significant in Zone A only mode 861 (Table V), suggesting that the contradictory result obtained on 862 DoY 256 is probably an artifact due to the small sample size. 863

Note that one drawback of the Zone A only mode is the larger 864 amount of data gaps in the soil moisture images. Therefore, 865 the use of both modes is a compromise between application 866 coverage and accuracy in the disaggregation output. 867

### 868 G. Distinguishing Between SMOS and DisPATCH Errors

By solving the extent mismatch between 40-km resolution 869 remote sensing observation and localized *in situ* measurements, 870 DisPATCH could be used as a tool to help improve the validation 871 strategies of SMOS data in low-vegetated semi-arid regions. It 872 also would reduce the coverage requirements identified by [41] 873 for airborne validation campaigns. However, such a validation 874 approach requires separating the different error sources that 875 may be attributed to SMOS soil moisture and to DisPATCH. 876 One solution is to estimate the errors attributed to DisPATCH 877 and then deduce the errors attributed to SMOS soil moisture. To 878 estimate the errors that are associated with the disaggregation 879

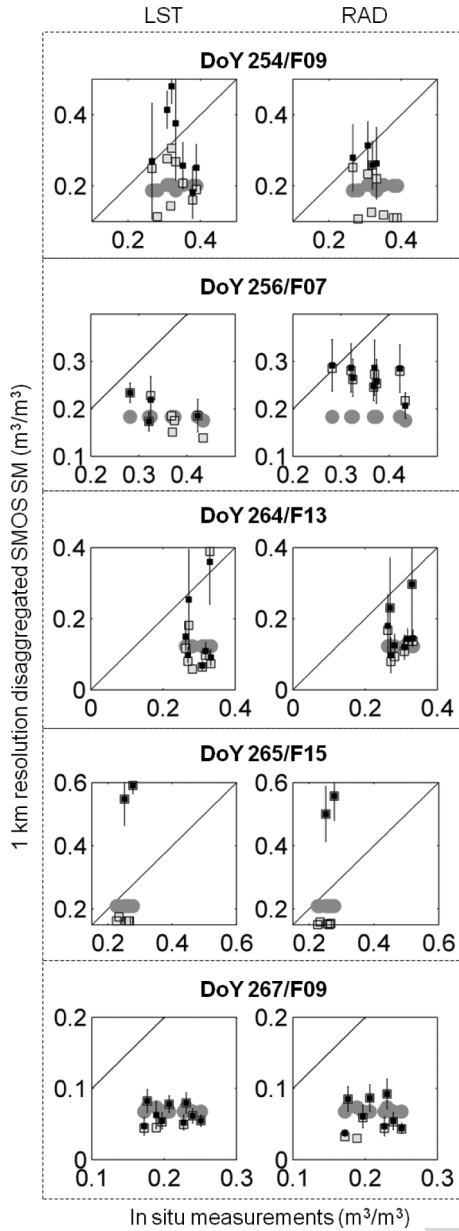


Fig. 9. Scatterplots of 1-km resolution disaggregated SMOS soil moisture versus 1-km resolution aggregated *in situ* measurements for each of the five date-farm data sets during AACES-2. The filled circles correspond to disaggregation with no 1-km information, empty squares to Zone A+B+C mode and black squares to Zone A only mode. For the Zone A only mode, the uncertainty in disaggregated soil moisture is represented by vertical errorbars.

methodology, it is suggested to analyze the spatial correlation between 1-km disaggregated SMOS soil moisture and 882 *in situ* measurements. If the correlation is significant, then the 883 disaggregation product is likely to be sufficiently accurate for 884 validating SMOS data.

Note that the errors in DisPATCH are in part coupled with 886 the errors in SMOS soil moisture, particularly because SMOS 887 is an input to DisPATCH. However, any uncertainties in SMOS 888 soil moisture should not impact the disaggregation results at a 889 distance shorter than the SMOS data sampling length (15 km). 890 This is the reason why such a validation strategy should be 891 conducted with ground measurements made within a distance 892 radius of 15 km.

In this study case, five date-farm units including DoY 893 46/F15, DoY 46/F16, DoY 49/F17, DoY 49/F18, and DoY 894 49/F20 indicate a significant correlation between disaggregated 895 SMOS soil moisture and *in situ* measurements. For these units, 896 the root mean square error in disaggregated SMOS soil mois- 897 ture is mainly explained by a bias in disaggregated soil moisture 898 (see Table IV). However, no conclusion can be drawn from 899 these data because: 1) the bias is sometimes positive (DoY 900 46/F15, DoY 49/F20), and sometimes negative (DoY 46/F16, 901 DoY 49/F17, DoY 49/F18); and 2) the comparison is made only 902 once for each farm, which does not allow analyzing the tempo- 903 ral behavior. Such a validation approach could be undertaken 904 in the near future using the OzNet (<http://www.oznet.org.au/>, 905 [42]) soil moisture monitoring network, providing continuous 906 measurements at 68 sites within the Murrumbidgee catchment 907 area. 908

#### H. Subpixel Variability and Assimilation Perspectives

909

DisPATCH is successively run in LST or RAD mode and in 910 Zone A+B+C or Zone A only mode during AACES-1. Fig. 10 911 plots for each case the estimated uncertainty in disaggregated 912 soil moisture (computed as the standard deviation of the disag- 913 gregation output ensemble) against the subpixel variability of 914 1-km resolution *in situ* measurements (computed as the stan- 915 dard deviation of the *in situ* measurements made within 916 1-km pixels). The data corresponding to DoY 51 are plotted 917 separately because of the time gap between HDAS/SMOS 918 (DoY 51) and MODIS (DoY 54) collection time. It is interest- 919 ing to observe that the estimated uncertainty in disaggregated 920 soil moisture is closely related to the observed subpixel vari- 921 ability of *in situ* measurements. Hence,  $\sigma_{SM, 1 \text{ km}}$  could be used 922 as a proxy for representing the soil moisture variability at scales 923 finer than 1-km resolution. Concerning the data on DoY 51, the 924 linear regression is clearly off the 1:1 line. This is consistent 925 with a decrease of the spatial variability in soil moisture during 926 a dry down period [43]. In particular, the spatial variability 927 in soil moisture is expected to be lower on DoY 54 than on 928 DoY 51. 929

The correlation between the estimated uncertainty in disag- 930 ggregated soil moisture and the subpixel soil moisture variability 931 makes an additional link between DisPATCH output and assim- 932 ilation schemes into hydrological models. A number of optimal 933 assimilation methodologies have been developed to combine 934 model predictions with remote sensing observations. However, 935 any so-called optimal assimilation technique stops being opti- 936 mal if the uncertainty in remotely sensed data is unknown or 937 estimated with a large uncertainty. In the perspective of assim- 938 ilating disaggregated SMOS data into land surface models, one 939 should keep in mind that the error information on observable 940 variables is as crucial as the observations themselves, e.g., [44]. 941

## V. SUMMARY AND CONCLUSION

942

DisPATCH is an algorithm dedicated to the disaggregation of 943 soil moisture observations using high-resolution soil tempera- 944 ture data. It converts soil temperature fields into soil moisture 945 fields given a semi-empirical soil evaporative efficiency model 946

TABLE V  
 DisPATCH IS RUN IN THE ZONE A ONLY MODE, AND STATISTICAL RESULTS ARE LISTED IN TERMS OF ROOT MEAN SQUARE DIFFERENCE (RMSD), MEAN DIFFERENCE (BIAS), CORRELATION COEFFICIENT (R), AND SLOPE OF THE LINEAR REGRESSION BETWEEN 1-km RESOLUTION DISAGGREGATED SMOS SOIL MOISTURE AND 1-km AGGREGATED *In Situ* MEASUREMENTS. THE RESULTS OBTAINED USING THE RADIANCE-DERIVED LAND SURFACE TEMPERATURE DATA (RAD MODE) AND USING THE OFFICIAL MODIS LAND SURFACE TEMPERATURE DATA (LST MODE IN PARENTHESIS) ARE COMPARED. THE MEAN AND STANDARD DEVIATION OF GROUND MEASUREMENTS ( $\langle SM_{HDAS} \rangle$  AND  $\sigma_{HDAS}$ ), THE NUMBER OF CONSIDERED 1-km PIXELS AND STATISTICAL SIGNIFICANCE (P-VALUE) ARE ALSO LISTED FOR EACH DATE-FARM UNIT

DoY/Farm	$\langle SM_{HDAS} \rangle$ ( $m^3/m^3$ )	$\sigma_{HDAS}$ ( $m^3/m^3$ )	Number of 1 km pixels	RMSD* ( $m^3/m^3$ )	Bias* ( $m^3/m^3$ )	R† (-)	Slope† (-)	p-value (-)
28/F05	0.04	0.02	7 (7)	0.04 (0.04)	-0.04 (-0.04)	- (-)	- (-)	0.72 (0.80)
30/F07	0.02	0.03	8 (8)	0.02 (0.02)	-0.02 (-0.02)	- (-0.70)	- (-0.08)	0.20 (0.05)
30/F08	0.03	0.02	7 (7)	0.02 (0.02)	-0.02 (-0.02)	- (-0.95)	- (-0.03)	0.11 (0.001)
46/F15	0.29	0.05	8 (8)	0.09 (0.09)	0.09 (0.08)	- (0.66)	- (1.4)	0.13 (0.07)
46/F16	0.34	0.06	3 (2)	0.07 (0.14)	-0.06 (-0.12)	- (-)	- (-)	0.96 (-)
49/F17	0.21	0.06	8 (8)	0.02 (0.04)	0.02 (-0.02)	0.79 (-)	0.71 (-)	0.02 (0.64)
49/F18	0.25	0.07	1 (0)	- (-)	- (-)	- (-)	- (-)	0.20 (0.20)
49/F20	0.20	0.09	4 (4)	0.05 (0.02)	0.05 (0.01)	0.98 (0.92)	1.1 (0.42)	0.02 (0.08)
51/F19	0.24	0.08	0 (1)	- (-)	- (-)	- (-)	- (-)	0.19 (0.19)
51/F20	0.20	0.10	6 (6)	0.09 (0.09)	-0.09 (-0.09)	- (-)	- (-)	0.70 (0.45)
AACES-1 mean‡	0.21 (0.25)	0.08 (0.07)	6 (6)	0.04 (0.06)	0.04 (0.05)	0.89 (0.79)	0.91 (0.91)	0.02 (0.08)
254/F09	0.33	0.07	4 (7)	0.05 (0.12)	-0.03 (-0.02)	- (-)	- (-)	0.70 (0.30)
256/F07	0.36	0.10	8 (4)	0.12 (0.15)	-0.10 (-0.13)	- (-)	- (-)	0.13 (0.43)
264/F13	0.30	0.07	8 (7)	0.14 (0.17)	-0.13 (-0.14)	- (-)	- (-)	0.64 (0.86)
265/F15	0.25	0.06	2 (2)	0.26 (0.30)	0.26 (0.30)	- (-)	- (-)	- (-)
267/F09	0.21	0.07	8 (9)	0.15 (0.15)	-0.15 (-0.15)	- (-)	- (-)	0.77 (0.85)
AACES-2 mean‡	-	-	- (-)	- (-)	- (-)	- (-)	- (-)	>0.10 (>0.10)

\* RMSD and bias values are computed if the number of 1 km pixels>1.

† R and slope values are reported if p-value<0.10.

‡ the mean values computed for AACES-1 and AACES-2 include only statistically significant (p-value<0.10) results and discard extensive dry days DoY 28-30.

947 and a first-order Taylor series expansion around the field-mean  
 948 soil moisture. In this study, the disaggregation approach is ap-  
 949 plied to 40-km resolution version-4 SMOS level-2 soil moisture  
 950 using 1-km resolution MODIS data. The objective is to test  
 951 DisPATCh under different surface and atmospheric conditions  
 952 using the very intensive ground measurements collected in  
 953 southeastern Australia during the 2010 summer and winter  
 954 AACES campaigns. Those measurements are aggregated at  
 955 the downscaling resolution (1 km) and subsequently compared  
 956 to the disaggregated SMOS soil moisture. Over the study  
 957 area, climatic (evaporative demand), meteorologic (presence  
 958 of clouds), and vegetation (cover and water status) conditions  
 959 are strong constraints on disaggregation results. The quality  
 960 of disaggregation products varies greatly according to season:  
 961 while the correlation coefficient between disaggregated and  
 962 *in situ* soil moisture is 0.7 during the summer AACES, it  
 963 is about zero during the winter AACES, consistent with a  
 964 weaker coupling between evaporation and surface moisture  
 965 in temperate than in semi-arid climate. Moreover, vegetation  
 966 cover prevents the soil temperature to be retrieved from thermal  
 967 infrared data and the vegetation water stress may increase the  
 968 remotely sensed land surface temperature independent of near-  
 969 surface soil moisture. By separating the 1-km pixels where  
 970 MODIS temperature is mainly controlled by soil evaporation,

from those where MODIS temperature is controlled by both  
 971 soil evaporation and vegetation transpiration, the correlation  
 972 coefficient between disaggregated and *in situ* soil moisture is  
 973 increased from 0.70 to 0.85 during the summer AACES cam-  
 974 paign. Also, cloud cover totally obscures the surface during rain  
 975 events, and on clear sky days, the water vapor in the atmosphere  
 976 significantly affects the quality of land surface temperature  
 977 data. It is found that the 5-km resolution atmospheric correction  
 978 of the official MODIS temperature data has significant impact  
 979 on DisPATCh output. An alternative atmospheric correction at  
 980 40-km resolution increases the correlation coefficient between  
 981 disaggregated and *in situ* soil moisture from 0.72 to 0.82 during  
 982 the summer AACES. 983

The above limitations must be kept in mind when using  
 984 DisPATCh as a tool for validating SMOS soil moisture. Over  
 985 semi-arid areas, disaggregation can solve the extent mismatch  
 986 between the 40-km resolution SMOS data and localized *in situ*  
 987 measurements. However, the validation of SMOS using Dis-  
 988 PATCh requires separation of the errors associated with SMOS  
 989 data and the errors associated with DisPATCh. As SMOS data  
 990 are an input to DisPATCh, the errors in DisPATCh are also  
 991 linked to the uncertainty in SMOS soil moisture. Nevertheless,  
 992 one way to identify the error sources specifically attributed  
 993 to DisPATCh is to analyze the spatial correlation between  
 994

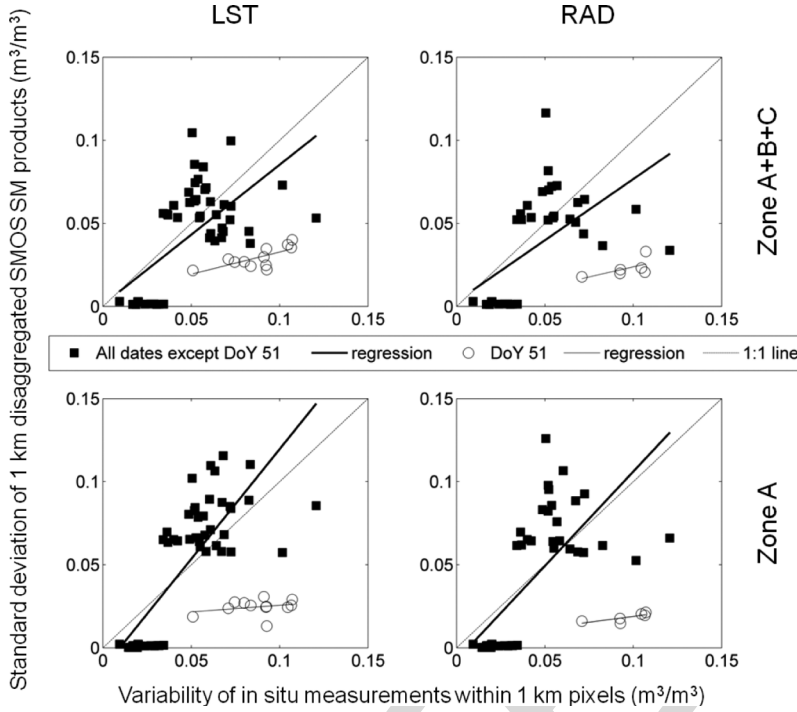


Fig. 10. Estimated uncertainty in disaggregated soil moisture ( $\sigma_{SM}$ , 1 km) versus subpixel variability of 1 km resolution *in situ* measurements for DisPATCH run in LST or RAD mode and Zone A+B+C or Zone A only mode.

995 disaggregated SMOS data and the *in situ* measurements made  
996 at a distance larger than the downscaling resolution (1 km with  
997 MODIS data) and smaller than the SMOS data sampling length  
998 (15 km).

999 Based on the results obtained using the AACES *in situ*  
1000 measurements, several improvements of DisPATCH can be  
1001 suggested:

- 1002 • Use of the MODIS land surface temperature quality index  
1003 to select the SMOS pixels with the highest MODIS data  
1004 quality.
- 1005 • Correcting the MODIS land surface temperature for  
1006 topography and illumination effects [45]. Within a 40-km  
1007 SMOS resolution pixel, the elevation range may be very  
1008 significant and thus induce a variability in land sur-  
1009 face temperature that is not attributed to surface soil  
1010 moisture.
- 1011 • Use of ancillary air temperature data to constrain the  
1012 estimation of end-members. The unstressed vegetation  
1013 temperature  $T_{v,min}$  could be set to the air temperature  
1014 instead of the minimum MODIS land surface temperature.  
1015 This would make the estimation of  $T_{v,min}$  less dependent  
1016 on the representativeness of the surface conditions met  
1017 within the SMOS pixel [24].
- 1018 • Accounting for the dependency of soil evaporative effi-  
1019 ciency to potential evaporation, by replacing the model in  
1020 [26] with the model in [38].
- 1021 • Estimating an optimal downscaling resolution for each  
1022 season: as the sensitivity of soil evaporative efficiency to  
1023 soil moisture is lower in the winter months than in the sum-  
1024 mer months, aggregating DisPATCH output may improve  
1025 the quality of disaggregation products at the expense of  
1026 spatial resolution [17].

A robust disaggregation methodology of SMOS soil moisture 1027 at 1-km resolution, which would provide both disaggregated 1028 soil moisture and its uncertainty at 1-km resolution is a crucial 1029 step toward the application of SMOS data to hydrological 1030 studies.

## REFERENCES

- [1] E. G. Njoku and L. Li, "Retrieval of land surface parameters using passive 1033 microwave measurements at 6–18 GHz," *IEEE Trans. Geosci. Remote 1034 Sens.*, vol. 37, no. 1, pp. 79–93, Jan. 1999. 1035
- [2] C. S. Draper, J. P. Walker, P. J. Steinle, R. A. M. D. Jeu, and 1036 T. R. H. Holmes, "An evaluation of AMSR-E derived soil moisture 1037 over Australia," *Remote Sens. Environ.*, vol. 113, no. 4, pp. 703–710, 1038 Apr. 2009. doi:10.1016/j.rse.2008.11.011. 1039
- [3] C. Kummerow, W. S. Olson, and L. Giglio, "A simplified scheme for 1040 obtaining precipitation and vertical hydrometeor profiles from passive 1041 microwave sensors," *IEEE Trans. Geosci. Remote Sens.*, vol. 34, no. 5, 1042 pp. 1213–1232, Sep. 1996. 1043
- [4] M. Grecu and E. N. Anagnostou, "Overland precipitation estimation from 1044 TRMM passive microwave observations," *J. Appl. Meteor.*, vol. 40, no. 8, 1045 pp. 1367–1380, Aug. 2001. 1046
- [5] T. J. Jackson, M. H. Cosh, R. Bindlish, P. J. Starks, D. D. Bosch, 1047 M. Seyfried, D. C. Goodrich, M. S. Moran, and J. Du, "Validation of 1048 advanced microwave scanning radiometer soil moisture products," *IEEE 1049 Trans. Geosci. Remote Sens.*, vol. 48, no. 12, pp. 4256–4272, Dec. 2010. 1050 doi:10.1109/TGRS.2010.2051035. 1051
- [6] Y. H. Kerr, P. Waldteufel, J.-P. Wigneron, S. Delwart, F. Cabot, 1052 J. Boutin, M. J. Escorihuela, J. Font, N. Reul, C. Gruhier, S. E. Juglea, 1053 M. R. Drinkwater, A. Hahne, M. Martin-Neira, and S. Mecklenburg, 1054 "The SMOS mission: New tool for monitoring key elements of the 1055 global water cycle," *Proc. IEEE*, vol. 98, no. 5, pp. 666–687, May 2010. 1056 doi:10.1109/JPROC.2010.2043032. 1057
- [7] P. Matos, A. Gutiérrez, and F. Moreira, *SMOS LI Processor Discrete 1058 Global Grids Document*, vol. SMOS-DMS-TN-5200. Lisboa, Portugal: 1059 DEIMOS Engenharia, 2004, V1.4. 1060
- [8] S. Bircher, J. E. Balling, N. Skou, and Y. Kerr, "SMOS validation by 1061 means of an airborne campaign in the Skjern river catchment, Western 1062 Denmark," *IEEE Trans. Geosci. Remote Sens.*, 2011, to be published. 1063 AQ11
- [9] C. Gruhier, P. de Rosnay, S. Hasenauer, T. Holmes, R. de Jeu, 1064 Y. Kerr, E. Mougin, E. Njoku, F. Timouk, W. Wagner, and M. Zribi 1065

- 1066 (2010, Jan.). Soil moisture active and passive microwave products:  
1067 Intercomparison and evaluation over a Sahelian site. *Hydrol. Earth Syst.*  
1068 *Sci. [Online]*, 14(1), pp. 141–156. Available: www.hydrol-earth-syst-  
1069 sci.net/14/141/2010/
- 1070 [10] J.-C. Calvet, N. Fritz, F. Froissard, D. Suquia, A. Petipia, and B. Piguet,  
1071 “In situ soil moisture observations for the CAL/VAL of SMOS: The  
1072 SMOSMANIA network,” in *Proc. IGARSS*, Barcelona, Spain, 2007,  
1073 pp. 1196–1199.
- 1074 [11] S. Peischl, J. P. Walker, M. Allahmoradi, D. Barrett, R. Gurney, Y. Kerr,  
1075 E. Kim, J. Le Marshall, C. Rüdiger, D. Ryu, and N. Ye, “Towards vali-  
1076 dation of SMOS using airborne and ground data over the Murrumbidgee  
1077 catchment,” in *Proc. MODSIM*, Cairns, Australia, 2009, pp. 3733–3739.
- 1078 [12] M. H. Cosh, T. J. Jackson, S. M. Moran, and R. Bindlish, “Temporal  
1079 persistence and stability of surface soil moisture in a semi-arid water-  
1080 shed,” *Remote Sens. Environ.*, vol. 112, no. 2, pp. 304–313, Feb. 2008.  
1081 doi:10.1016/j.rse.2007.07.001.
- 1082 [13] P. de Rosnay, C. Gruhier, F. Timouk, F. Baup, E. Mougin, P. Hiernaux,  
1083 L. Kergoat, and V. Le Dantec, “Multi-scale soil moisture measurements  
1084 at the Gourma meso-scale site in Mali,” *J. Hydrol.*, vol. 375, no. 1/2,  
1085 pp. 241–252, Aug. 2009. doi:10.1016/j.jhydrol.2009.01.015.
- 1086 [14] N. S. Chauhan, S. Miller, and P. Ardanuy, “Spaceborne soil moisture esti-  
1087 mation at high resolution: A microwave-optical/IR synergistic approach,”  
1088 *Int. J. Remote Sens.*, vol. 24, no. 22, pp. 4599–4622, Nov. 2003.
- 1089 [15] M. Piles, A. Camps, M. Vall-llossera, I. Corbella, R. Panciera, C. Rüdiger,  
1090 Y. H. Kerr, and J. P. Walker, “Downscaling SMOS-derived soil moisture  
1091 using MODIS visible/infrared data,” *IEEE Trans. Geosci. Remote Sens.*,  
1092 vol. 49, no. 9, pp. 3156–3166, Sep. 2011.
- 1093 [16] O. Merlin, A. Al Bitar, J. P. Walker, and Y. Kerr, “An improved algorithm  
1094 for disaggregating microwave-derived soil moisture based on red, near-  
1095 infrared and thermal-infrared data,” *Remote Sens. Environ.*, vol. 114,  
1096 no. 10, pp. 2305–2316, Oct. 2010. doi:10.1016/j.rse.2010.05.007.
- 1097 [17] O. Merlin, A. Al Bitar, J. P. Walker, and Y. Kerr, “A sequential model  
1098 for disaggregating near-surface soil moisture observations using multi-  
1099 resolution thermal sensors,” *Remote Sens. Environ.*, vol. 113, no. 10,  
1100 pp. 2275–2284, Oct. 2009. doi:10.1016/j.rse.2009.06.012.
- 1101 [18] O. Merlin, J. Walker, R. Panciera, R. Young, J. Kalma, and  
1102 E. Kim, “Soil moisture measurement in heterogeneous terrain,” in *Proc.*  
1103 *MODSIM—International Congress Modelling Simulation Modelling*  
1104 *Simulation Society Australia New Zealand*, Dec. 2007, pp. 2604–2610.
- 1105 [19] Y. H. Kerr, P. Waldteufel, P. Richaume, P. Ferrazzoli, and J.-P. Wigneron,  
1106 *SMOS Level 2 Processor Soil Moisture Algorithm Theoretical Basis*  
1107 *Document (ATBD)*, vol. SO-TN-ESL-SM-GS-0001. Toulouse, France:  
1108 CESBIO, May 2011, V3.f.
- 1109 [20] Y. H. Kerr, P. Waldteufel, P. Richaume, J. P. Wigneron, P. Ferrazzoli,  
1110 A. Mahmoodi, A. Al Bitar, F. Cabot, C. Gruhier, D. Leroux, A. Mialon,  
1111 and S. Delwart, “The SMOS soil moisture retrieval algorithm,” *IEEE*  
1112 *Trans. Geosci. Remote Sens.*, 2011.
- 1113 [21] O. Merlin, C. Rüdiger, P. Richaume, A. Al Bitar, A. Mialon, J. P. Walker,  
1114 and Y. Kerr, “Disaggregation as a top-down approach for evaluating  
1115 40 km resolution SMOS data using point-scale measurements: Application  
1116 to AACES-1,” in *Proc. SPIE, Remote Sens. Agriculture, Ecosystems,*  
1117 *Hydrol. XII*, Toulouse, France, 2010, pp. 782.401-1–782.401-8.
- 1118 [22] K. Nishida, R. R. Nemani, J. M. Glassy, and S. W. Running, “Develop-  
1119 ment of an evapotranspiration index from Aqua/MODIS for monitoring  
1120 surface moisture status,” *IEEE Trans. Geosci. Remote Sens.*, vol. 41, no. 2,  
1121 pp. 493–501, Feb. 2003.
- 1122 [23] G. Gutman and A. Ignatov, “The derivation of the green vegetation fraction  
1123 from NOAA/AVHRR data for use in numerical weather prediction  
1124 models,” *Int. J. Remote Sens.*, vol. 19, pp. 1533–1543, 1998.
- 1125 [24] O. Merlin, B. Duchemin, O. Hagolle, F. Jacob, B. Coudert, G. Chehbouni,  
1126 G. Dedieu, J. Garatza, and Y. Kerr, “Disaggregation of MODIS surface  
1127 temperature over an agricultural area using a time series of Formosat-2  
1128 images,” *Remote Sens. Environ.*, vol. 114, no. 11, pp. 2500–2512,  
1129 Nov. 2010. doi:10.1016/j.rse.2010.05.025.
- 1130 [25] A. C. T. Pinheiro, J. Descloitres, J. L. Privette, J. Susskind, L. Iredell, and  
1131 J. Schmaltz, “Near-real time retrievals of land surface temperature within  
1132 the MODIS rapid response system,” *Remote Sens. Environ.*, vol. 106,  
1133 no. 3, pp. 326–336, Feb. 2007. doi:10.1016/j.rse.2006.09.006.
- 1134 [26] J. Noilhan and S. Planton, “A simple parameterization of land surface  
1135 processes for meteorological models,” *Monthly Weather Rev.*, vol. 117,  
1136 no. 3, pp. 536–549, 1989.
- 1137 [27] O. Merlin, J. P. Walker, A. Chehbouni, and Y. Kerr, “Towards deter-  
1138 ministic downscaling of SMOS soil moisture using MODIS derived soil  
1139 evaporative efficiency,” *Remote Sens. Environ.*, vol. 112, no. 10, pp. 3935–  
1140 3946, Oct. 2008. doi:10.1016/j.rse.2008.06.012.
- 1141 [28] M. S. Moran, T. R. Clarke, Y. Inoue, and A. Vidal, “Estimating crop water  
1142 deficit using the relation between surface-air temperature and spectral  
1143 vegetation index,” *Remote Sens. Environ.*, vol. 49, no. 3, pp. 246–263, 1994.  
1144
- [29] T. N. Carlson, R. R. Gillies, and E. M. Perry, “A method to make use of thermal infrared temperature and NDVI measurements to infer soil water content and fractional vegetation cover,” *Remote Sens. Rev.*, vol. 52, pp. 45–49, 1994.
- [30] O. Merlin, G. Chehbouni, J. P. Walker, R. Panciera, and Y. Kerr, “A simple method to disaggregate passive microwave based soil moisture,” *IEEE Trans. Geosci. Remote Sens.—SMOS Special Issue*, vol. 46, no. 3, pp. 786–796, Mar. 2008. doi:10.1109/TGRS.2007.914807.
- [31] W. P. Kustas and J. M. Norman, “Evaluation of soil and vegetation heat flux predictions using a simple two-source model with radiometric temperatures for partial canopy cover,” *Agricultural Forest Meteorol.*, vol. 94, no. 1, pp. 13–29, 1999.
- [32] M. C. Anderson, J. M. Norman, G. R. Diak, W. P. Kustas, and J. R. Mecikalski, “A two-source time-integrated model for estimating surface fluxes using thermal infrared remote sensing,” *Remote Sens. Environ.*, vol. 60, no. 2, pp. 195–216, May 1997.
- [33] O. Merlin and G. Chehbouni, “Different approaches in estimating heat flux using dual angle observations of radiative surface temperature,” *Int. J. Remote Sens.*, vol. 25, no. 1, pp. 275–289, 2004.
- [34] T. J. Lee and R. A. Pielke, “Estimating the soil surface specific humidity,” *J. Appl. Meteorol.*, vol. 31, no. 5, pp. 480–484, 1992.
- [35] T. S. Komatsu, “Towards a robust phenomenological expression of evaporation efficiency for unsaturated soil surfaces,” *J. Appl. Meteorol.*, vol. 42, no. 9, pp. 1330–1334, Sep. 2003.
- [36] O. Merlin, J. P. Walker, J. D. Kalma, E. J. Kim, J. Hacker, R. Panciera, R. Young, G. Summerell, J. Hornbuckle, M. Hafeez, and T. J. Jackson, “The NAFe’06 data set: Towards soil moisture retrieval at intermediate resolution,” *Adv. Water Resour.*, vol. 31, pp. 1444–1455, 2008. doi:10.1016/j.advwatres.2008.01.018.
- [37] Z. Wan and J. Dozier, “A generalized split-window algorithm for retrieving land-surface temperature from space,” *IEEE Trans. Geosci. Remote Sens.*, vol. 34, no. 4, pp. 892–905, Jul. 1996.
- [38] O. Merlin, A. Al Bitar, V. Rivalland, P. Béziat, E. Ceschia, and G. Dedieu, “An analytical model of evaporation efficiency for unsaturated soil surfaces with an arbitrary thickness,” *J. Appl. Meteorol. Climatol.*, vol. 50, no. 2, pp. 457–471, Feb. 2011. doi:10.1175/2010JAMC2418.1.
- [39] N. Agam, W. P. Kustas, M. C. Anderson, F. Li, and C. M. U. Neale, “A vegetation index based technique for spatial sharpening of thermal imagery,” *Remote Sens. Environ.*, vol. 107, no. 4, pp. 545–558, 2007.
- [40] E. E. Small and S. A. Kure, “Tight coupling between soil moisture and the surface radiation budget in semiarid environments: Implications for land-atmosphere interactions,” *Water Resour. Res.*, vol. 39, no. 10, p. 1278, Oct. 2003. doi:10.1029/2002WR001297.
- [41] C. Rüdiger, J. P. Walker, and Y. H. Kerr, “On the airborne spatial coverage requirement for microwave satellite validation,” *IEEE Geosci. Remote Sens. Lett.*, vol. 8, no. 4, pp. 824–828, Jul. 2011.
- [42] R. Young, J. Walker, N. Yeoh, A. Smith, K. Ellett, O. Merlin, and A. Western, *Soil Moisture and Meteorological Observations from the Murrumbidgee Catchment*. Melbourne, Australia: Dept. Civil Environ. Eng., Univ. Melbourne, 2008.
- [43] A. J. Teuling, R. Uijlenhoet, R. Hurkmans, O. Merlin, R. Panciera, J. Walker, and P. A. Troch, “Dry-end surface soil moisture variability during NAFe’06,” *Geophys. Res. Lett.*, vol. 34, no. L17402, Sep. 2007.
- [44] W. T. Crow and E. F. Wood, “The assimilation of remotely sensed soil brightness temperature imagery into a land surface model using Ensemble Kalman filtering: A case study based on ESTAR measurements during SGP97,” *Adv. Water Resour.*, vol. 26, pp. 137–149, 2003.
- [45] Q. K. Hassan, C. P.-A. Bourque, F.-R. Meng, and R. M. Cox, “A wetness index using terrain-corrected surface temperature and normalized difference vegetation index derived from standard MODIS products: An evaluation of its use in a humid forest-dominated region of eastern Canada,” *Sensors*, vol. 7, no. 10, pp. 2028–2048, 2007.

**Olivier Merlin**, photograph and biography not available at the time of publication.

**Christoph Rüdiger**, photograph and biography not available at the time of publication.

1211 **Ahmad Al Bitar**, photograph and biography not available at the time of  
1212 publication.

**Jeffrey P. Walker**, photograph and biography not available at the time of 1215  
1216 publication.

1213 **Philippe Richaume**, photograph and biography not available at the time of  
1214 publication.

**Yann H. Kerr**, photograph and biography not available at the time of 1217  
1218 publication.

IEEE  
Proof

## AUTHOR QUERIES

AUTHOR PLEASE ANSWER ALL QUERIES

Please be aware that the authors are required to pay overlength page charges (\$200 per page) if the paper is longer than 6 pages. If you cannot pay any or all of these charges please let us know.

AQ1 = Please provide publication update in Ref. [8].

AQ2 = Please provide volume, issue number, page range and month of publication in [20].

END OF ALL QUERIES

IEEE Proof